THESIS

This is to certify that the

thesis entitled

A Study of Binary Mixture Boiling
Boiling Site Density and Subcooling Boiling

presented by

Tze-On Hui

has been accepted towards fulfillment
of the requirements for

M.S. degree in Mechanical Engineering

John Thome is in Germany for the term.
He has given me the authority to confirm
all corrections have been made.

Major professor

Date June 13, 1983

R W Bartlomew
Committee Member

A STUDY OF BINARY MIXTURE BOILING: BOILING SITE DENSITY AND SUBCOOLING BOILING

By

Tze On Hui

A THESIS

Submitted to
Michigan State University
in partial fulfillment of the requirements

MASTER OF SCIENCE

DEPARTMENT OF MECHANICAL ENGINEERING

1983

ABSTRACT

A STUDY OF BINARY MIXTURE BOILING:
BOILING SITE DENSITY AND SUBCOOLING BOILING

By

Tze On Hui

Boiling site densities have been measured for ethanol-water and ethanol-benzene mixtures at 1.01 bar. Site densities were obtained photographically for a vertically oriented heated test surface. The effects of composition, heat flux, and subcooling on the boiling site density were studied.

For ethanol-water mixtures the boiling site density increased about two orders of magnitude from pure water (relatively large bubbles) to the azeotrope composition (relatively small bubbles). This dramatic increase was noted to be caused by the nature of activation of the boiling surface; inception of individual boiling sites at low ethanol compositions and inception of boiling of the whole surface upon the activation of the first boiling site at medium and high ethanol compositions.

For ethanol-benzene mixtures the boiling site density formed an unexpected maximum to the left of the azeotrope point while forming a minimum to the right. This phenomenon was postulated to be caused by condensation or evaporation of the more volatile component during the waiting period of the bubble growth

cycle. Activation of the first boiling site caused rapid activation of the entire boiling surface at all compositions.

The effect of subcooling (0 to 20 °C) on the boiling site density was observed to behave in three ways: (1) monotomically decreasing, (2) displaying a maximum, or (3) displaying a minimum. The boiling site density was found to increase with increasing heat flux as expected from previous single component studies.

Pool boiling curves were obtained for subcoolings ranging from 0 to 20 °C for heat fluxes up to 100 kW/m^2. The heat transfer coefficient, based on $(T_{wall}-T_{bulk})$, was found to decrease with increasing subcoolings. The decrease in the heat transfer coefficient in the mixtures for a given level of subcooling was less than that for the single components and azeotropic mixtures.

TABLE OF CONTENTS

LIST OF TABLES..... vi

LIST OF FIGURES..... vii

LIST OF SYMBOLS..... x

1.0 INTRODUCTION 1

2.0 REVIEW OF BOILING 9

2.1 Bubble growth rates 9

2.1.1. Van Stralen's derivation..... 10

2.1.2. Thome's equation for bubble growth rate in binary mixtures..... 14

2.2 Bubble departure diameter and frequency..... 16

2.2.1. Bubble departure diameter..... 16

2.2.2. Bubble departure frequency..... 19

2.3. Bubble nucleation..... 20

2.4. Temperature profile of the thermal boundary layer adjacent to a heated surface during nucleate pool boiling..... 28

2.5 The influence of subcooling on pool boiling heat transfer..... 32

3.0 EXPERIMENTAL DESIGN AND PROCEDURE..... 38

3.1 Experimental design and procedures..... 38

3.1.1. Heating surfaces..... 38

3.1.2. Electrical circuit for surface heater..... 40

3.1.3. Description of experimental rig and overall set up 43

3.1.4. Temperature measurement..... 46

3.2 Experimental procedure and calculation..... 46

3.2.2. Determining the boiling site density..... 51

3.2.3. Calculation for heat transfer coefficient.. 52

4.0 RESULTS AND DISCUSSION 55

4.1. Heat transfer coefficient vs. mixture composition..... 57

4.1.1. Ethanol-water mixtures..... 57

4.1.2. Ethanol-benzene mixtures..... 62

4.2. Heat transfer coefficient vs. subcooling... 67

4.3. Non-dimensional heat transfer coefficient vs. mixture composition..... 67

4.3.1. Ethanol-water mixtures..... 67

4.3.2. Ethanol-benzene mixtures..... 74

4.4. Boiling site density vs. mixture composition 74

4.4.1. Ethanol-water mixture..... 74

4.4.2. Ethanol-benzene mixtures..... 82

4.5. Boiling site density vs. subcooling..... 89

4.6. Boiling site density vs. heat flux..... 96

4.7. Boiling site density vs. wall temperature.. 100

4.8. $(B.S.D._{EXP})/(B.S.D._{I})$ vs. mixture composition..... 104

5.0 CONCLUSION..... 108

APPENDIX A Preparation of a mixture of known composition 110

APPENDIX B Calculation for heat loss..... 113

APPENDIX C Experimental data..... 117

LIST OF REFERENCES 135

LIST OF TABLES

2.1. The influence of subcooling on the heat transferred by one bubble.....31

2.2. Effect of subcooling on heat transfer coefficient.....35

3.1. Experimental conditions: mixture composition, heat fluxes, and subcooling.....49

LIST OF FIGURES

1.1 Phase equilibrium diagram for an ideal binary mixture system..... 3

1.2 Phase equilibrium diagram for an azeotropic mixture system..... 4

1.3 Pool boiling curves with boiling site densities (site/cm^2) for the water-MEK system at 1.0 bar by Van Stralen..... 7

2.1 Bubble growth model of Van Stralen for a spherical vapor bubble growing in a superheated binary system..... 12

2.2 Dependence of bubble departure and heat transfer coefficient on composition obtained by Tolubinskiy and Ostrovskiy..... 17

2.3 Bubble departure diameter for nitrogen-argon mixtures by Thome..... 17

2.4 Bubble departure frequency for nitrogen-argon mixtures..... 18

2.5 Bubble departure diameter in nitrogen-argon mixtures vs. bubble inertia force term..... 18

2.6 Variation in the advancing contact angle with composition for ethanol-water mixtures measured by Eddington and Kenning at 20°C against nitrogen gas..... 22

2.7 Vapor trapping model of Singh et al..... 23

2.8 Incipient and deactivation superheats for liquid nitrogen-argon mixtures 23

2.9 Incipient and deactivation superheats for ethanol-water mixtures..... 24

2.10 Calculated vapor nucleus radius vs. mole fraction of ethanol..... 25

2.11 Amplitude of temperature fluctuations vs. height above surface..... 31

2.12 Average diameter, nucleation frequency, and growth rate for vapor bubbles as a function of subcooling..... 31

2.13 Experimental boiling heat transfer data for a horizontal stainless steel cylinder immersed in water 35

2.14 Variation of surface-heat with bulk subcooling 36

2.15 Variation of active site with bulk subcooling 36

2.16 Variation of average bubble frequency with bulk subcooling..... 36

3.1 Test surface no. 1..... 39

3.2 Boiling surface set-up..... 41

3.3 Test surface no. 2..... 42

3.4 Power supply circuit 44

3.5 Experimental boiling rig..... 45

3.6 Experimental set-up..... 47

4.0 Definition of a linear mixing law for the azeotropic ethanol-benzene system..... 56

4.1, 4.2, 4.3, 4.4

Heat transfer coefficient vs. percent ethanol for ethanol-water mixtures.....
58, 59, 60, 61

4.5, 4.6, 4.7, 4.8

Heat transfer coefficient vs. percent ethanol for ethanol-benzene mixtures.....
63, 64, 65, 66

4.9,4.10, 4.11, 4.12

Heat transfer coefficient vs. subcooling.....
68, 69, 70, 71

4.13, 4.14

H(exp)/H(I) vs. composition for ethanol-water mixtures.....
72,73

4.15, 4.16

H(exp)/H(I) vs. composition for ethanol-benzene mixtures..... 75, 76

4.17, 4.18, 4.19, 4.20

Site density vs. percent ethanol for ethanol-water mixture..... 77,78, 79, 80

4.21, 4.22, 4.23, 4.24a

Site density vs. percent ethanol for ethanol-benzene mixture..... 83, 84, 85, 86

4.24b Phase diagram for ethanol-benzene system 88

4.25,4.26, 4.27, 4.28, 4.29, 4.30

Site density vs. subcooling..... 91, 92, 93, 94, 95, 96

4.31, 4.32, 4.33

Site density vs. heat flux..... 97, 98, 99

4.34, 4.35, 4.36

Site density vs. wall temperature..... 101, 102, 103

4.38, 4.39, 4.40

$(B.S.D._{exp})/(B.S.D._{I})$ vs. composition.... 105, 106, 107

A-1 Values for fin efficiency..... 116

NOMENCLATURE

Az	azeotrope or azeotropic composition
$B.S.D._{exp}$	experimental boiling site density (sites/cm^2)
$B.S.D._I$	ideal boiling site density (sites/cm^2)
C_p	liquid specific heat (kJ/kg · °C)
D	liquid mass diffusivity (m^2/s)
D_d	bubble departure diameter
f	bubble departure frequency
F_b	buoyancy force
F_d	drag force
F_i	inertia force
F_p	excess pressure force on base area of bubble
F_σ	surface tension force
h	heat transfer coefficient (w/m^2 °C)
h_{exp}	experimental heat transfer coefficient (w/m^2 °C)
h_{fg}	latent heat of evaporation
h_I	ideal heat transfer coefficient (w/m^2 °C)
N_{sn}	Scriven number
dP_{sat}/dT	slope of saturation curve
q	heat flux (w/m^2)
R	vapor bubble radius
ΔT	wall superheat, $T_w - T_{sat}$
T_b	bulk temperature of liquid

ΔT_{eff}	effective wall superheat
ΔT_{inc}	incipient superheat, $T_{sup} - T_{sat}$
T_s	wall surface temperature
T_{sat}	saturation temperature
T_w	wall temperature
T_1, T_2, T_3	temperature measurements underneath heating surface
t_g	binary mixture bubble growth time
t_{g_I}	ideal binary mixture bubble growth time
t_w	waiting period
x	mass fraction of volatile component at bubble interface
$\tilde{x}$	mole fraction of volatile component in liquid phase
x_b	mass fraction of volatile component in bulk liquid
y	mass fraction of volatile component in the vapor bubble
$\tilde{y}$	mole fraction of volatile component in vapor bubble

GREEK SYMBOLS

α_L	liquid thermal diffusivity (m^2/s)
δ	extrapolated superheated-layer thickness
δ_m	mass diffusion shell thickness
$\Delta\theta$	rise in local saturation temperature
ρ_L	liquid density (kg/m^3)
ρ_V	vapor density (kg/m^3)
σ	surface tension (N/m)
$\tilde{\tau}$	average bubble growth time

Chapter 1

Introduction

Boiling is a physical process of great practical significance and has been the subject of intensive research for many years. Many of these research projects were motivated by the need for nuclear power vapor generator design and safety and the sharp rise in energy cost. Most of the research efforts have been directed on the boiling characteristics of single component liquids. But mixture boiling research is important in the design of two-phase heat exchange equipment in the chemical and petrochemical processing industries, the refrigeration industry, the air separation industry, and the liquid natural gas industry as examples.

The boiling of binary and multicomponent liquid mixtures is quite different from single component boiling. The thermodynamics of vapor-liquid phase equilibria of mixtures allow the vapor and liquid phase to be of differing compositions. Thus, the boiling of a liquid mixture is distinct from single component boiling in that the driving force for heat transfer is in turn linked to mass transfer. The evaporation rate can be severely retarded in the mixture because the rate of mass diffusion is usually much slower than that of heat diffusion in the liquid phase.

A working knowledge of the elementary principles of vapor-liquid phase equilibria is required for an understanding of mixture boiling. Phase equilibrium diagrams are used to describe the relationship between temperature, pressure, and the compositions in the two phases at saturation. Figure 1.1 shows the phase equilibrium diagram for an ideal binary system at constant pressure. Saturation temperature is plotted on the vertical axis. Mole fractions of the more volatile component in the liquid and vapor phases are plotted on the horizontal axis. The more volatile component is that with the lower boiling point at the pressure of interest. The dew point line denotes the variation in equilibrium vapor mole fraction with saturation temperature. The bubble point line depicts the functional dependency of the liquid mole fraction on the saturation temperature. It is evident that $\tilde{y} > \tilde{x}$ for the more volatile component and $\tilde{y} < \tilde{x}$ for the less volatile component. This is expected intuitively since the more volatile component is above its normal boiling point while the reverse is true for the less volatile component.

Figure 1.2 illustrates a temperature-composition phase diagram for a binary mixture system forming an azeotrope at $\tilde{x}_{az}$. At the azeotrope, the compositions of the liquid and vapor phase are identical. To the left side of the azeotrope, $\tilde{y} > \tilde{x}$, and to the right $\tilde{y} < \tilde{x}$. The slope of the bubble point line changes from negative to positive as the azeotrope is passed from left to right. However, the product $(\tilde{y}-\tilde{x})(dT/d\tilde{x})$ is always positive as a consequence. The

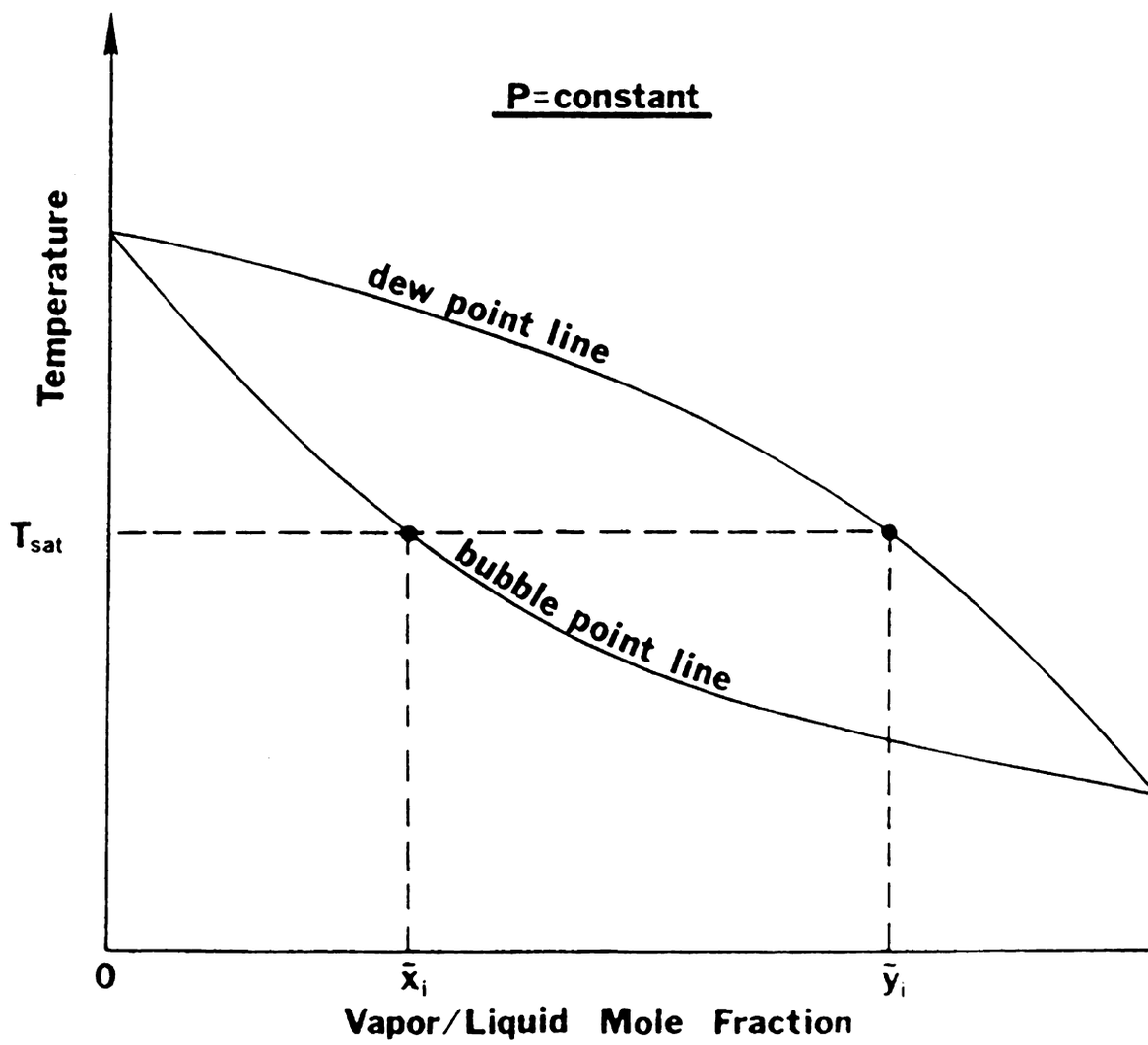

Figure 1.1
Phase equilibrium diagram for an ideal binary mixture system

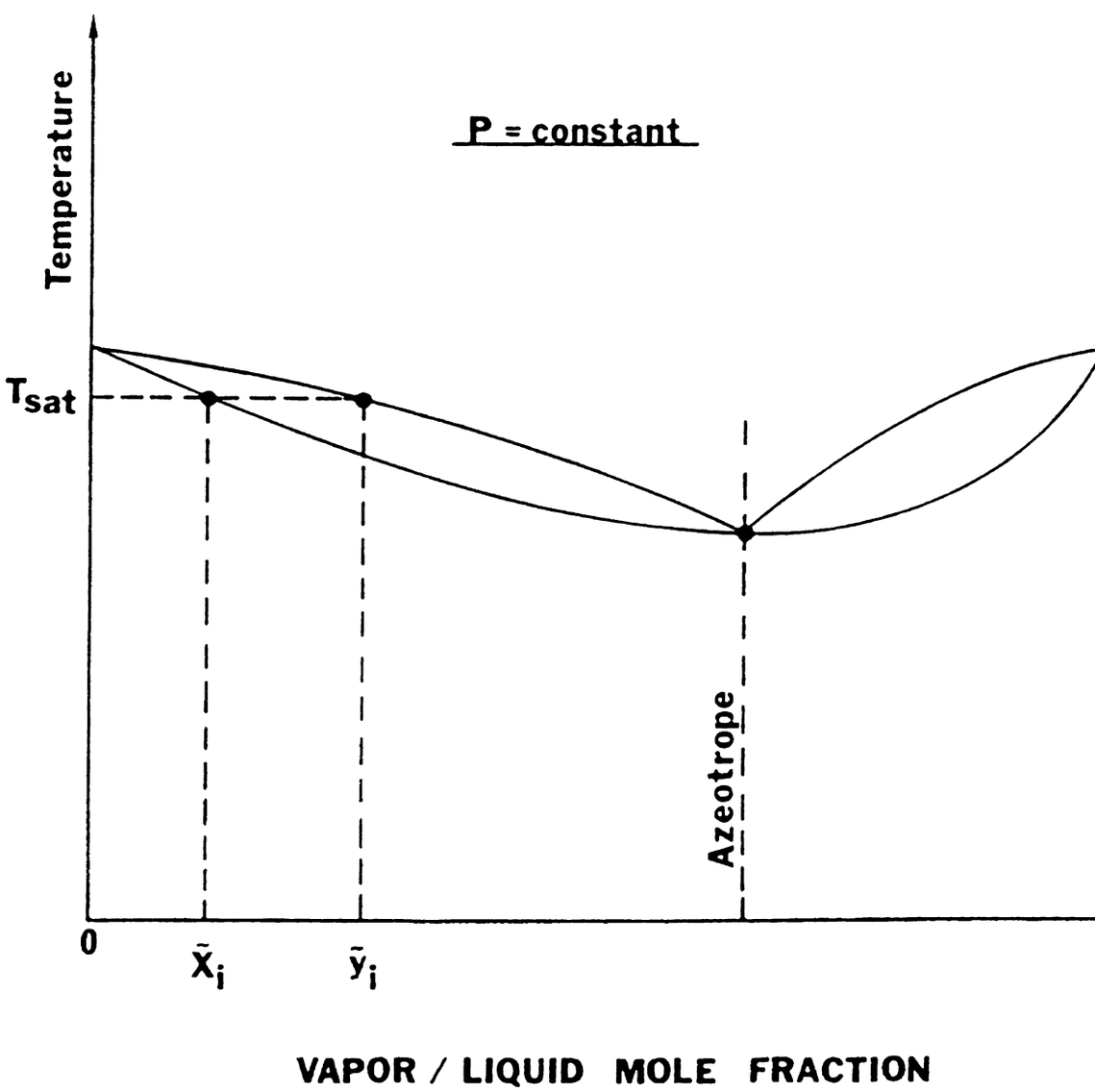

Figure 1.2
Phase equilibrium for an azeotropic mixture system

azeotrope behaves like a single component liquid since the compositions in both phases are the same.

The boiling heat transfer coefficient of binary mixtures can be drastically smaller than that predicted by using an ideal linear mixing law on single component boiling heat transfer coefficients. Thus, the fundamental mechanisms causing this variation need to be studied and ultimately, a method is needed to predict the boiling heat transfer coefficient for binary mixtures. An objective of the present experimental program is to determine the effects of composition and subcooling on the boiling site density. Boiling site density is defined as the number of active boiling sites per unit area. The boiling heat transfer coefficient also will be measured in order to ascertain the dependence of the heat transfer coefficient on the boiling site density. The boiling site density is an important parameter because it affects the rate of total vapor generation and thermal boundary layer removal. Consequently, it plays a significant role in the overall enhancement of the heat transfer rate in nucleate pool boiling compared to single phase natural convection.

No analytical information is available at the present time to predict the site density as a function of composition and the degree of subcooling. The only previous experimental work on site density in binary liquid mixtures as a function of composition was performed by Van Stralen (1). However, his results seem impractical since his study was performed on a very thin wire (0.2 mm in diameter) which is much smaller

than the diameter of the bubbles themselves. His tests covered a number of aqueous systems. Figure 1.3 depicts the results for water, methyl ethyl ketone (MEK), and a mixture of 4.1% wt. MEK. At a constant heat flux of 0.3 MW/m^2, for instance, the number of boiling sites per cm^2 in pure water is 30 and in MEK over 200, but for the 4.1% mixture only one site per unit area is active. Thus, the variation in the boiling site density at constant heat flux shows a marked minimum.

Several parameters are important in any model for predicting the site density: the boiling incipience criteria, the dynamic contact angle, and the thickness and the temperature profile of the thermal boundary layer. These parameters will be elaborated in Chapter 2.

The experimental program involves performing boiling heat transfer experiments in which composition, heat flux, and the degree of bulk subcooling are varied. Two binary mixture systems were chosen for the study: ethanol-water and ethanol-benzene. In the aqueous binary mixtures of ethanol and water, the dynamic contact angle and surface tension vary substantially as the composition changes. Therefore, a large variation in the boiling site density with composition is expected for this mixture system. On the other hand, the variation of boiling site density for ethanol and benzene mixtures is expected to be smaller since the surface tension does not change as much for this non-aqueous binary system. Also, the contact angle is thought

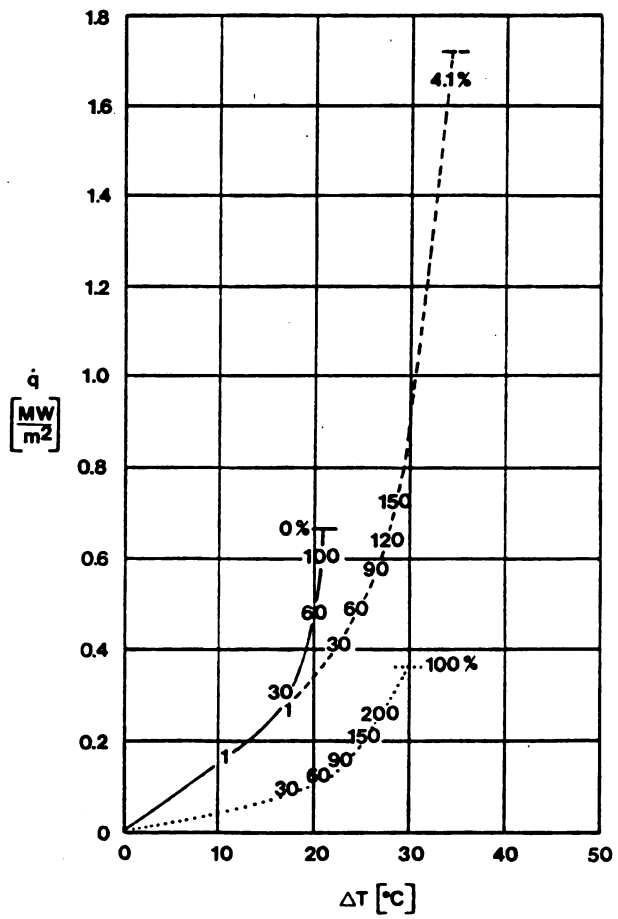

Figure 1.3
Pool boiling curves with boiling site densities (sites/cm^2) for the water-MEK system at 1.0 bar by Van Stralen (1)

to be fairly constant. For each experimental condition, photographs of the boiling surface are taken at a shutter speed of 1000 HZ. The boiling site density is obtained from the photographs. The heat transfer coefficient is obtained by calculating the wall temperature of the boiling test surface and the heat flux through a prescribed area.

Chapter 2 is a state-of-the-art review on the areas of importance in the present study. Chapter 3 describes the experimental design and procedure. Experimental results and a discussion of these results will be presented in Chapter 4. Chapter 5 presents the conclusions of the study.

Chapter 2

Review of boiling

It has been well established from experimental studies that the boiling heat transfer coefficient of binary mixtures is much lower than that predicted by using an ideal linear mixing law on their single component values. In the following sections, fundamental phenomenological topics such as bubble growth rate, bubble departure diameter, bubble departure frequency, bubble incipience, and boiling site density are presented in the context to explain the lower heat transfer coefficient for binary mixtures. A section will be devoted to discussing the effects of subcooling on the boiling heat transfer process and its effect on the different parameters will be examined.

2.1 Bubble growth rates

The bubble growth rate of a single component liquid is limited by the rate of heat transfer to the bubble interface to provide for the latent heat of evaporation. In binary mixtures, however, the growth rate depends upon the rate of mass diffusion of the more volatile component as well as upon the diffusion of heat. During the growth of the bubble,

the more volatile component is evaporated preferentially since its mole fraction in the vapor phase, $\tilde{y}$, is greater than its mole fraction in the liquid phase, $\tilde{x}$ (Figure 2.1). Due to this preferential evaporation, the volatile component is depleted near the bubble interface and must be replenished by mass diffusion through the depleted layer. Consequently, the bubble growth rate is slowed down. The local saturation temperature rises also, due to the higher composition of the less volatile component. Thus the effective driving force for heat conduction to the evaporating interface, ΔT_{eff}, is lowered.

2.1.1 Van Stralen's derivation of bubble growth rate equation for binary mixture

In the next two sections, derivations for bubble growth rates for binary mixtures will be presented. The first derivation will be the pioneer work of Van Stralen (2) who extended the theory for spherically symmetric bubble growth in a uniformly superheated liquid for single component liquids to include binary mixtures. Next, Thome's model (3) is presented. Thome's model extends Van Stralen's model by considering a further rise in the local saturation temperature due to the evaporation of neighboring sites and a previously departed bubble.

Van Stralen starts his derivation by using a mass balance equation at the bubble interface. The rate of

preferential evaporation of the more volatile component is equated to its rate of mass diffusion through the interface,

$$\rho_v(y-x)dR/dt = \rho_L D(\partial x/\partial r)_{r=R} \qquad (2.1)$$

The mass fraction of the more volatile component drops from a value of x_b to x across a spherical diffusion shell of thickness δ_m (see Figure 2.1). Assuming the mass concentration gradient across the diffusion shell to be linear, one gets

$$(\partial x/\partial r)_{r=R} = \frac{x_b - x}{\delta_m} \qquad (2.2)$$

Substitution of equation 2.2 into equation 2.1 gives

$$dR/dt = (\rho_L/\rho_v)(x_b-x/y-x)(D/\delta_m) \qquad (2.3)$$

To approximate the value of δ_m, Van Stralen uses a model for one-dimensional transient mass diffusion through a spherical shell, i.e.

$$\delta_m = (\pi Dt/3)^{1/3} \qquad (2.4)$$

The bubble growth rate is then given as

$$dR/dt = (\rho_v/\rho_L)(x_b-x/y-x)\frac{D}{(\pi Dt/3)^{1/2}} \qquad (2.5)$$

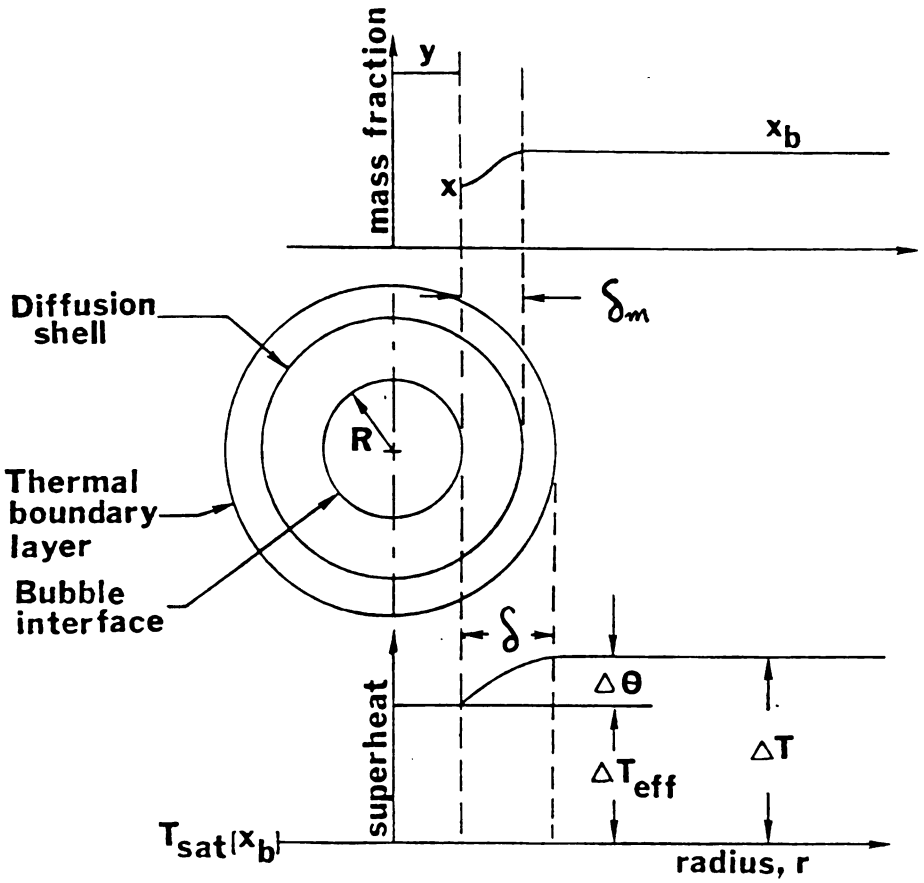

(a)

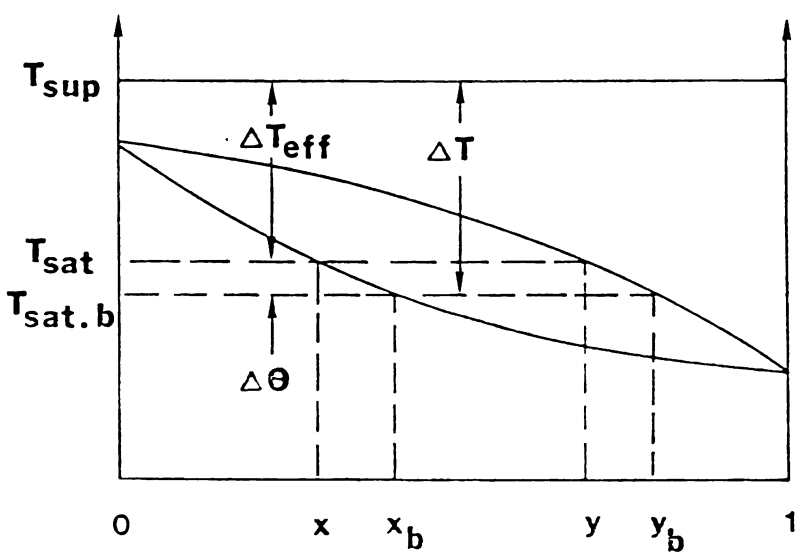

(b)

Figure 2.1 Bubble growth model of Van Stralen (2) for a spherical vapor bubble growing in a superheated binary mixture. (a) temperature and composition profiles; (b)process illustrated on phase diagram.

Van Stralen next examines the bubble growth rate in light of the Plesset and Zwick (4) bubble growth equation based on a heat balance:

$$R = (12/\pi)^{1/2} \frac{\rho_L C_p}{\rho_v h_{fg}} \Delta T (\alpha_L t)^{1/2} \qquad (2.6)$$

or differentiating equation (2.6),

$$dR/dt = (\rho_L/\rho_v)(C_p/h_{fg}) \frac{\Delta T \alpha_L}{(\pi \alpha_L t/3)^{1/2}} \qquad (2.7)$$

As pointed out earlier, the effective superheat, ΔT_{eff}, will be reduced by an increase in the local saturation temperature, $\Delta\theta$, at the bubble interface (Figure 2.1) such that

$$\Delta T_{eff} = \Delta T - \Delta\theta \qquad (2.8)$$

Substitution of ΔT_{eff} into equation 2.7 gives

$$dR/dt = (\rho_L C_p/\rho_v h_{fg})(\Delta T - \Delta\theta) \frac{\alpha_L}{(\frac{\pi}{3} \alpha_L t)^{1/2}} \qquad (2.9)$$

Combining equations 2.5 and 2.9, Van Stralen's equation for bubble growth for binary mixtures becomes

$$R = (12\alpha_L/\pi)^{1/2} (\rho_L C_p \Delta T/\rho_v h_{fg}) \frac{t^{1/2}}{1-(y-x)(\alpha_L/D)(C_p/h_{fg})(dT/dx)} \qquad (2.10)$$

Note that in the above equation, the value for $\Delta\theta$ is approximated by

$$\Delta\theta = (x_b - x/y - x)\, x_b \left[1 - K(x_b) \right] (dT/dx)_{x=x_b} \qquad (2.10a)$$

where $K(x_b)$ is the equilibrium constant at x_b .
This is in the same form as the Plesset and Zwick equation for single component liquids except that it is multiplied by the term

$$\frac{1}{1-(y-x)(\alpha_L/D)^{1/2}(C_p/h_{fg})\,(dT/dx)}$$

Since the value of this term is less than or equal to one, a smaller growth rate is predicted for binary mixtures.

2.1.2 Thome's equation for bubble growth rate in binary mixtures

Thome's equation is an extension of Van Stralen's equation. By comparing equation 2.9 and equation 2.10, one gets

$$\Delta T_{eff} = \Delta T - \Delta\theta = \Delta T N_{sn} \qquad (2.11)$$

where

$$N_{sn} = \left[1 - (y-x)(\alpha_L/D)^{1/2}(C_p / h_{fg})(dT/dx) \right]^{-1} \qquad (2.12)$$

Thome argues that equation 2.11 is an appropriate modification for the effective superheat for a single bubble growing in a liquid that was initially at the bulk saturation temperature. Application of Konovalov's rule dictates that (y-x) and (dT/dx) are always of opposite sign such that $N_{sn} \leq 1$.

On a boiling surface, bubbles are growing next to each other and even for a given site, the liquid is depleted of the more volatile component to some extent due to the preferential evaporation by a previously departed bubble. Therefore, the local liquid at the start of the growth stage is no longer at the bulk saturation temperature. The effective superheat is thus further reduced and Thome postulates that this rise in the local boiling point is similar in magnitude to $\Delta\theta$. Therefore, the modified effective superheat is given as

$$\Delta T_{eff} = \Delta T - \Delta\theta_1 - \Delta\theta_2 \qquad (2.13)$$

where

$$\Delta\theta_2 = (1-N_{sn})(\Delta T - \Delta\theta_1) \qquad (2.14)$$

Consequently, the effective wall superheat for bubble growth is given as

$$\Delta T_{eff} = N_{sn}^2 \Delta T \qquad (2.15)$$

and Thome's equation for bubble growth becomes

$$R = (12\alpha_L/\pi)^{1/2} (\rho_L c_{p/} \rho_v h_{fg}) N_{sn}^2 \Delta T t^{1/2} \qquad (2.16a)$$

2.2 Bubble departure diameter and frequency

2.2.1 Bubble departure diameter

The general trend of experimental results shows that bubble departure diameters in binary mixtures are significantly smaller than those for the two single component liquids. Figure 2.2 is an example of the experimental results by Tolubinskiy, Ostroviskiy, and coworker (5). Both binary systems of ethanol-water and methanol-water demonstrated a minimum in the bubble departure diameter at the maximum in $|\tilde{y}-\tilde{x}|$. Thome (6) carried out similar experiments for the argon-nitrogen system and found a similar trend in the bubble departure diameter and frequency. (see Figures 2.3 and 2.4)

To investigate the physical reason for the smaller bubble departure diameter in binary mixtures, the forces acting on a bubble growing on a heated surface are given by Kreshock and Siegel's equation (7) as

$$F_b + F_p = F_i + F_\sigma + F_d \qquad (2.16b)$$

where F_b = buoyancy force

F_p = excess pressure force on base area of bubble

F_i = inertia force

F_σ = surface tension force

F_d = drag force

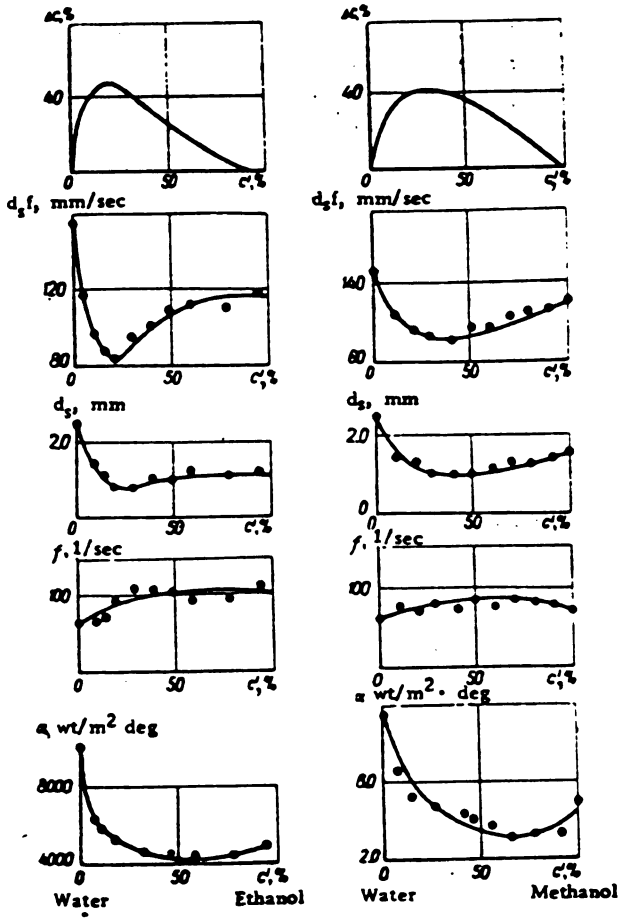

Figure 2.2 Dependence of bubble departure and heat transfer coefficient on composition ($q = 116\ kW/m^2$) obtained by Tolubinskiy and Ostrovskiy (5)

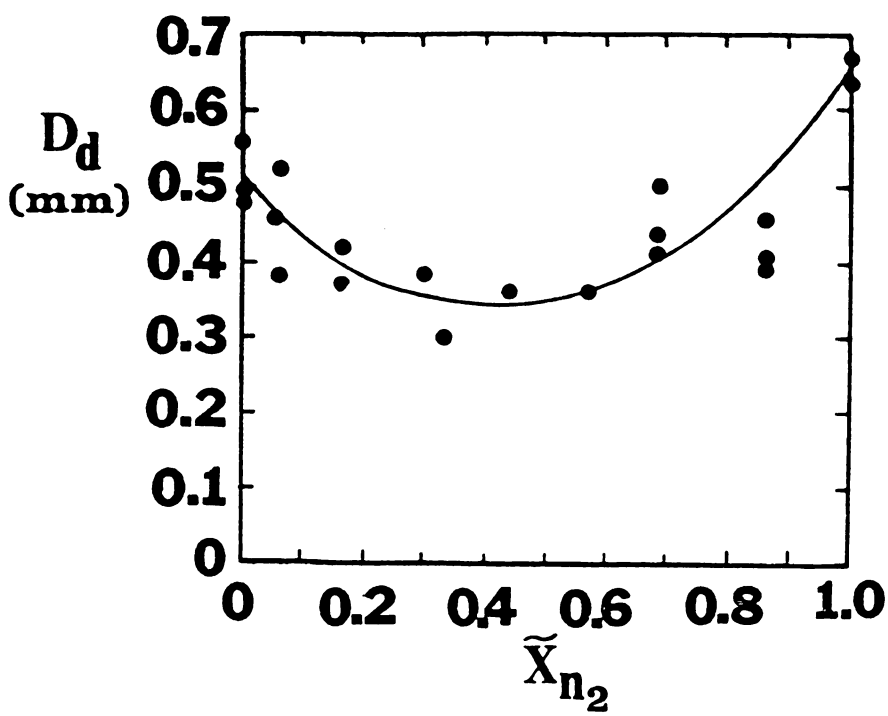

Figure 2.3 Bubble departure diameter at $q = 2.1\ kW/m^2$ for nitrogen-argon mixtures by Thome (6)

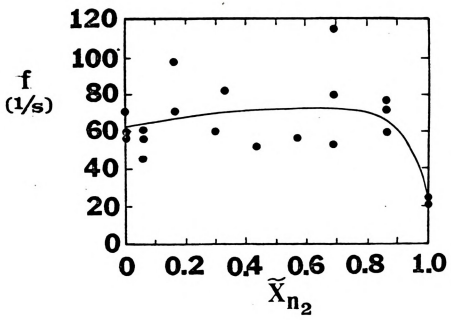

Figure 2.4
Bubble departure frequency at $q = 2.1\ kW/m^2$ for nitrogen-argon mixture by Thome (6)

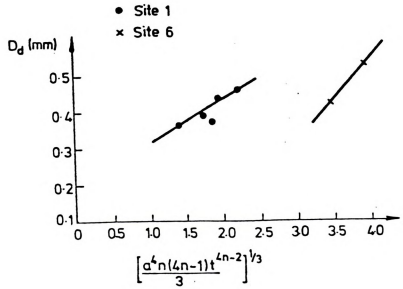

Figure 2.5
Bubble departure diameter in nitrogen-argon mixtures vs. bubble inertia force term, Thome and Davey (7). Site #1 is an artificial site of 52 μm dia. and site #6 is a naturally occuring site.

Using this model, Thome (8) noted that an effect of the slower bubble growth rate in binary mixtures is to decrease the inertia and drag force terms. If the drag force is considered insignificant in comparision to the inertia force, and applying the usual bubble growth law of

$$R = at^n \qquad (2.16c)$$

where a and n are empirical constants, then the bubble departure diameter, D_d, is found to be proportional to the inertia term as

$$D_d \sim \left[a^4 n(4n-1)t^{4n-2}\right]^{1/3} \qquad (2.16d)$$

Using the experimental values of a and n obtained for the nitrogen-argon system (9), Thome was able to demonstrate that the reduced inertia force term does correlate the smaller bubble departure diameters in the binary mixtures (Figure 2.5).

2.2.2 Bubble departure frequency

The bubble departure frequency, f, is defined as

$$f = 1/(t_g + t_w) \qquad (2.17a)$$

The bubble growth time, t_g, is determined by the bubble growth rate and the bubble departure diameter, which in turn is governed by forces acting on the bubble. Thome showed that the ratio of the bubble growth time in a binary mixture to that in an ideal mixture is

$$\frac{t_g}{t_{g_I}} = (N_{sn})^{2/5} \qquad (2.17b)$$

Since $N_{sn} \leqslant 1$, a shorter bubble growth time is predicted for binary mixtures.

During the departure of a bubble from a heated surface, the surrounding thermal boundary layer is stripped and must be reformed in order that the vapor embryo in the cavity can begin to grow again. This time interval is called the waiting time, t_w. Several physical parameters that can affect the waiting time are the bubble nucleation superheat required, the thermal diffusivity of the liquid mixture, and the wall superheat.

Experimental data of Thome (9) and Tolubinskiy and Ostrovskiy (5) showed that the combined effect of bubble departure diameter and frequency is to yield a lower vaporization rate and thus can partially explain the lower heat transfer rate for binary mixtures.

2.3 Bubble nucleation

In this section, the nucleation criteria for a vapor embryo trapped in a cavity on a heated wall will be discussed. Observations show that bubbles growing on a heated surface originate as minute vapor nuclei trapped in pits and cracks

on the surface. The nucleation criteria are important for two reasons. First, it is important to know the superheat temperature required for boiling to initiate. It is also important for predicting the number of boiling sites per unit area on the boiling surface.

The incipient superheat required for thermal and mechanical equilibrium for a vapor nucleus of radius r trapped in the micro-structure of a heated surface is given as

$$\Delta T_{inc} = T_{sup} - T_{sat} = 2\sigma / (r \frac{dp_{sat}}{dT}) \qquad (2.18)$$

Shock (10) has evaluated ΔT_{inc} for the binary system of ethanol-water based on equation 2.18. Comparing the calculated values with those obtained experimentally, he concluded that the wetting characteristics can be a principal parameter controlling ΔT_{inc}. The dynamic contact angle for water is about 70° but drops off toward 0° as the mole fraction of ethanol is increased (Figure 2.6). Using the model of Singh et al (11) shown in Figure 2.7, the effect of a small contact angle, θ, is to decrease the size, i.e. the radius , of the vapor nucleus trapped and hence the nucleation superheat is increased.

Recently, experiments (12) were performed with the binary systems of nitrogen-argon and ethanol-water and the results supported Shock's claim concerning the importance of the wetting characteristic on boiling incipience. Both

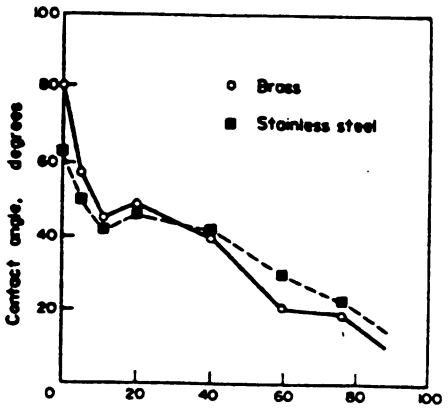

Ethanol, % mass

Figure 2.6 Variation in the advancing contact angle with composition for ethanol-water mixtures measured by Eddington and Kenning at 20 °C against nitrogen gas. Reference 26

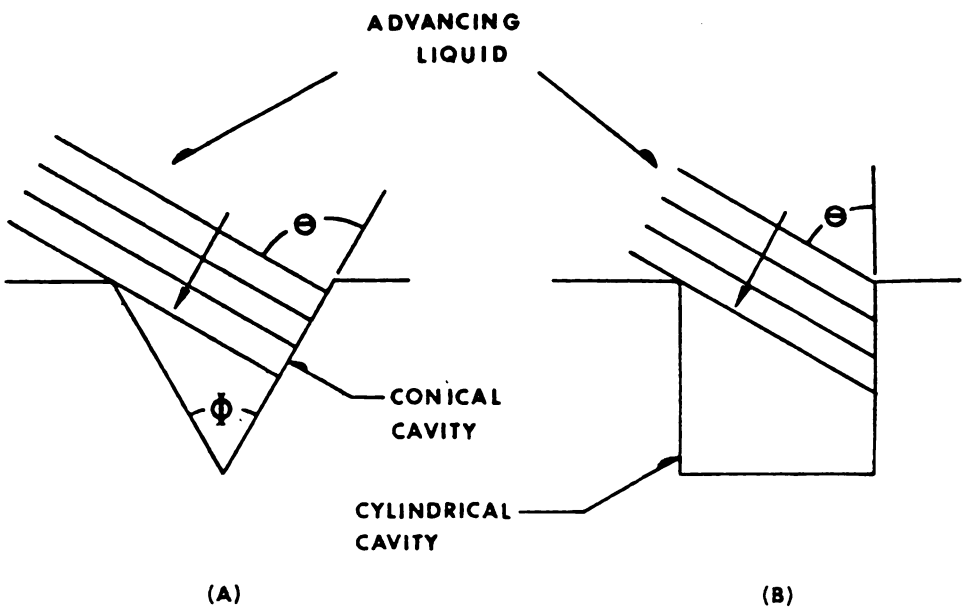

Figure 2.7 Vapor trapping model of Singh et al. (11) for (a) a conical cavity (b) a cylindrical cavity.

experiments were carried out to determine the effect of composition on boiling incipience and boiling site deactivation. In the experiments with liquid nitrogen-argon mixtures, no change was observed in the incipient superheat as a function of composition. Furthermore, the deactivation superheat coincided in value with the incipient superheat. In choosing the nitrogen-argon system, it was known a priori that no large variation in σ , dp_{sat}/dT, or contact angle occurred. Therefore no significant variation in the incipient superheat was expected. The solid line in Figure 2.8 depicted theoretical value from equation 2.18 for ΔT_{inc} based on values of σ , dp_{sat}/dT, and a vapor radius value of 1.0 μm. The deviation of the experimental value from the theoretical value might be due to a smaller contact angle for nitrogen.

A large variation in ΔT_{inc} was obtained for the ethanol-water binary system. This was expected since large variations in the values for σ and contact angle exist for this system. The results are shown in Figure 2.9. A maximum value of $44^{\circ}C$ was found for the mixture at a mole fraction of about 0.5. Again, the solid line gives the value of ΔT_{inc} calculated by using equation 2.18 and a vapor nucleus radius of r. A large discrepancy is noted.

By substituting their experimental values of ΔT_{inc} into equation 2.18, Thome et al (12) obtained the calculated values of the vapor nucleus radii (Figure 2.10). The large decrease in the radius can be explained by the rapidly decreasing value of the contact angle as the mole fraction

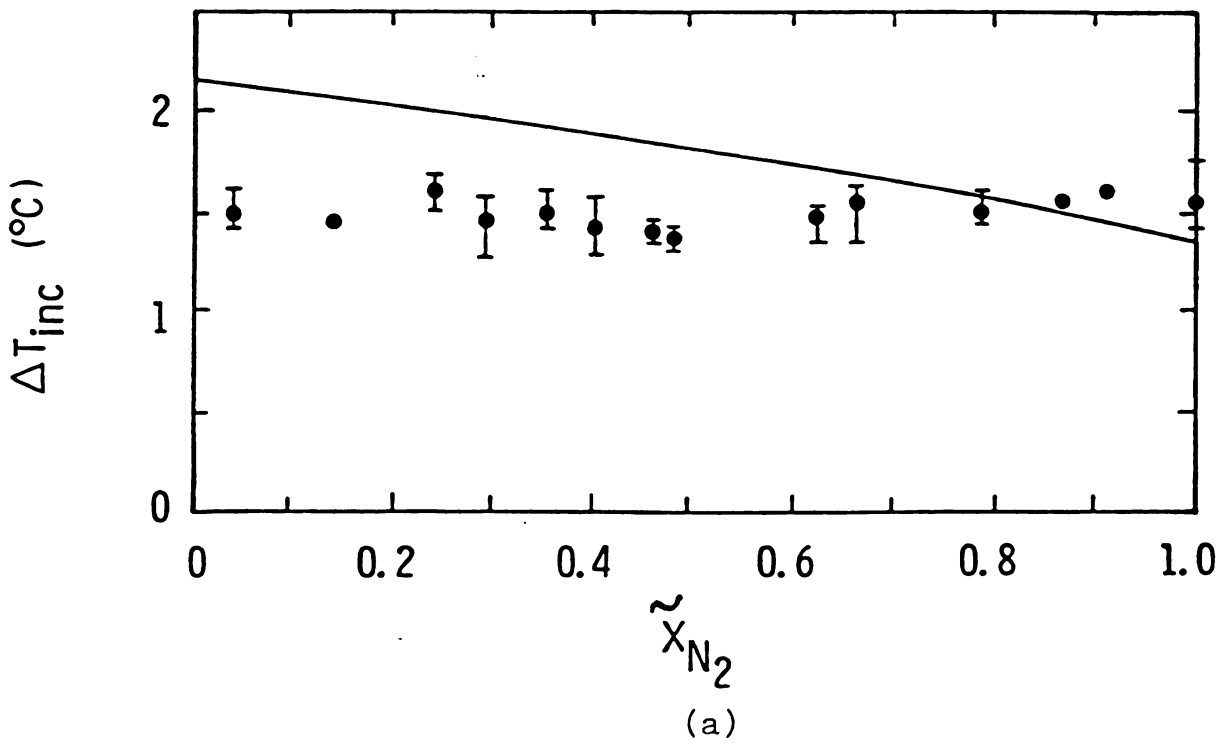

(a)

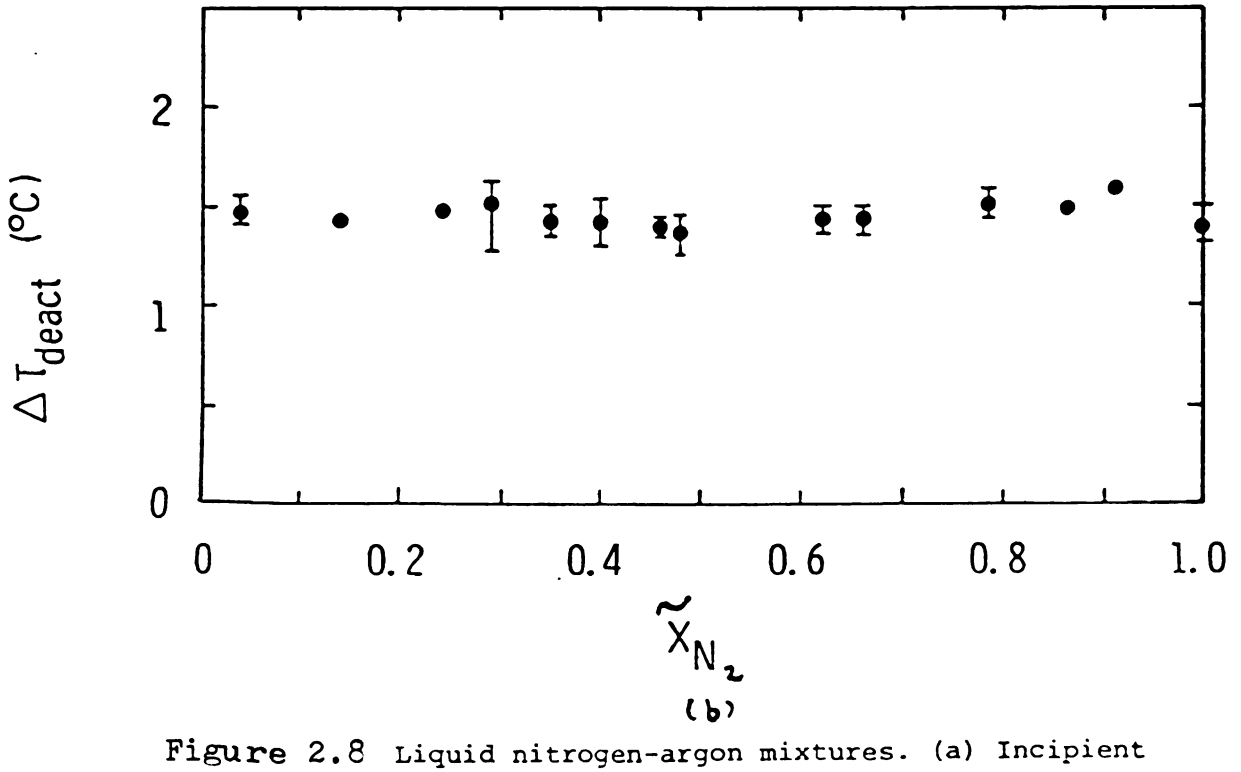

(b)

Figure 2.8 Liquid nitrogen-argon mixtures. (a) Incipient superheats; (b) Deactivation superheats.

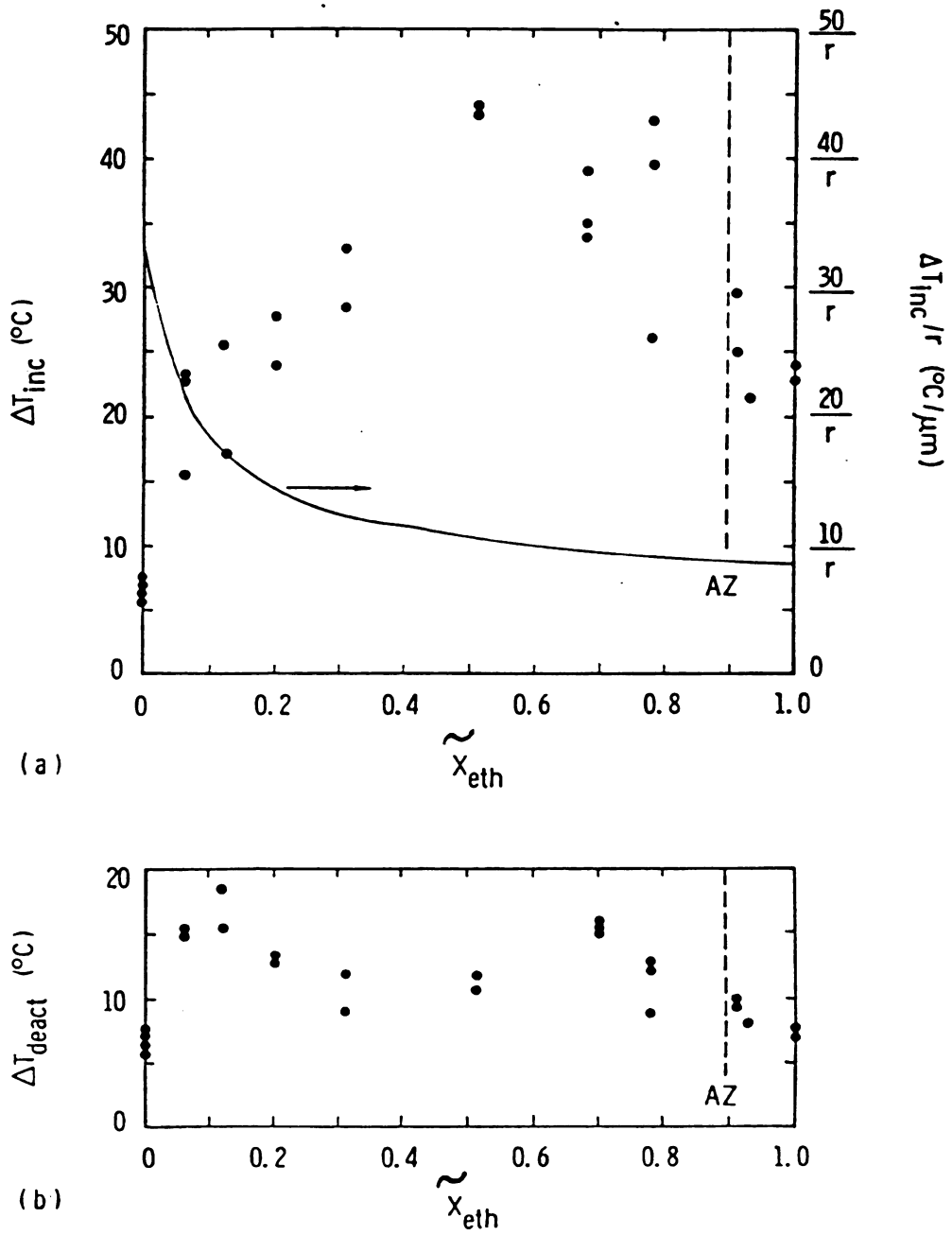

Figure 2.9 Ethanol-water mixtures (a) Incipient superheats; (b) Deactivation superheats.

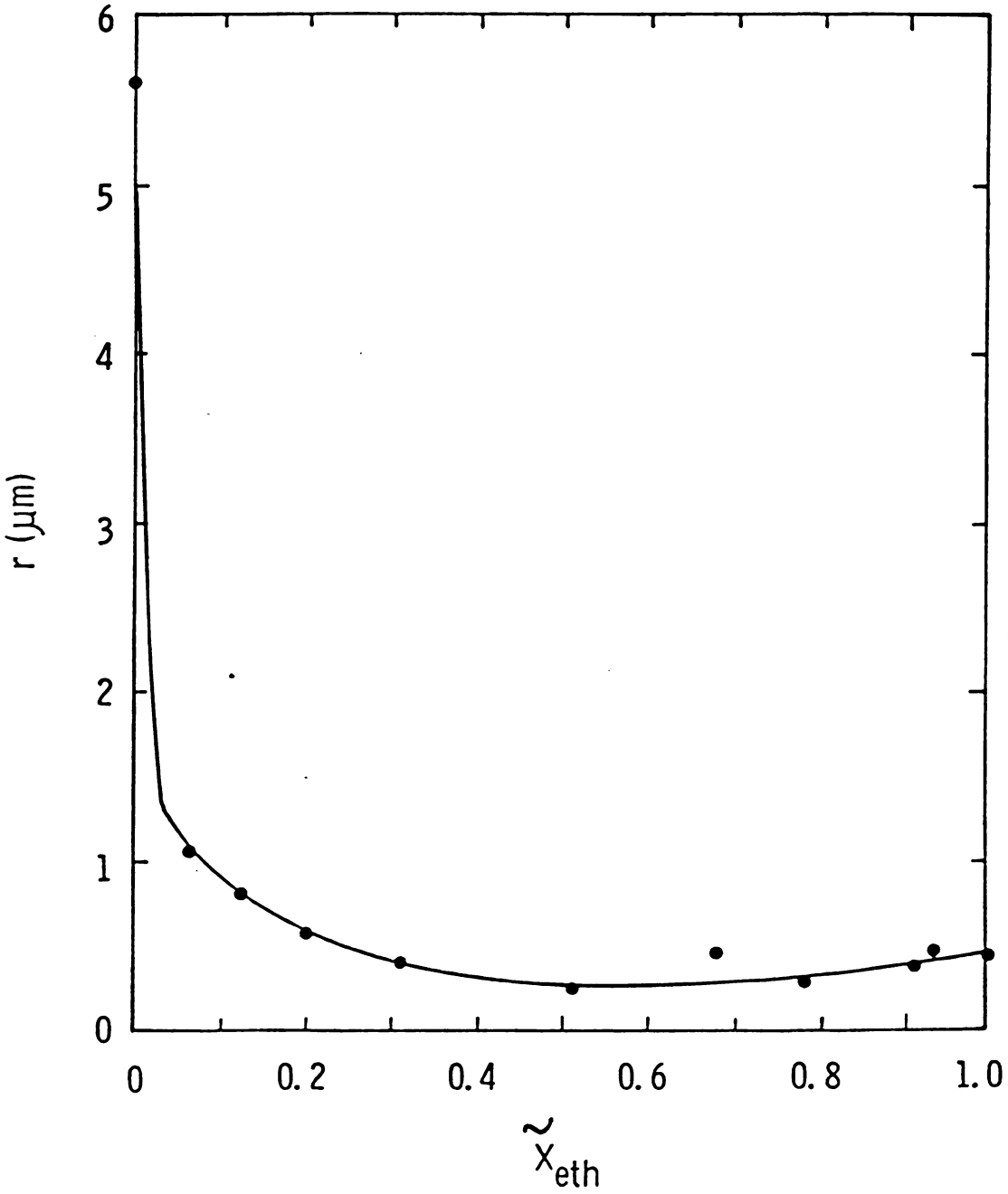

Figure 2.10 Calculated vapor nucleus radius vs. mole fraction ethanol.

of ethanol in the mixture is increased.

Equation 2.18 was derived for the case of a vapor nucleus surrounded by superheat liquid of constant temperature. For a vapor nucleus growing on a heated surface, it is surrounded by a thermal boundary layer with a temperature gradient. Recognizing the significance of the temperature gradient in the thermal boundary layer when the height of the vapor nucleus is comparable to the thickness of the thermal layer led several investigations (13,14,15,16) to develop more detailed corrections for $\Delta T_{inc.}$

The analysis of Hsu (14) can be divided into two parts. First, it is important to know the temperature profile within the thermal boundary layer. Secondly, a new criterion for nucleation must be defined. Hsu approximates the problem of the thermal boundary layer as one of one-dimensional transient conduction of heat into a slab. The thickness of the slab is a parameter called δ. Beyond the slab, the turbulent agitation is so strong that the temperature is essentially at the bulk temperature, T_b. At steady state, the temperature profile within δ is linear.

To establish the criterion for the initiation of bubble growth, Hsu argues that it is necessary for the thermal layer surrounding the bubble nucleus to be at a temperature equal to or greater than the temperature of the bubble nucleus in order to give an inward flow of heat through the bubble interface to provide the latent heat of vaporization. But the temperature of the vapor bubble is

defined previously as T_{sup} and given by equation 2.18 as

$$\Delta T_{inc} = T_{sup} - T_{sat} = 2\sigma/(r \frac{dp_{sat}}{dT}) \qquad (2.18)$$

The temperature of the thermal layer at the top of the bubble must be equal to or greater than T_{sup}. The results of Hsu's analysis can be summarized as follows:

1. Given a wall temperature, there are an upper limit and a lower limit for the vapor nucleus radii for nucleation to occur. Equation 2.18, on the other hand, has a lower limit only.

2. For a given vapor nucleus of radius r, Hsu's value for ΔT_{inc} is higher than that given by equation 2.18.

3. Hsu's analysis points to the importance of the thermal boundary layer in understanding incipience. It is important to know the temperature profile as well as its thickness.

2.4 Temperature profile of the thermal boundary layer adjacent to a heated surface during nucleate pool boiling

The thickness of the superheated boundary layer adjacent to the heating surface and the temperature profile within it have long been recognized as significant parameters in nucleate boiling. It is this highly superheated region which is responsible for the origin and growth of a vapor

bubble. To a large degree, the thickness of this region and its temperature distribution control the growth rate of a vapor bubble as well as its departure size. In addition, these parameters play a significant role in determining the size range of active cavities on a given surface.

Several experiments were carried out to measure the temperature profiles within the thermal boundary layer (17, 18, 19). Marcus and Dropkin (17) used thermocouple junctions with a diameter of less than .002 in. (.0051 cm) in their experiments with water. Their results showed that the temperature profile is linear very near the heating surface. The linear region of the temperature profile exhibited similarity with respect to the "extrapolated superheat-layer thickness", δ, regardless of the heat flux applied. That is, for all of their data, the temperature profile from the wall to about $0.57\,\delta$ is given as

$$\frac{T - T_b}{T_w - T_b} = 1 - \frac{y}{\delta}, \qquad 0 \leq y \leq 0.57 \qquad (2.19)$$

For the region above $0.57\,\delta$, the temperature profile is expressed in the form of

$$\frac{T - T_b}{T_w - T_b} = C(y/\delta)^{-n} \qquad (2.20)$$

where n and C are functions of the heat flux applied. The

"extrapolated superheat-layer thickness", δ , is defined as the height of the intersection between the tangent to the temperature profile at the surface and the constant liquid bulk temperature line. Figure 2.11 is an example of their result.

The value of δ , which is a measure of the super-heated region adjacent to the surface, appears to be primarily a function of the heat transfer coefficient. The experimental results of Marcus and Dropkin were satisfactorily correlated in the form

$$\delta = C_i h^d \qquad (2.21)$$

where C_i and d are functions of the liquid and the surface used. It should be noted that the instantaneous temperature at any point in the superheated boundary layer is a widely and rapidly fluctuating variable. The amplitude of these fluctuations varies with the height above the boiling surface. It reaches a maximum value a small distance from the surface and decreases to a very small value as it approaches the surface. Thus the surface appears to act as a smoothing agent inhibiting the agitation in the liquid. Similar results were obtained for water, Freon-113, and methyl alcohol in the experiments performed by Lippert and Dougall (18).

Wiebe and Judd (19) carried these experiments one step further by considering the effect of subcooling on the thermal boundary layer. Their result showed that the wall

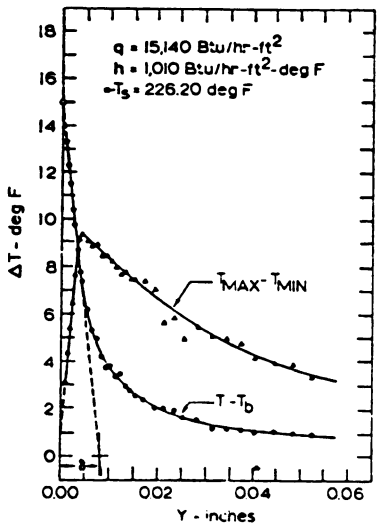

Figure 2.11 Amplitude of temperature fluctuations versus height above surface; high heat flux. Curve also shows average temperature profile and definition of extrapolated superheated layer thickness.

T_L	ΔT_2	$(T_w - T_L)$, deg F	R_{max}, in.	$R^2_{max}/(T_w - T_L) \times 10^3$	$\frac{1}{\tau}$, cycles/sec	$R^2_{max}/(T_w - T_L)\frac{1}{\tau}$
177	35	80	0.022	0.85	909	0.77
140	72	117	0.019	0.80	1100	0.88
100	112	157	0.016	0.64	1430	0.92
62	150	195	0.013	0.43	2000	0.86

Table 2.1 The influence of subcooling on the heat transferred by one bubble.

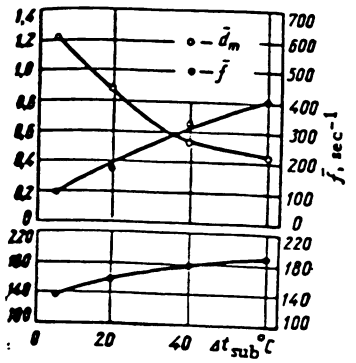

Figure 2.12 Average diameter $\bar{d}_m$, nucleation frequency $\bar{f}$ and growth rate $\overline{d_m f}$ for vapor bubbles at p= 1 bar as a function of the subcooling.

temperature is relatively insensitive to the degree of subcooling, $T_{sat} - T_b$. At a heat flux of 20,000 BTU/Hr-ft^2 (63.08 kW/m^2), the wall superheat dropped from approximately 20 °F to 10 °F (11.1 °C to 5.6 °C) while the subcooling was increased to 50 °F (27.8 °C). When the heat flux was increased to 100,000 BTU/Hr-ft^2 (315.40 kW/m^2), the wall superheat remained relatively constant at 40 °F (22.2 °C) while the subcooling was increased from 0 °F to 90 °F (0 to 50 °C). One might then conclude that the wall superheat is relatively insensitive to subcooling in the well established boiling region. The effect of less subcooling is to decrease the thickness of the extrapolated superheated-layer thickness, δ. Thus, similar boiling conditions can be brought about by independent changes in heat flux or subcooling.

2.5 The influence of subcooling on pool boiling heat transfer

It was stated earlier that given a fixed heat flux, the wall superheat, $T_w - T_{sat}$, remains essentially unchanged while subcooling may be changed by a large factor (by as much as 100 °F or 150 °F). Engelberg-Forster and Greif (20) have proposed an explanation for the apparent insensitivity of the heat transfer rate to subcooling based upon a "vapor-liquid exchange" mechanism. They postulated that the primary mechanism of nucleate boiling heat transfer is the stripping or displacement of the superheat thermal boundary layer by

the departing vapor bubble. This process may be visualized as a kind of pumping action in which a layer of hot liquid is displaced and replaced by cold liquid from the bulk.

When a bubble grows to a maximum size of R_{max}, it causes the exchange of a liquid volume proportional to $(R_{max})^3$. The rate of heat energy transferred per boiling site is then given as

$$q \sim C_p \rho_L (R_{max})^3 (T_w - T_b)/\tau \qquad (2.22)$$

where τ is the average time between each growth cycle. The insensitivity of heat flux to subcooling can be explained by combining the effects of subcooling on each of the parameters in equation 2.22. Tolubinskiy and Konstanchuk (21) and Ellion (22) performed experiments with water to study the effects of subcooling on R_{max} and τ. Ellion's experimental data are shown in Table 2.1 and those of Tolubinskiy and Konstanchuk are shown in Figure 2.12. Both data sets point to the fact that R_{max} decreases while $1/\tau$ increases as subcooling is increased. Column 5 of Table 2.1 shows that the product $R_{max}^3 \cdot (T_w - T_b)$ decreases as subcooling increases, despite the fact that higher subcooling increases the total temperature difference between the heating surface and the bulk liquid. Column 7 depicts the heat transfer rate per boiling site. By comparing column 7 with column 2, it is seen that while subcooling was changed by more than 400 percent, the product appearing in equation 2.22 changed only by about 15%, an insignificant variation in view of experimental accuracy.

The analysis of Engelberg-Forster and Greif (20) has some drawbacks. The volume of the hot liquid displaced is more accurately described as being proportional to $(KR_{max})^2 \delta$, where δ is the thickness of the thermal boundary layer. K is a factor multiplying R_{max} to give the area of influence in the liquid by the bubble. K, intuitively, will depend upon factors such as the viscosity of the liquid, the bubble growth rate, the velocity at the moment of departure, and the boiling site density on the heating surface. They failed also to consider that the boiling site density might be affected by the change in subcooling.

Fand and Deswani (23) performed a detailed study on the effect of subcooling on the wall temperature of a heating surface. Their results are shown in Figure 2.13. Figure 2.13 is a plot of the surface temperature, T_s, as a function of the bulk temperature of the liquid, T_b. At a given heat flux, T_s possesses a maximum, which occurs at progressively higher degrees of subcooling with increasing heat flux. Table 2.2 gives the calculated values for the heat transfer coefficient as a function of subcooling (note that $T_s = T_w$). The heat transfer coefficient, h, is defined as

$$h = q/(T_w - T_b) \qquad (2.22a)$$

Sultan and Judd's (24) experimental results on the effect of subcooling on the wall temperature, boiling site density, and average bubble frequency are shown in Figures 2.14, 2.15, and 2.16. Figures 2.14 and 2.15 suggest a

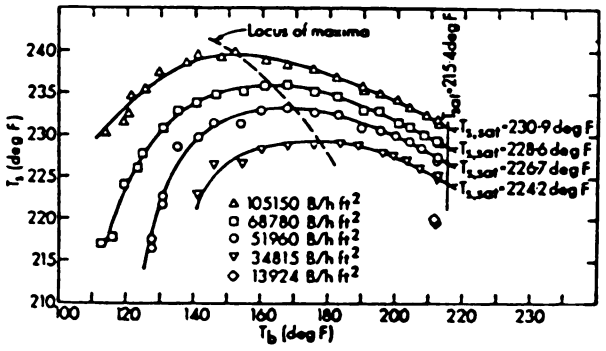

Figure 2.13 Experimental boiling heat transfer data for a horizontal stainless steel cylinder (Dia. = 0.4555 in.) immersed in water.

Table 2.2 Effect of subcooling on heat transfer coefficient (Calculated from figure 3 of Fand and Keswani (22))

1	2	3	4	5
q (BTU/ Hr-ft^2)	T_w (F)	T_b (F)	$T_{sat} - T_b$ (F)	h (BTU/ Hr-ft^2-F
51960	226.7	212	0	3535
51960	228.6	204	8	2112
51960	230.9(max)	190	22	1270
51960	230.9	142	70	584
51960	228.6	136	76	561
51960	226.7	132	80	548
51960	224.2(min)	129	83	545

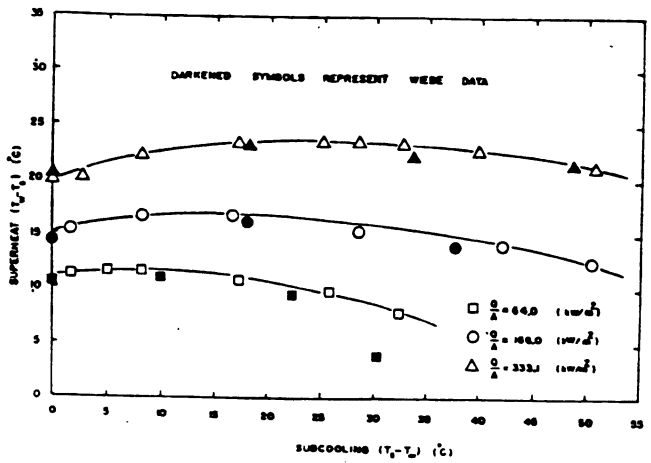

Figure 2.14 Variation of surface-heat with bulk subcooling.

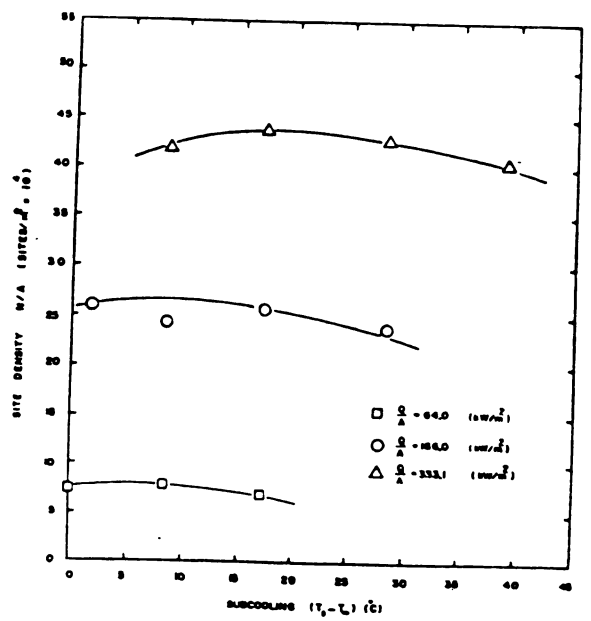

Figure 2.15 Variation of active site with bulk subcooling.

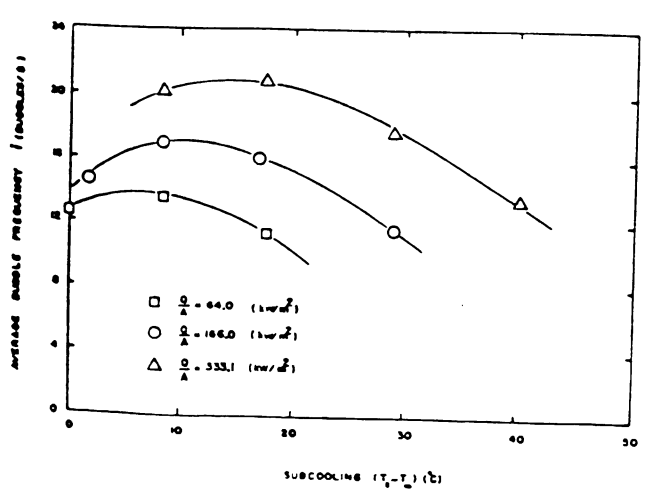

Figure 2.16 Variation of average bubble frequency with bulk subcooling.

direct dependence of site density upon the wall temperature. Contrary to the results of Tolubinskiy and Konstanchuk (21) and Ellion (22), Sultan and Judd's data showed a maximum in the average bubble frequency when plotted against subcooling.

Chapter 3

Experimental Design and Procedures

3.1 Experimental Design

All experiments were performed at the Boiling Heat Transfer Laboratory at Michigan State University. This section describes the experimental design and set up.

3.1.1 Heating surfaces

Two different heating test surfaces made of brass were used in performing the boiling experiments for the two binary systems. At the beginning of each trial, the test surface was prepared by rubbing the heating test section with a fine emery paper (silicon carbide 320) and then finished with a crocus cloth. It should be noted also that a circle with a diameter of 19.1 cm is inscribed on the test section. In the counting of the site density, only bubbles inside this circle are considered. Surface no. 1 (see Figure 3.1) was used for mixtures of ethanol and water. The outer section of the test surface was made very thin (0.4 mm) to minimize the conduction heat loss in the radial direction. Therefore, the major portion of thermal energy is transferred through

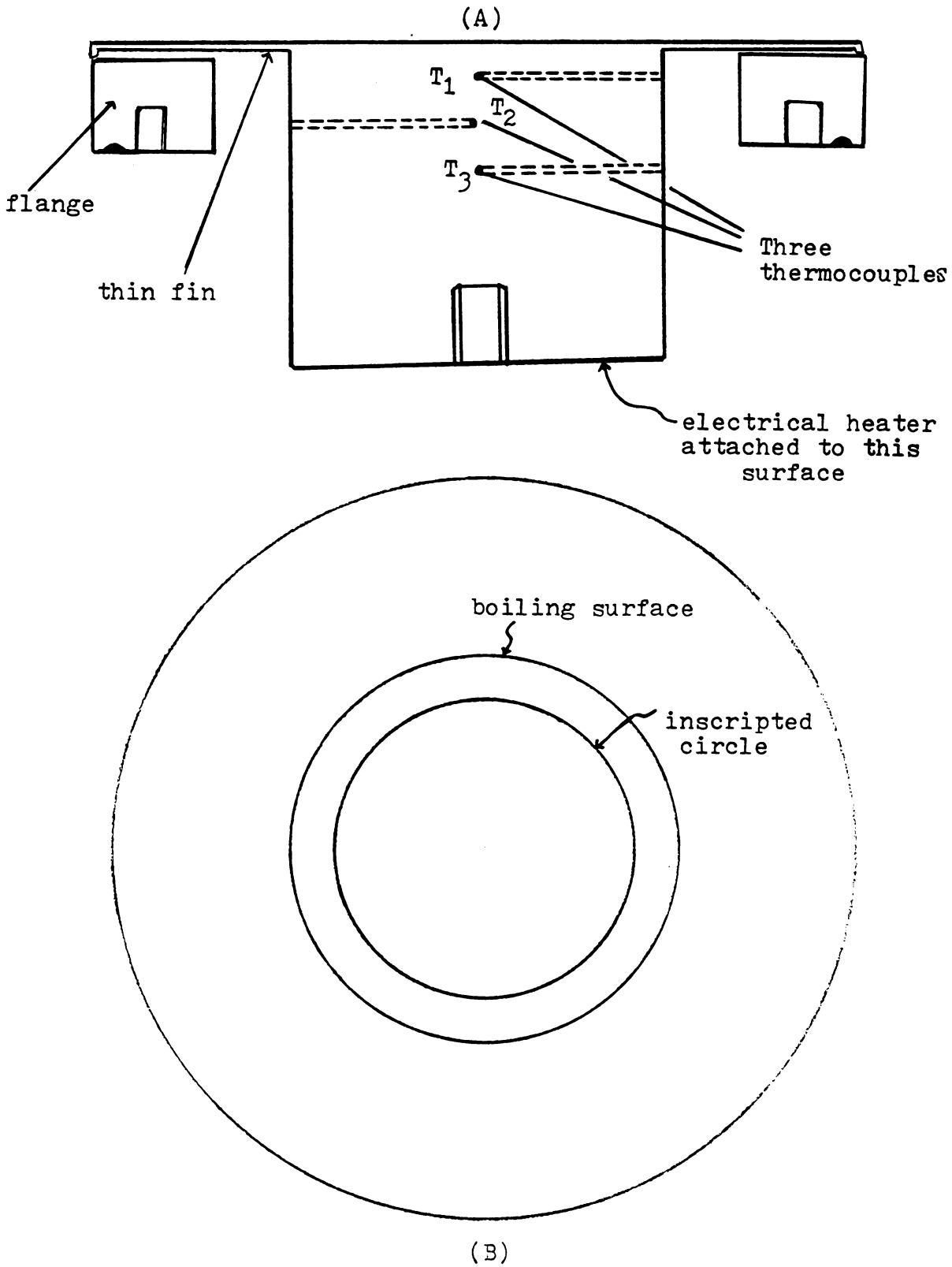

Figure 3.1 Test surface no. 1; (A) SIDE VIEW, (B) TOP VIEW

the midsection since the boiling heat transfer rate on the inner section is much higher than the heat transfer rate by natural convection on the outer section. An adhesive with high temperature resistance and low thermal conductivity was used to attach a circular ring to the bottom of the thin section of the test surface. The ring is in turn screwed to a cylindrical shell (see Figure 3.2).

When surface no. 1 was used for ethanol-benzene mixtures, it was discovered that the mixtures chemically attack the adhesive used, thus creating a leakage problem. For the mixtures of ethanol-benzene, surface no. 2 (Figure 3.3) was used instead. The surface is screwed directly to the cylindrical shell.

The bottom of the test surface, as shown in Figure 3.2, is fastened to an electrical heater by means of a screw. A high thermal conductivity grease is used to lower the thermal contact resistance between the bottom of the test surface and the heater. The heater was specially designed and built with a nichrome heating filament. Its resistance is about 1.4 ohms. The maximum current used in the experiments is about 12 amperes.

3.1.2 Electrical circuit for surface heater

To measure the total heat flux passing through the test surface, it is necessary to know the current and voltage across the heater filament. Section 3.2.3 presents a more

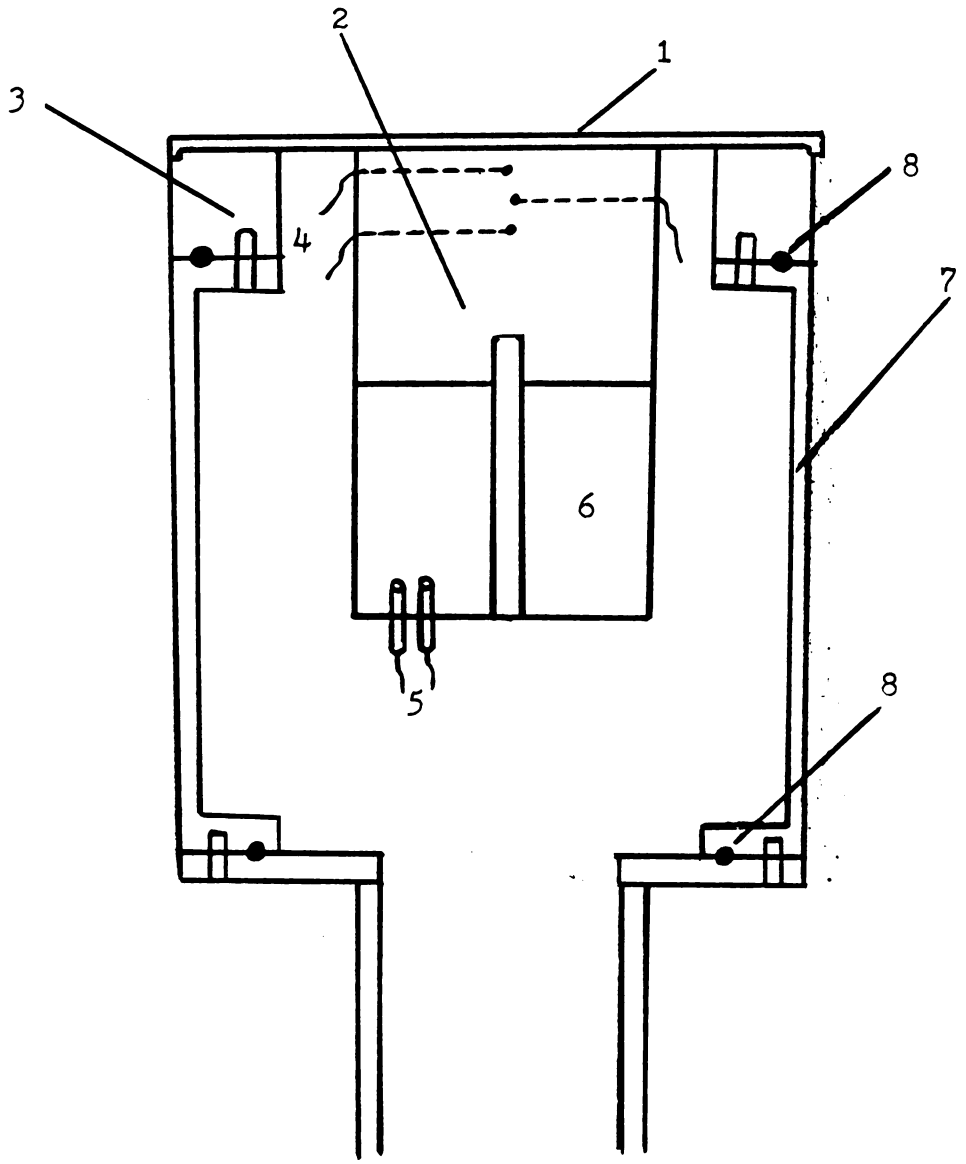

Figure 3.2 Boiling surface set-up (legend; 1-test surface, 2-test surface base, 3-circular ring attached to the test surface using low conductivity adhesive, 4-thermocouple wire, 5-power lead for electric heater, 6-electric heater, 7-cylindrical shell, 8-o-rings)

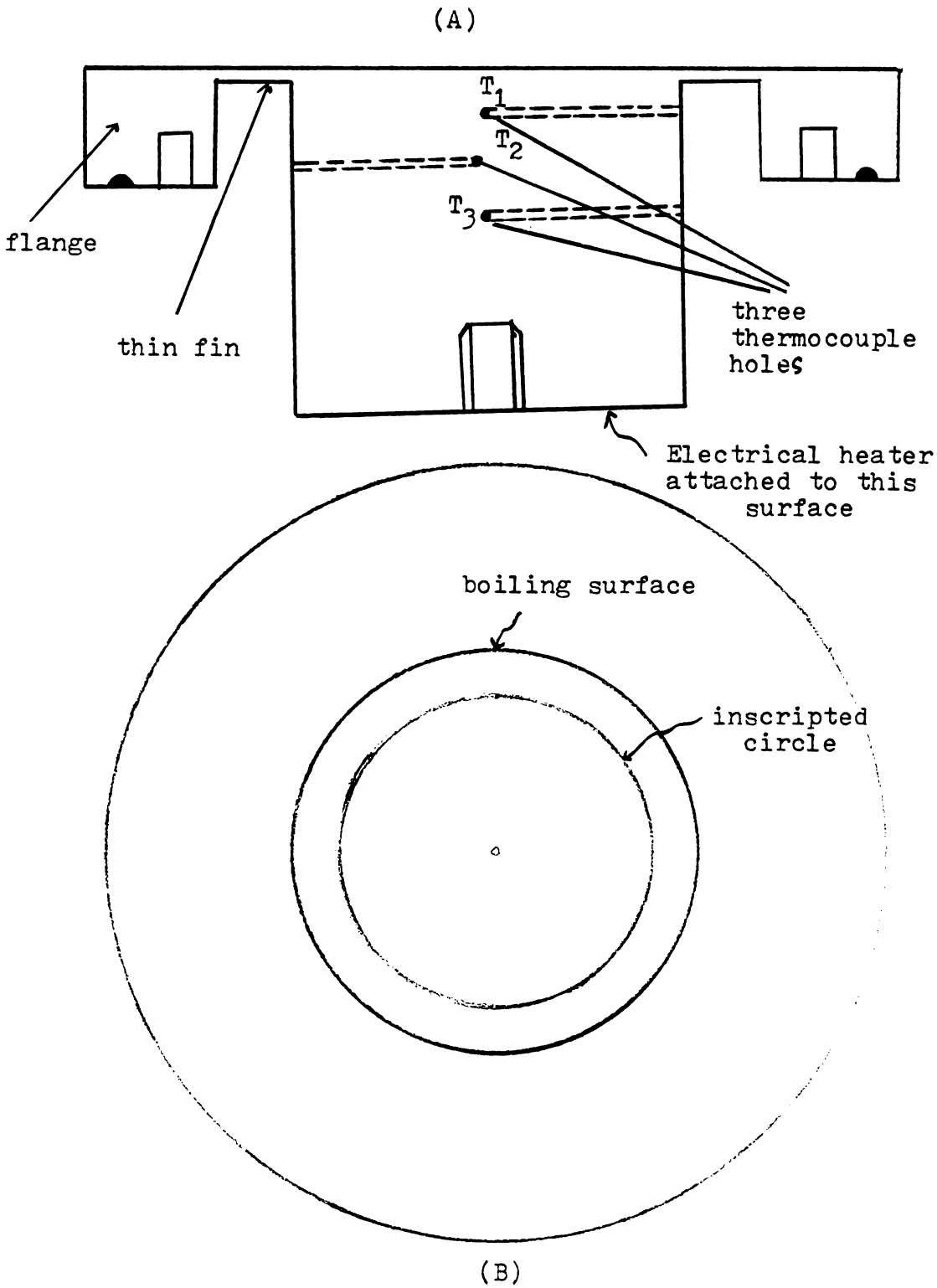

Figure 3.3 Test surface no. 2; (A) side view, (B) top view

detailed description on the conversion of the power of the heater into heat flux for the heating surface. Figure 3.4 is a schematic diagram of the circuitry for the surface heater.

Two voltage measurements are made by a digital multimeter. The first measurement gives the voltage across the heater itself. A shunt with a known resistance of 1 m $\pm$ 1% is used to indirectly measure the current passing through the heater. By measuring the voltage across the shunt, one can obtain a value for the current by dividing the voltage by the known resistance of 1 mΩ. The power is then given as:

Power = (Voltage across heater) X (current) (3.1)

3.1.3 Description of experimental rig and overall set up

A schematic diagram of the boiling rig is shown in Figure 3.5. The vessel is a 1/4 inch (6.4 mm) thick stainless steel cylinder cross (4 inches in internal diameter) with flanged ends. To maintain the desired temperature and pressure inside the vessel, a proportional temperature controller connected to an immersion heater and a condenser using water as coolant are used. The test surface is mounted vertically, facing a sight glass window.

For all of the test trials, it is desired to maintain the pressure inside the vessel at 14.7 p.s.i.a. (1.01 bar). In cases where subcooling is maintained in the bulk liquid,

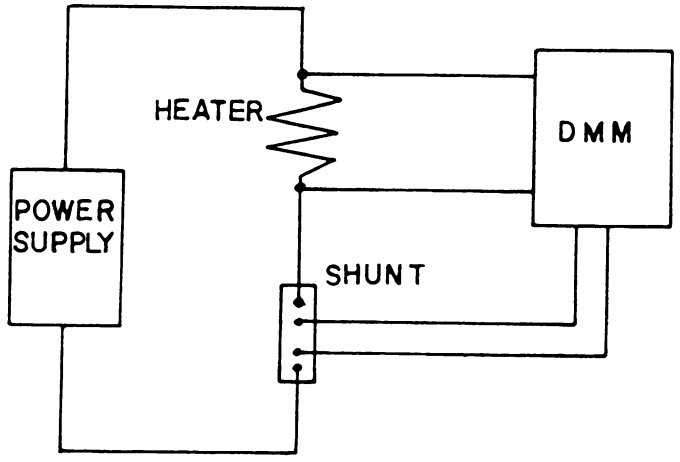

Figure 3.4 Power supply circuit

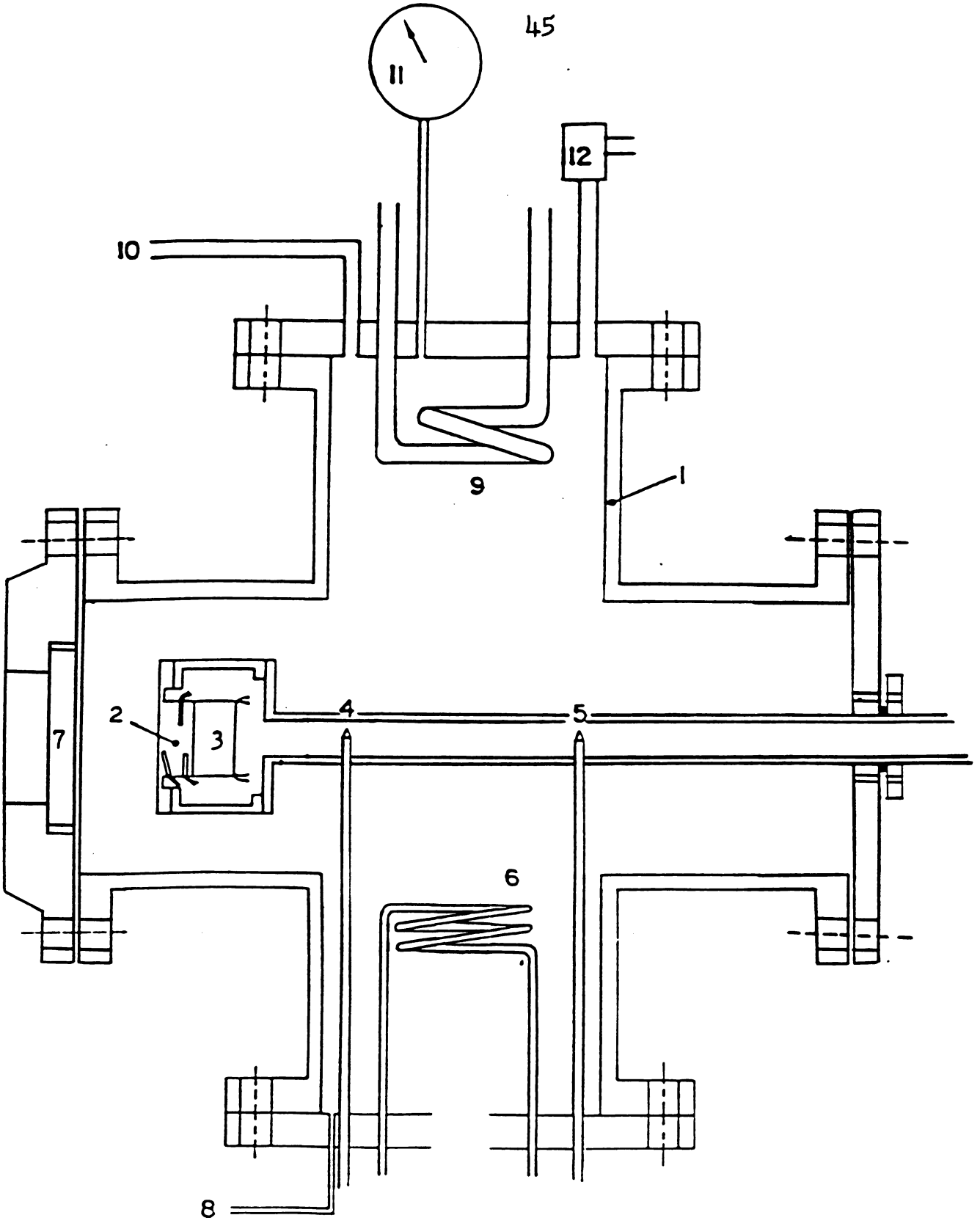

Figure 3.5 Nucleate pool boiling rig (1-stainless steel vessel, 2-test surface, 3-electric heater, 4-bulk liquid thermocouple, 5-temperature controller thermocouple, 6-immersion heater, 7-sight glass windows, 8-liquid fill line, 9-condenser, 10-valve to vacuum pump/atmosphere, 11-pressure gauge, 12-safety relief valve.

nitrogen gas is fed into the vessel at the valve located at position 10 of Figure 3.5. A system of pressure regulators is used so that the pressure is maintained at 14.7 ± .3 p.s.i.a. (1.01 ± 0.02 bar). Figure 3.6 shows the overall set up for the experiments.

3.1.4 Temperature measurement

Copper-constantan thermocouples and digital temperature indicators are used for temperature measurements. The estimated maximum error for each measurements is ± 0.2 °C. Two thermocouples (at positions 4 and 5 in Figure 3.5) are used to measure the bulk temperature of the liquid. One of these measurements is interfaced with the temperature controller and the other with a digital temperature indicator. Three thermocouples are embedded at three different locations of the heating surface and their temperatures are read from another digital temperature indicator. The two digital temperature indicators are calibrated to agree with each other. The temperatures of the test section are used to extrapolate the wall temperature (see section 3.2.3) of the heating surface.

3.2 Experimental procedure and calculations

The purpose of this study is to investigate the effect of heat flux, composition, and degree of subcooling on the

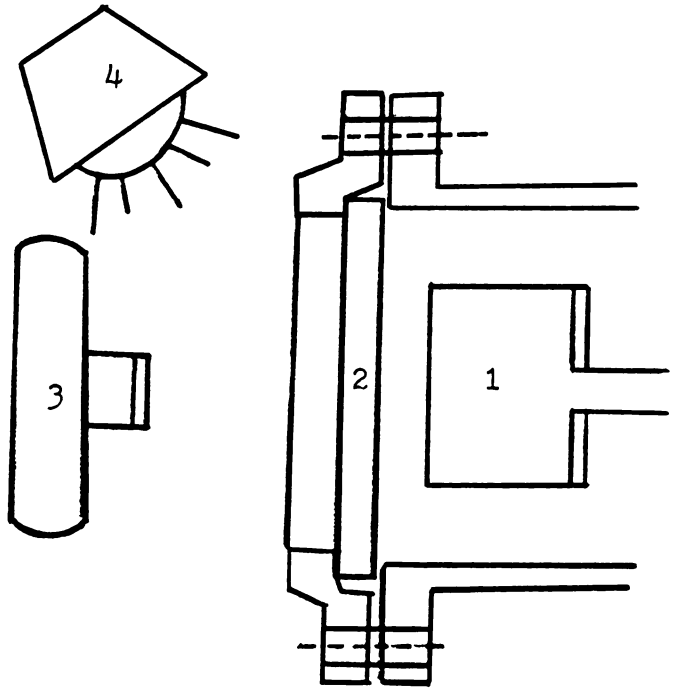

Figure 3.6 : Experimental set-up (legend; 1-boiling surface, 2-viewing window, 3-camera, 4-lighting)

boiling site density and the boiling heat transfer coefficient of binary mixtures. Also, qualitatively at least, a fundamental relationship between the boiling site density and the boiling heat transfer coefficient is being sought. Two binary mixture systems were chosen : ethanol-water and ethanol-benzene. As mentioned in Chapter 1, it is known a priori that a large variation in the dynamic contact angle existed for the ethanol-water binary system. This variation is thought to be less significant for the ethanol-benzene system. Therefore, it is hoped that the experimental results of site density from the mixtures will help us to understand the importance of the dynamic contact angle on the site density.

Table 3.1 lists the compositions, heat fluxes, and subcoolings used in the experiments. Appendix A gives a summary of the procedure used to prepare a mixture of the desired composition. The following is an outline of the steps used in the experiment.

3.2.1 Experimental procedure

(1) The prepared mixture is fed into the vessel gradually (to minimize air bubble formation) until the level of the liquid is about 14 cm above the heating surface.

(2) The temperature controller for the bulk liquid is set to the saturation temperature corresponding to 14.7 p.s.i.a. (1.01 bar). The sytem is closed to the

Table 3.1 Experimental conditions; mixture composition, heat fluxes, and subcooling.

(A)

Mixture composition: Mole fraction of ethanol

Ethanol-water	Ethanol-benzene
0%	0%
15.00%	15.00%
28.67%	30.00%
49.04%	45.00%
60.00%	65.00%
70.00%	80.00%
80.00%	100.00%
89.40%	

(B)

Heat fluxes tested (kW/m^2)
97.39
74.62
55.48
38.54
24.41
13.74

(C)

Degree of subcooling, °C
0 C
5 C
10 C
15 C
20 C

atmosphere, but the excess pressure caused by the degassing process is released periodically.

(3) The experiment is ready to start when the saturation condition is reached. At this point , the liquid has been degassed.

(4) The power to the surface heater is turned on and increased gradually to give a heat flux of about 150 kW/m^2 in the inner section of the heating surface. This ensures that boiling is taking place and that all the possible boiling sites are activated. Boiling continues for approximately 5 minutes to achieve steady state condition.

(5) The power to the surface heater is then lowered to the desired level. A period of time is allowed for the system to reach a steady state condition. The temperatures (T_b, T_1, T_2, T_3) are then recorded and photographs of the boiling surface taken.

(6) Step 5 is repeated for the five other heat fluxes. (See Table 3.1 for a list of heat fluxes tested)

(7) The bulk temperature setting on the temperature controller is then lowered to the degree of subcooling desired. The system is allowed to reach the desired **bulk temperature.** At this point, the pressure is lower than 1.01 bar. Nitrogen gas is then fed into the system to make up for the pressure difference.

(8) Steps 4,5, and 6 are repeated for each subcooling condition. (See Table 3.1 for the different degrees

of subcooling tested.

(9) At the end of each experiment a sample of the mixture is taken from the vessel and its density measured at ~20°C to ensure that its composition remained the same. The heating surface is cleaned with crocus cloth to eliminate surface aging as a factor in the experiment.

3.2.2 Determining the boiling site density

Three photographs are obtained for each set of experimental conditions, i.e., mixture composition, heat flux, and degree of subcooling. For each active boiling site on the heating surface, the boiling cycle can be divided into the bubble growth time and the waiting time. During the waiting time, the thermal layer above the surface is being heated by transient heat conduction until it reaches a temperature high enough to reactivate the boiling site as defined by the nucleation criteria. Since the vapor nucleus is too small to be seen in the photograph, a counting of the boiling site density from any single photograph would underestimate the actual number of active sites. Therefore, a scheme is used to reduce this error in the counting procedure.

During the counting of each photograph, a piece of paper is placed directly underneath the photograph. The counting is done by punching a tiny hole in the center of the bubble. Thus the location of the boiling site is also recorded on

the piece of paper. This procedure is repeated for the two other photographs and in this manner the boiling sites of the three photographs are superimposed on the paper. The boiling site density is then obtained by counting the holes on the paper, which gives a better estimate of the actual boiling site density.

3.2.3 Calculation for heat transfer coefficient

The heat transfer coefficient is defined as:

$$h = q/(T_w - T_b)$$

(Note that several previous experimental studies have used T_{sat} instead of T_b in the definition of h) In the next two sections, calculation procedures for determining the heat flux through the boiling surface area, q, and the wall temperature will be discussed.

Heat flux through the boiling surface area

As mentioned earlier in Section 3.1.1, the heating surface has a total diameter of 2 inches (5.08 cm). The total area of this surface can be thought of as being two separate regions: a boiling heat transfer region and a natural convective heat transfer region. For our calculations, all the heat energy generated by the surface heater is assumed to pass through the heating surface . In order to obtain the heat flux through the boiling area (inner region with a diameter of 2.54 cm), heat loss by natural convection in the

outer region must be subtracted from the total heat transfer rate. It should be noted that the distinction of the two heat transfer mechanisms on the two regions is justified by experimental observations made on the heating surface.

The heat loss to the outer region is calculated by assuming it to be a case of heat transfer by conduction through a circumferential fin of rectangular profile. The heat which is conducted through the circumferential fin is removed by natural convection to the bulk liquid. For detailed discussion of this calculation, see Appendix B.

Heat losses through the fin ranged from 8% to about 65% depending upon the experimental conditions, i.e., this heat loss is more significant at low heat flux and high subcooling. The actual heat flux through the boiling test section is then adjusted appropriately in the calculation for the heat transfer coefficient.

Other designs incorporating an insulating material rather than the metallic fin could have been used to reduce heat losses but bubbles formed at the joint would have adversely affected the boiling site density measurements.

Wall temperature

Three thermocouples were placed at different distances underneath the heating surface. The heat energy generated by the electric heater is conducted to the test surface through a circular base located at its bottom (see Figures 3.1 and 3.3). Inside the cylindrical shell (Figure 3.2), it is assumed that the energy loss by natural convection to

air is insignificant. Thus the temperature profile along the length of the circular base is assumed to be linear and the wall temperature can be extrapolated by measurement of T_1, T_2, and T_3. However, two problems were encountered: (1) the temperature profile in the region between T_2 and T_3 is not quite linear due to the shape effect of the electric heater bolt hole, and (2) occasionally, a loose contact exists between the junction of the thermocouple and the point of temperature measurement in the cylindrical rod. The first problem is eliminated by using only T_1 and T_2 in extrapolating the wall temperature, T_w. The temperature profile of T_1, T_2, and T_3 is checked qualitatively to ensure that the junctions are in good contact with the wall of the drilled holes in the circular base.

Chapter 4

Results and Discussion

Experimental results are presented and discussed in this chapter. Seventeen experimental runs were performed: 10 experiments for ethanol-water mixtures and 7 experiments for ethanol-benzene mixtures. Experiments for two compositions of ethanol-water mixtures (at 70% and 80% mole fraction ethanol) were repeated and the results were consistent with each other. A tabulated form of all experimental data is presented in Appendix C. In the following sections, different aspects of the results are organized by presenting them in graphical form. Specifically, the effects of compositions, subcooling, heat flux, and wall temperature on boiling site density are examined. Presented also are plots of the heat transfer coefficient as a function of composition and the heat transfer coefficient as a function of subcooling. Finally, ratios of (h_{exp}/h_I) and (experimental boiling site density/ ideal boiling site density) at constant heat flux are plotted against mixture composition. The ideal quantities are defined by an ideal linear mixing law. An example showing the value of h_{exp} and h_I for ethanol-benzene mixtures is shown in Figure 4.0. Note that h_I is the ideal heat transfer coefficient calculated by using an ideal linear mixing law,

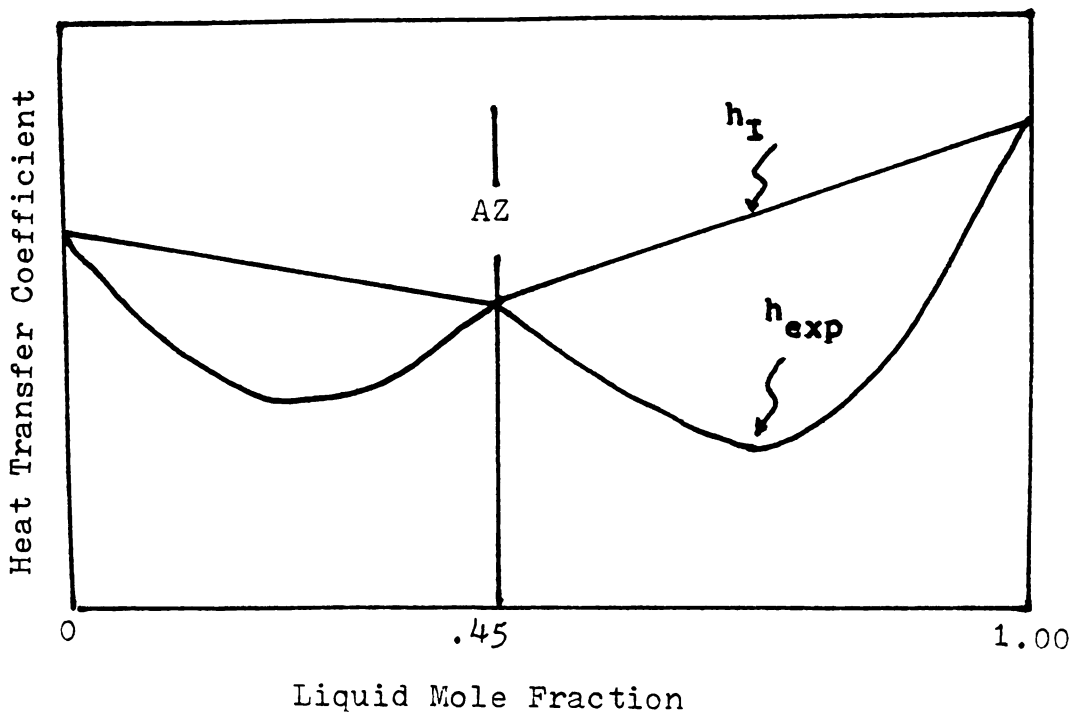

Figure 4.0 Definition of a linear mixing law for the azeotropic ethanol-benzene system

i.e. for $0 \leq \tilde{x} \leq \tilde{x}_{az}$

$$h_I = \frac{\tilde{x}}{\tilde{x}_{az}} \, h_{exp}\Big|_{\tilde{x} = \tilde{x}_{az}} + \frac{\tilde{x}_{az} - \tilde{x}}{\tilde{x}_{az}} \, h_{exp}\Big|_{\tilde{x} = 0} \qquad (4.1)$$

and $\tilde{x}_{az} \leq \tilde{x} \leq 1$

$$h_I = \frac{\tilde{x} - \tilde{x}_{az}}{1 - \tilde{x}_{az}} \, h_{exp}\Big|_{\tilde{x} = 1} + \frac{1 - \tilde{x}}{1 - \tilde{x}_{az}} \, h_{exp}\Big|_{\tilde{x} = \tilde{x}_{az}} \qquad (4.2)$$

4.1 Heat transfer coefficient vs. mixture composition

4.1.1 Ethanol-water mixtures

Figures 4.1, 4.2, 4.3, and 4.4 are graphs of the experimental heat transfer coefficient plotted against mixture composition for the ethanol-water system. For each heat flux used, five different levels of subcooling were maintained in the bulk liquid. The negative deviation of the actual heat transfer coefficient from that calculated by a linear mixing law is conclusive for high heat fluxes and low subcoolings. The minimum point for most of the curves occurs in the vicinity of about 30% mole fraction of ethanol. For the mixture composition of 30% ethanol at a heat flux of 97.39 kW/m^2 and 0 °C of subcooling, the predicted heat coefficient from a linear mixing law is calculated to be about 8.0 kW/m^2 °C. The experimental value is 3.9 kW/m^2 °C, a 51%

Figure 4.1

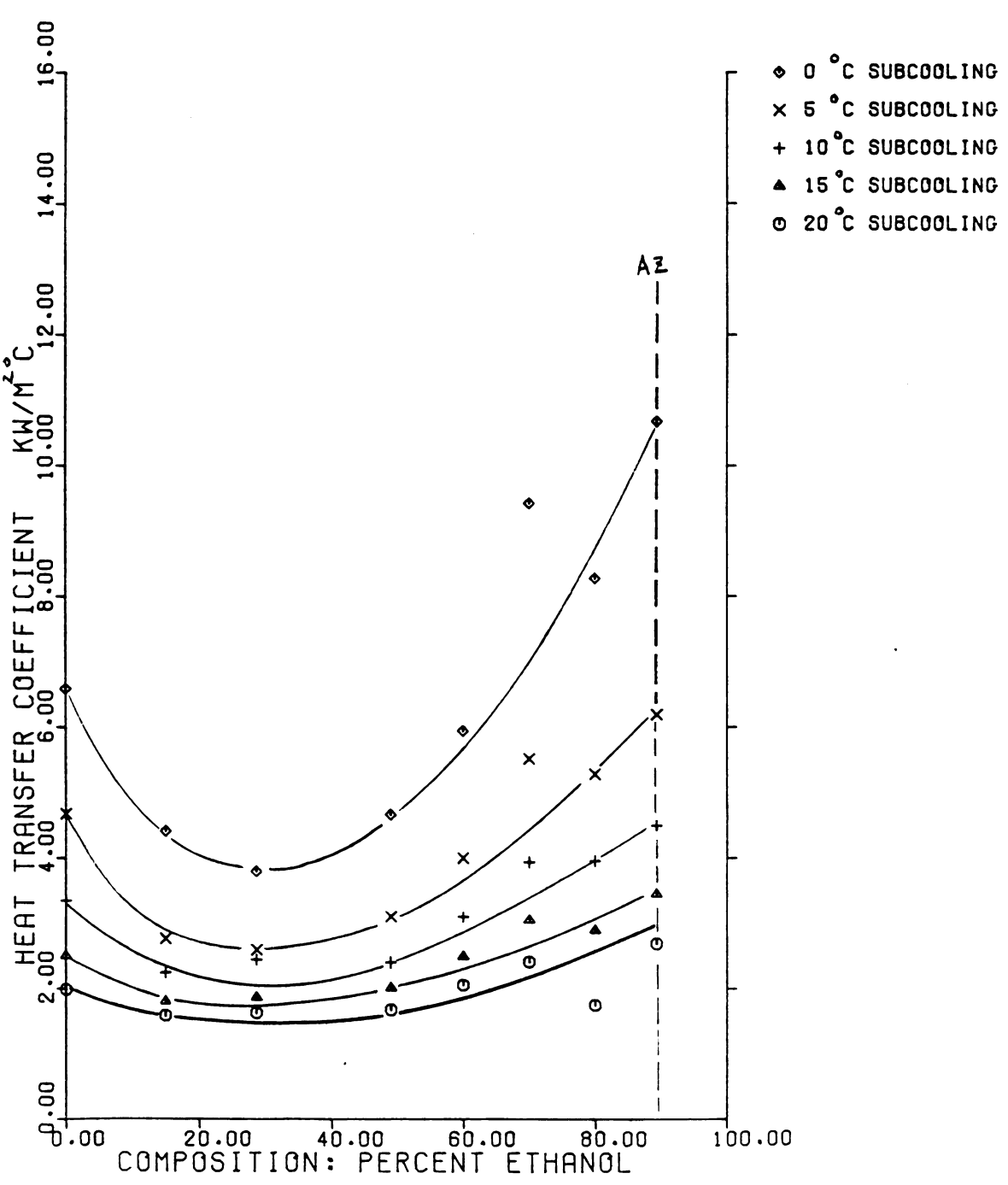
HEAT TRANS COEFF VS PERCENT ETHANOL
ETHANOL AND WATER MIXTURE
HEAT FLUX IS 97.39 KW/M²
0 °C SUBCOOLING
5 °C SUBCOOLING
10 °C SUBCOOLING
15 °C SUBCOOLING
20 °C SUBCOOLING
AZ
HEAT TRANSFER COEFFICIENT KW/M²°C
0.00
2.00
4.00
6.00
8.00
10.00
12.00
14.00
16.00
0.00
20.00
40.00
60.00
80.00
100.00
COMPOSITION: PERCENT ETHANOL

Figure 4.2

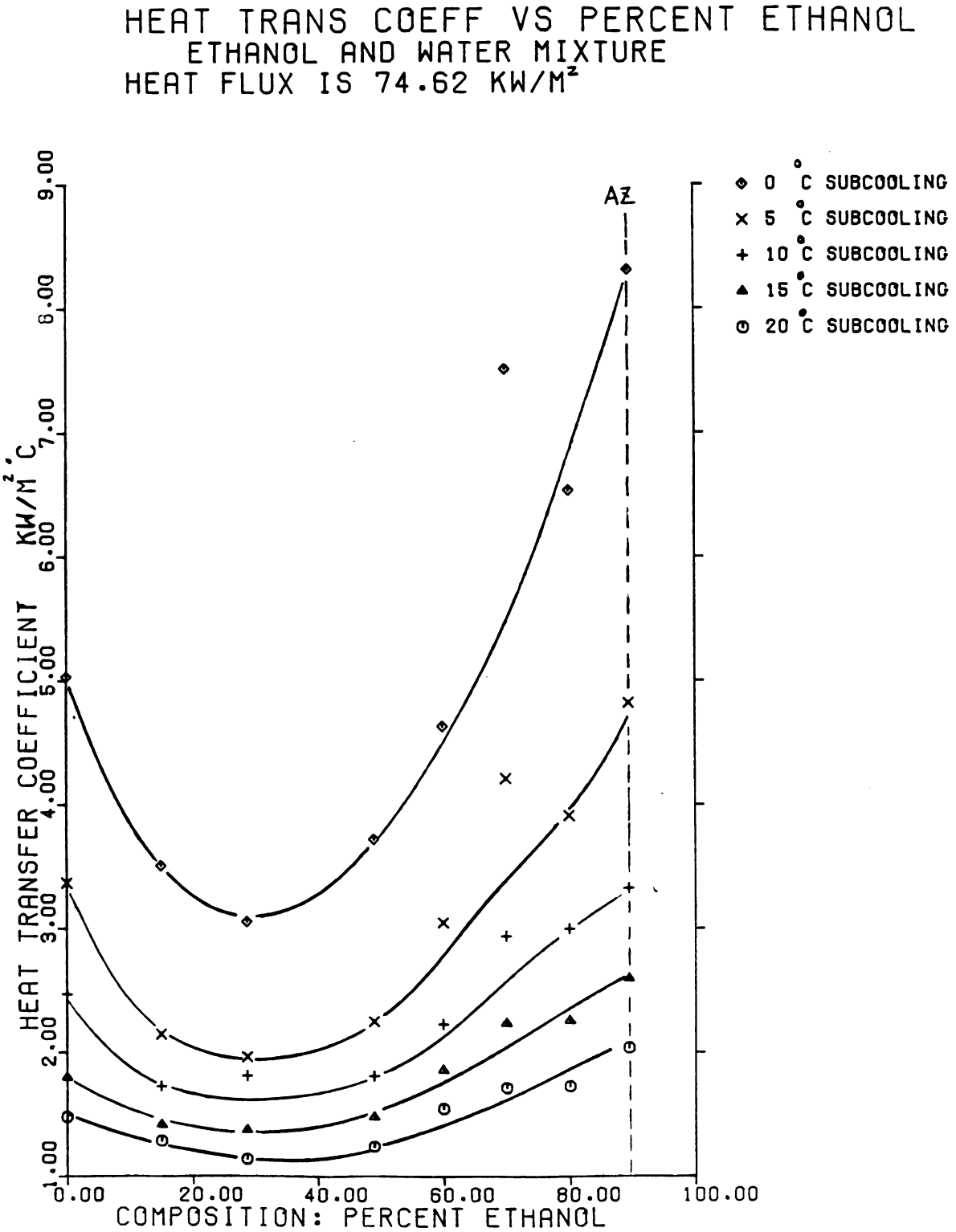
HEAT TRANS COEFF VS PERCENT ETHANOL
ETHANOL AND WATER MIXTURE
HEAT FLUX IS 74.62 KW/M²
HEAT TRANSFER COEFFICIENT KW/M² °C
1.00
2.00
3.00
4.00
5.00
6.00
7.00
8.00
9.00
AZ
0 °C SUBCOOLING
5 °C SUBCOOLING
10 °C SUBCOOLING
15 °C SUBCOOLING
20 °C SUBCOOLING
0.00
20.00
40.00
60.00
80.00
100.00
COMPOSITION: PERCENT ETHANOL

Figure 4.3

HEAT TRANS COEFF VS PERCENT ETHANOL
ETHANOL AND WATER MIXTURE
HEAT FLUX IS 38.54 KW/M^2

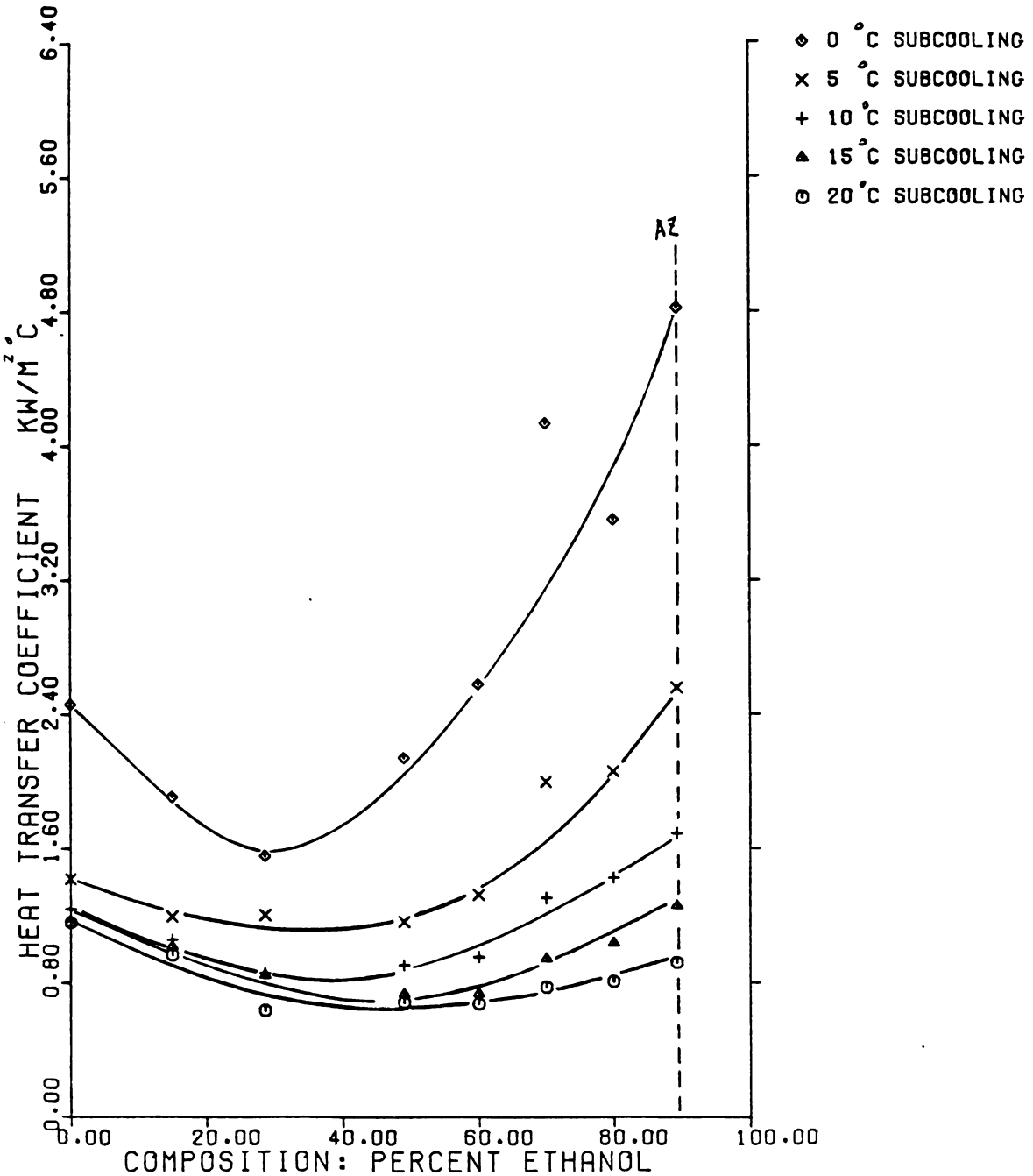

Figure 4.4

HEAT TRANS COEFF VS PERCENT ETHANOL
ETHANOL AND WATER MIXTURE
HEAT FLUX IS 13.74 KW/M^2

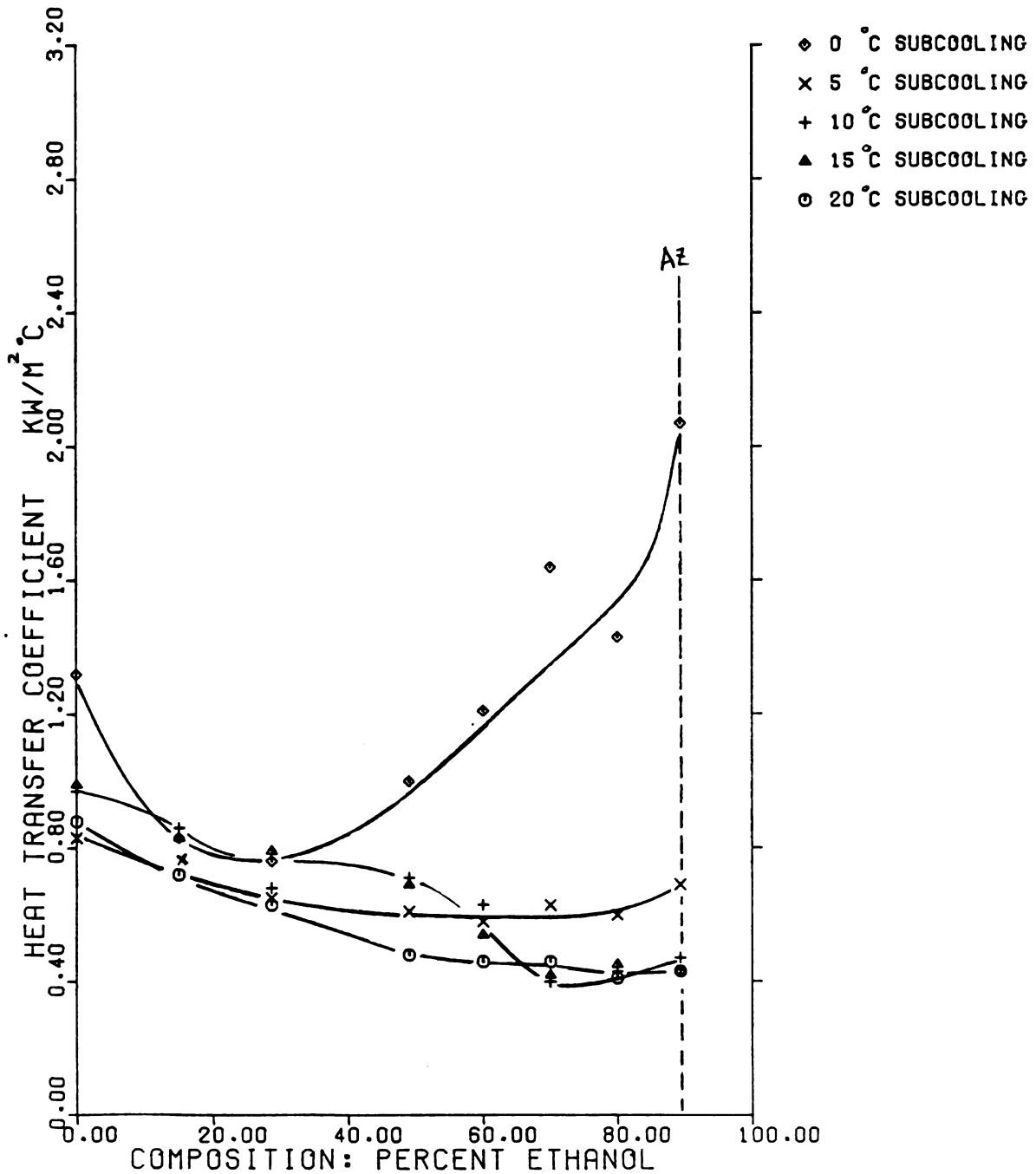

reduction from the predicted value. The deviations from the predicted values become smaller for lower heat fluxes and higher degrees of subcooling. This can be explained by the fact that at these conditions, natural convection becomes more significant in the heat transfer process and the heat transfer coefficient is less affected by the preferential evaporation of the more volatile component (i.e. ethanol). This is illustrated by Figure 4.4 where for subcoolings of 5, 10, 15, and 20 °C, the heat transfer coefficient can be accurately predicted by using a linear mixing law.

4.1.2 Ethanol-benzene mixtures

Some results for heat transfer coefficient as a function of mixture composition for ethanol-benzene mixtures are shown in Figures 4.5, 4.6, 4.7, and 4.8. The negative deviation from the ideal values is again obvious. Two minima are observed for this system: one at each side of the azeotropic mixture composition (45% mole fraction of ethanol). The azeotropic mixture thus seems to behave like a pure liquid. As in the case of the ethanol-water system, the deviation is more significant at high heat flux and low subcooling. The deviation from the ideal values, however, is smaller for this system than the ethanol-water system. For the minimum point at the composition of about 80%, at a heat flux of 97.39 kW/m^2 and 0 °C subcooling, a 27% reduction from the ideal value is obtained for the experimental heat transfer coefficient.

Figure 4.5

HEAT TRANS COEFF VS PERCENT ETHANOL
ETHANOL AND BENZENE MIXTURE
HEAT FLUX IS 97.39 KW/M^2

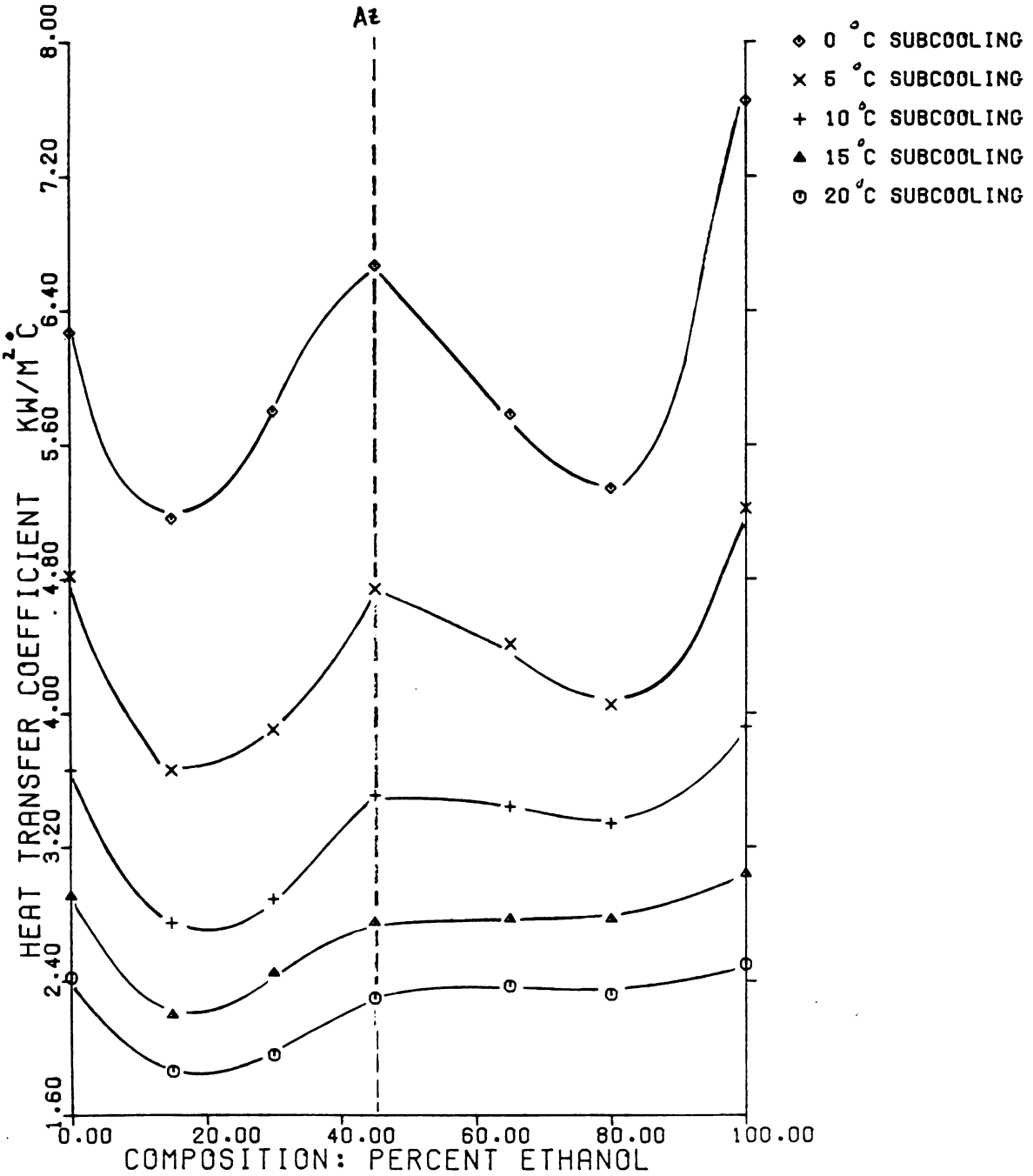

Figure 4.6

HEAT TRANS COEFF VS PERCENT ETHANOL
ETHANOL AND BENZENE MIXTURE
HEAT FLUX IS 38.54 KW/M^2

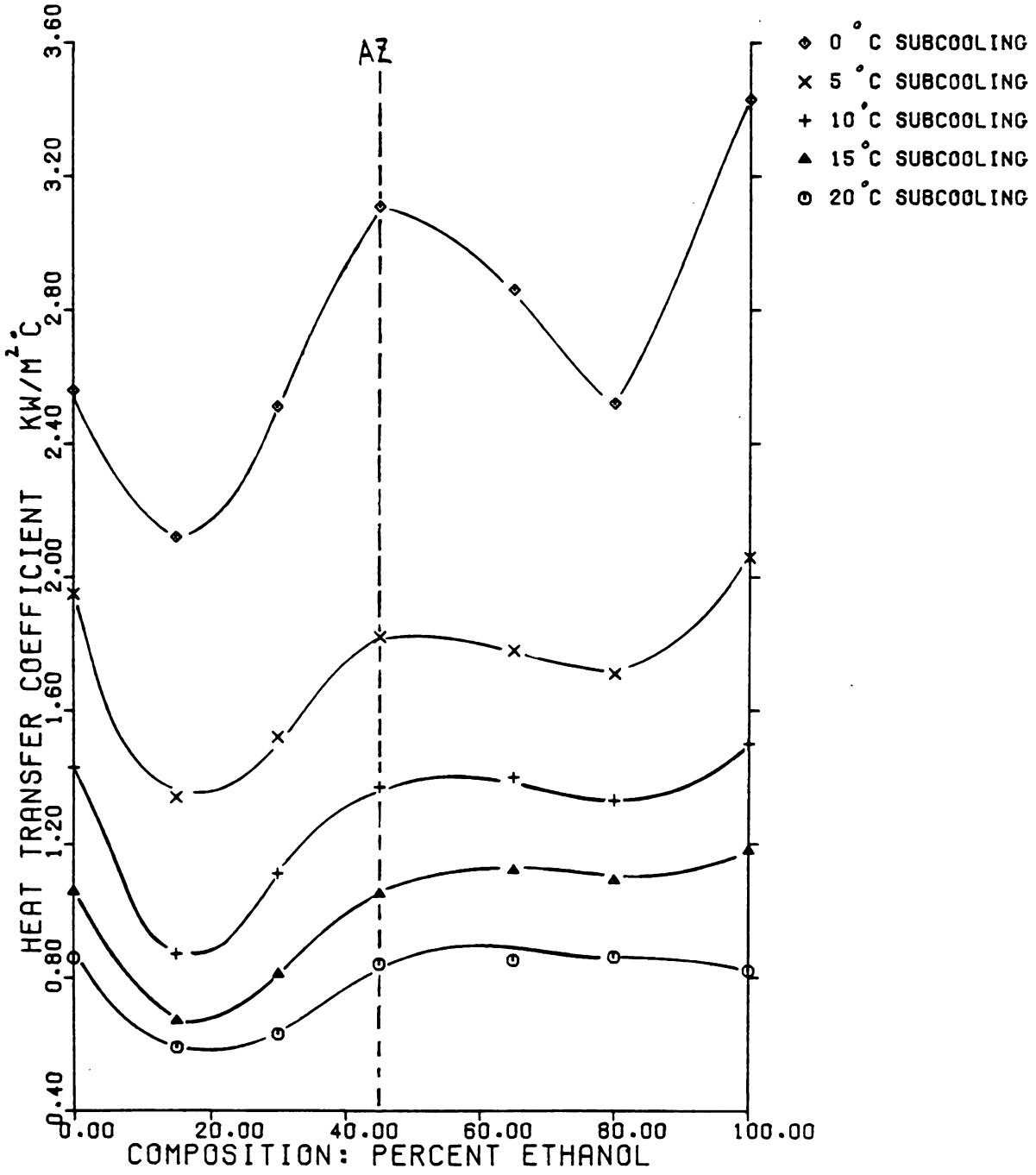

Figure 4.7

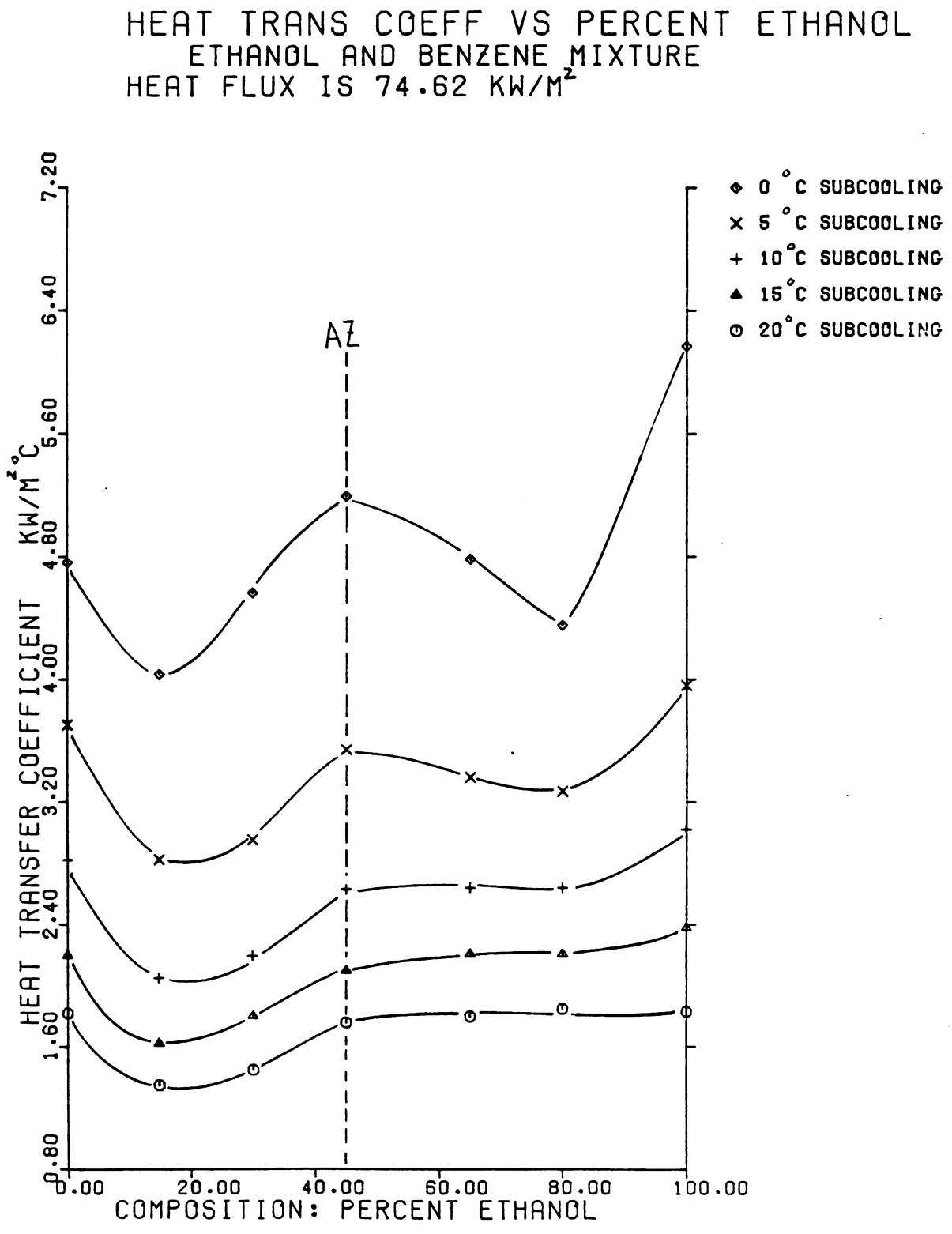
HEAT TRANS COEFF VS PERCENT ETHANOL
ETHANOL AND BENZENE MIXTURE
HEAT FLUX IS 74.62 KW/M2
0 °C SUBCOOLING
5 °C SUBCOOLING
10 °C SUBCOOLING
15 °C SUBCOOLING
20 °C SUBCOOLING
AZ
HEAT TRANSFER COEFFICIENT KW/M2°C
7.20
6.40
5.60
4.80
4.00
3.20
2.40
1.60
0.80
0.00
20.00
40.00
60.00
80.00
100.00
COMPOSITION: PERCENT ETHANOL

Figure 4.8

HEAT TRANS COEFF VS PERCENT ETHANOL
ETHANOL AND BENZENE MIXTURE
HEAT FLUX IS 13.74 KW/M^2

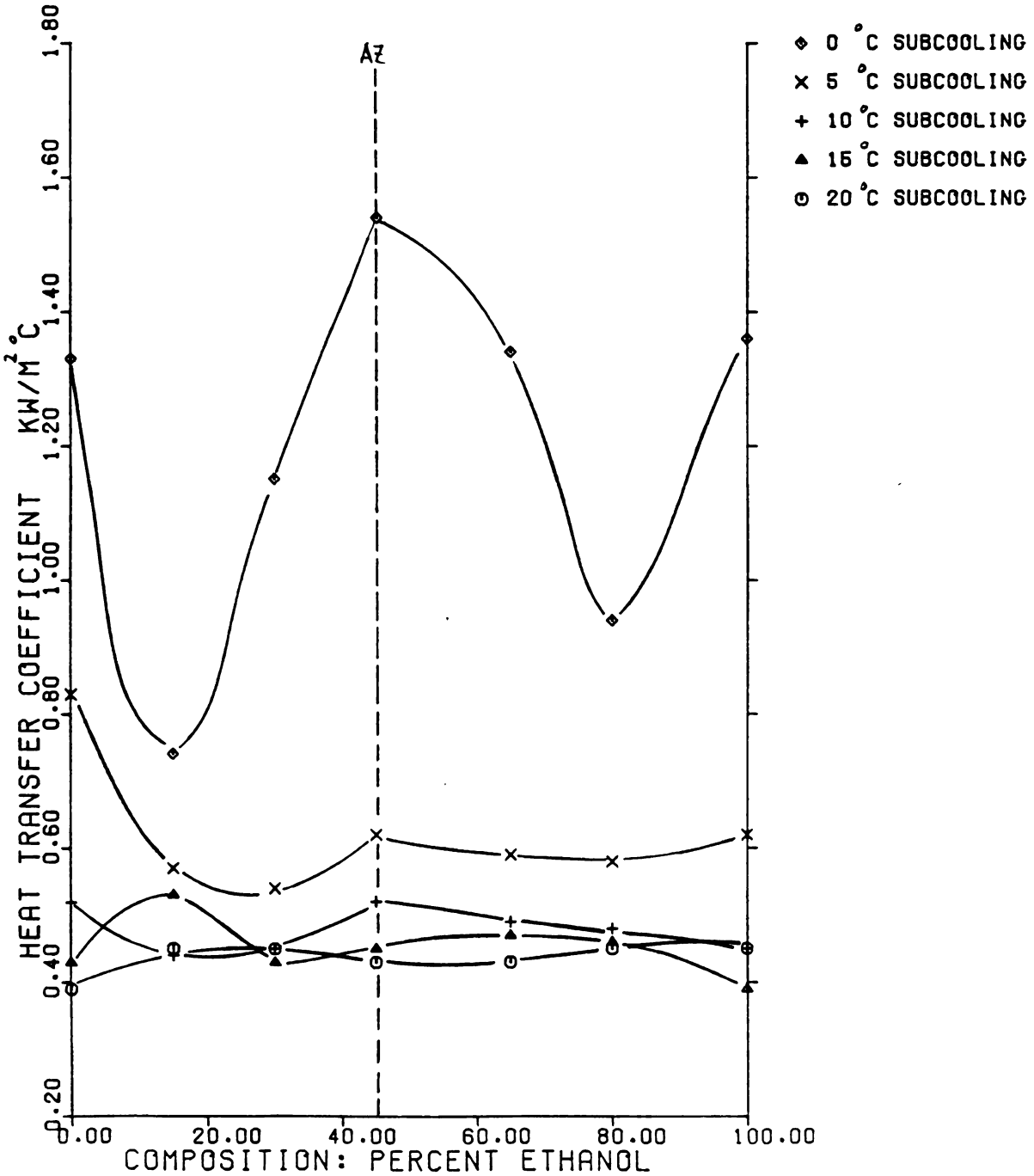

4.2 Heat transfer coefficient vs. subcooling

Figures 4.9, 4.10, 4.11, and 4.12 show the effect of subcooling on the heat transfer coefficient. Note that each figure is for one particular composition. The heat transfer coefficient is seen to decrease as the subcooling increases. This is due to the fact that T_w drops at a less extent than T_b, i.e. T_w is relatively insensitive to changes in subcooling. Also evident is the fact that the decreasing value of h is more significant at higher fluxes. This suggests that T_w is relatively insensitive to subcooling in the well established boiling region. On the other hand, since natural convection is the more dominant mode of heat transfer at lower heat fluxes, h is relatively insensitive to subcooling. It should be pointed out also that the results here show a similar trend to those obtained by Sterman, Vilamos, and Abramov (25).

4.3 Non-dimensional heat transfer coefficient, h_{exp}/h_I, vs. mixture composition

4.3.1 Ethanol-water mixtures

The value of the non-dimensional heat transfer coefficient, defined here as h_{exp}/h_I, indicates the extent of the negative deviation of the experimental value of h from that predicted by an ideal linear mixing law. In Figures 4.13 and 4.14 (at constant heat fluxes of 97.39 kW/m^2 and 74.62

Figure 4.9

HEAT TRANS COEFF VS SUBCOOLING
ETHANOL AND WATER MIXTURE
COMPOSITION- 60.00 PERCENT ETHANOL

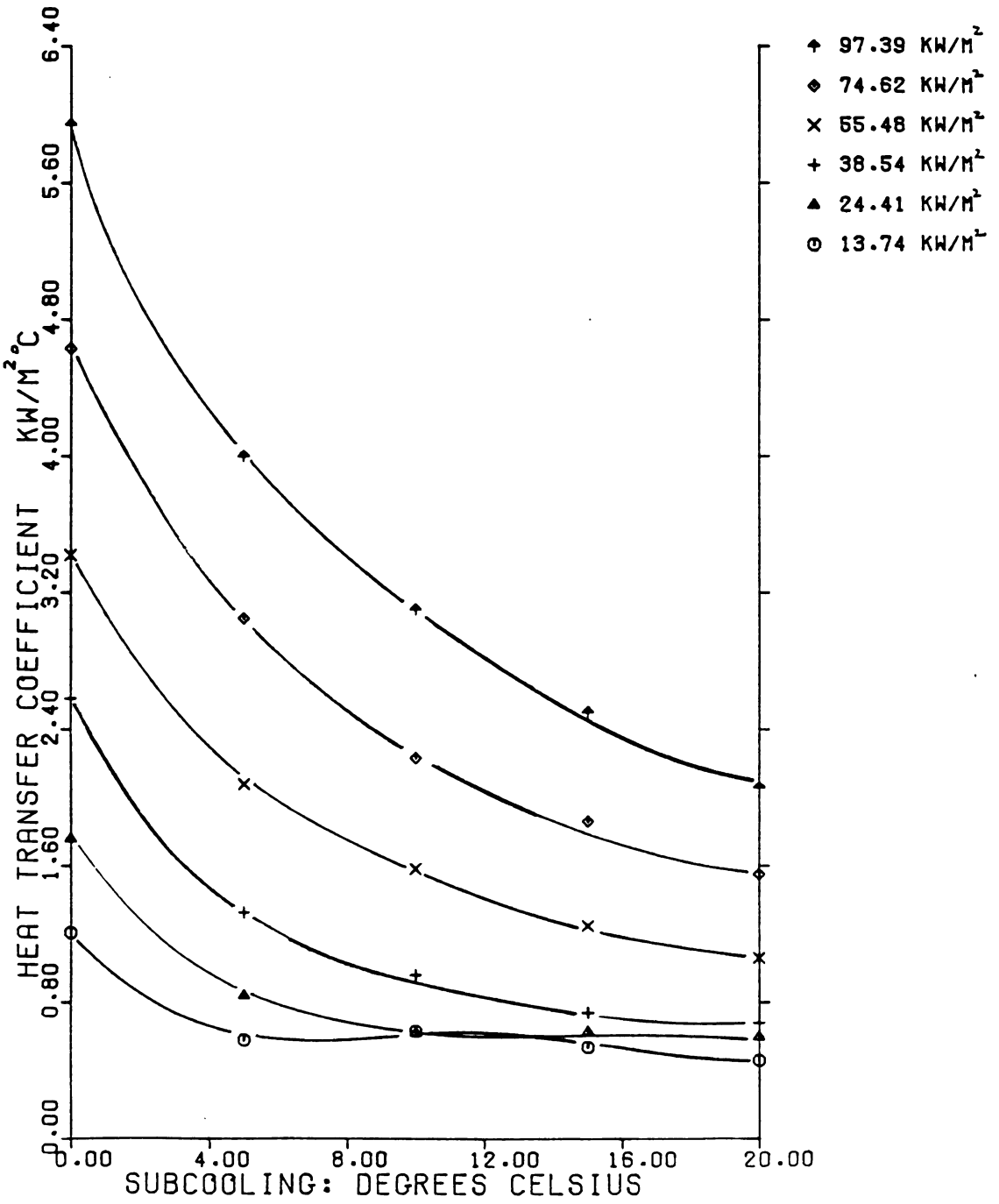

Figure 4.10

HEAT TRANS COEFF VS SUBCOOLING
ETHANOL AND BENZENE MIXTURE
COMPOSITION- 100.00 PERCENT ETHANOL

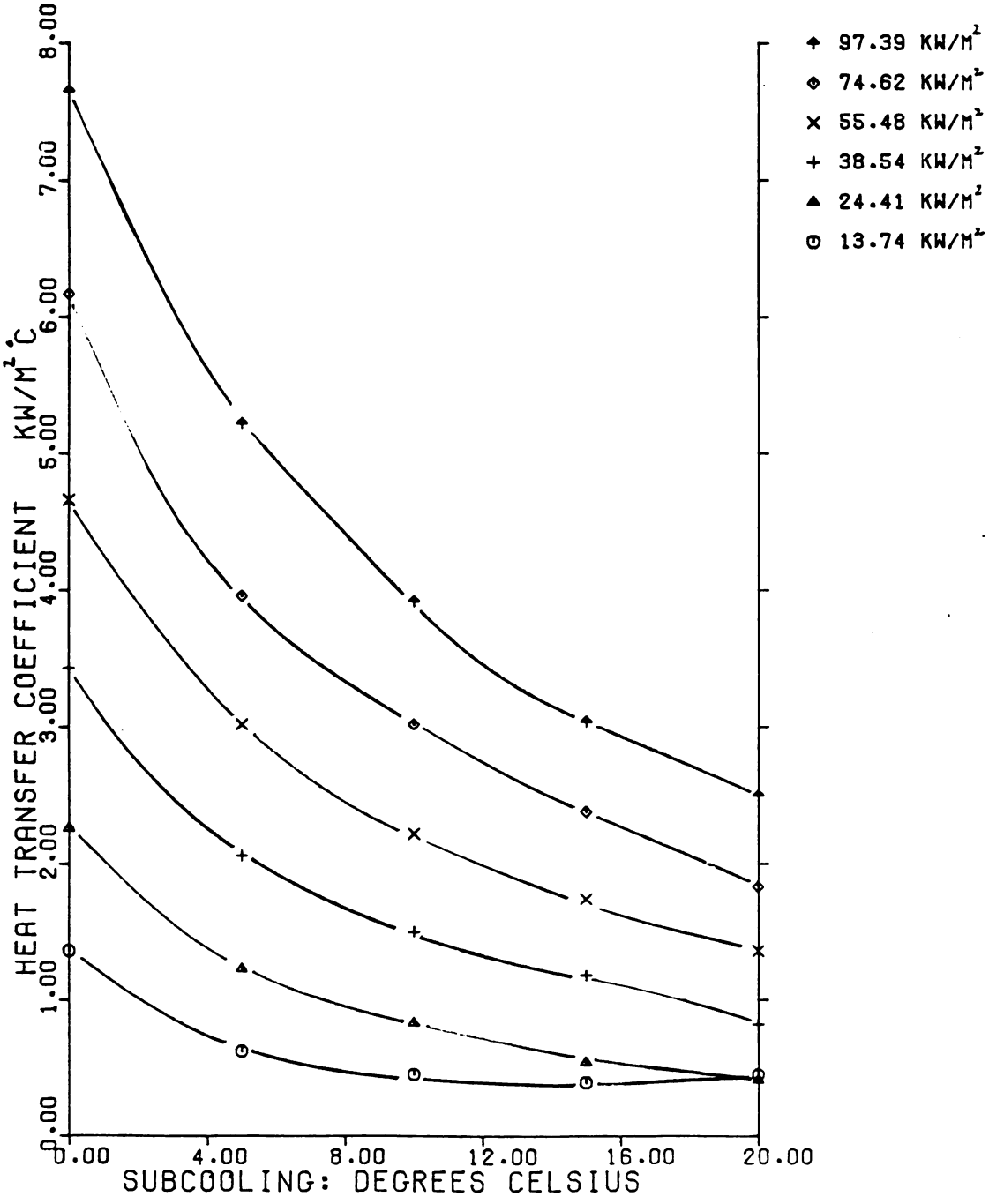

Figure 4.11
HEAT TRANS COEFF VS SUBCOOLING
ETHANOL AND BENZENE MIXTURE
COMPOSITION- 80.00 PERCENT ETHANOL

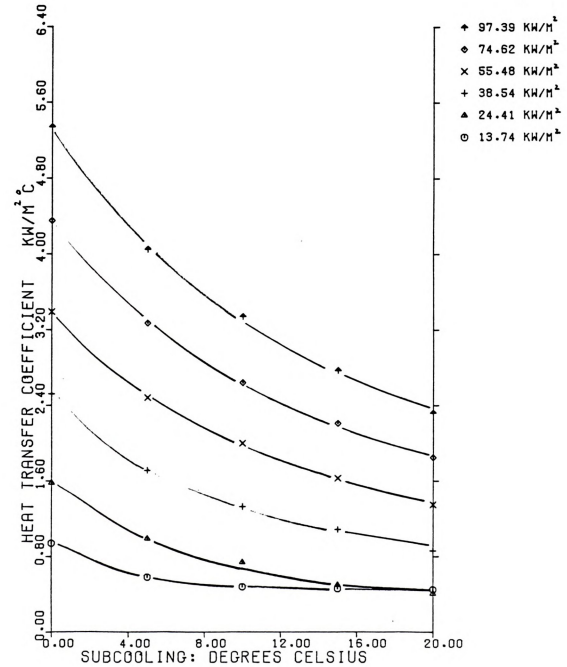

Figure 4.12

HEAT TRANS COEFF VS SUBCOOLING
ETHANOL AND BENZENE MIXTURE
COMPOSITION- 0.00 PERCENT ETHANOL

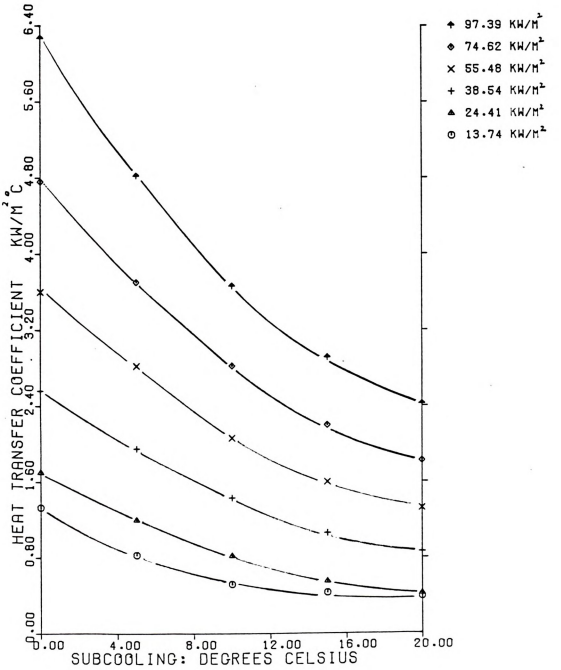

Figure 4.13

H(EXP)/H(I) VS. COMPOSITION
ETHANOL AND WATER MIXTURE
HEAT FLUX IS 97.39 KW/M^2

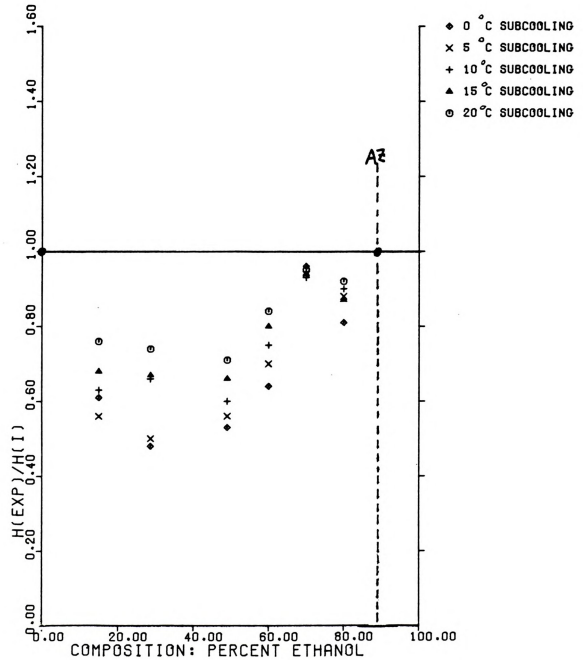

Figure 4.14

H(EXP)/H(I) VS. COMPOSITION
ETHANOL AND WATER MIXTURE
HEAT FLUX IS 74.62 KW/M^2

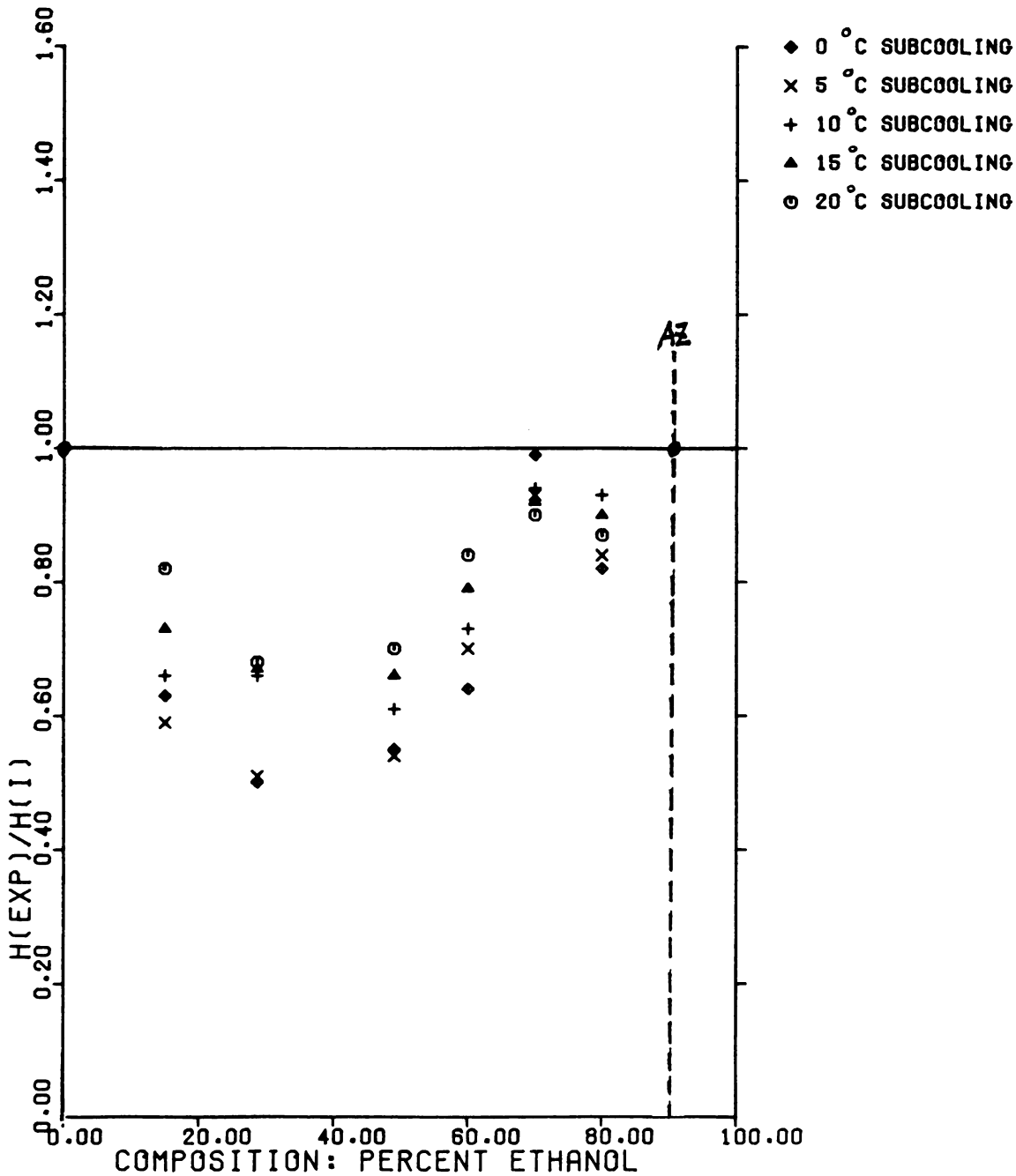

kW/m^2), the minimum values of h_{exp}/h_I occur in the neighborhood of 30% ethanol composition; the values being about 0.5 in both cases. For the composition region between 0% to 60%, the values of h_{exp}/h_I increased when subcooling is increased. Again, natural convection begins to be more significant at higher subcooling and the degradation in the boiling heat transfer process becomes less dominant. This trend is not as obvious for the data at the compositions of 70% and 80%.

4.3.2 Ethanol-benzene mixtures

Some values of h_{exp}/h_I for the ethanol-benzene mixtures are shown in Figures 4.15 and 4.16. As pointed out earlier, two mimima are obtained: one on each side of the azeotrope. The mimima of h_{exp}/h_I are in general less profound for this system compared to the ethanol-water system. In the region from 45% to 100% ethanol, h_{exp}/h_I increases as subcooling is increased. However, h_{exp}/h_I has its maximum values at 0 °C subcooling in the region from 0% to 45% ethanol. This is true at both heat fluxes: 97.39 kW/m^2 and 74.62 kW/m^2. No plausible explanation is available at the present time.

4.4 Boiling site density vs. mixture composition

4.4.1 Ethanol-water mixture

Figures 4.17, 4.18, 4.19, and 4.20 are experimental

Figure 4.15
H(EXP)/H(I) VS. COMPOSITION
ETHANOL AND BENZENE MIXTURE
HEAT FLUX IS 97.39 KW/M^2

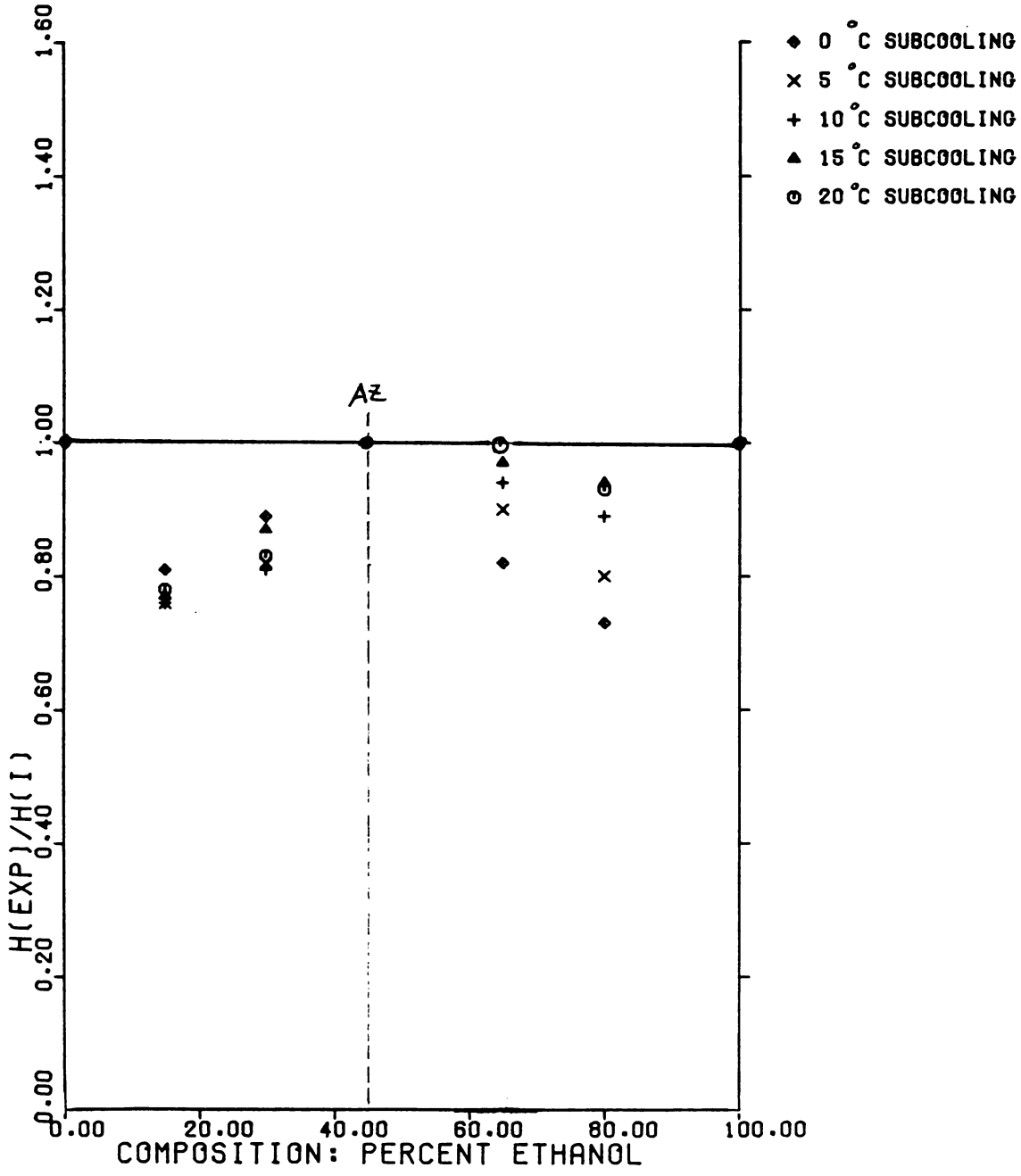

Figure 4.16
H(EXP)/H(I) VS. COMPOSITION
ETHANOL AND BENZENE MIXTURE
HEAT FLUX IS 74.62 KW/M^2

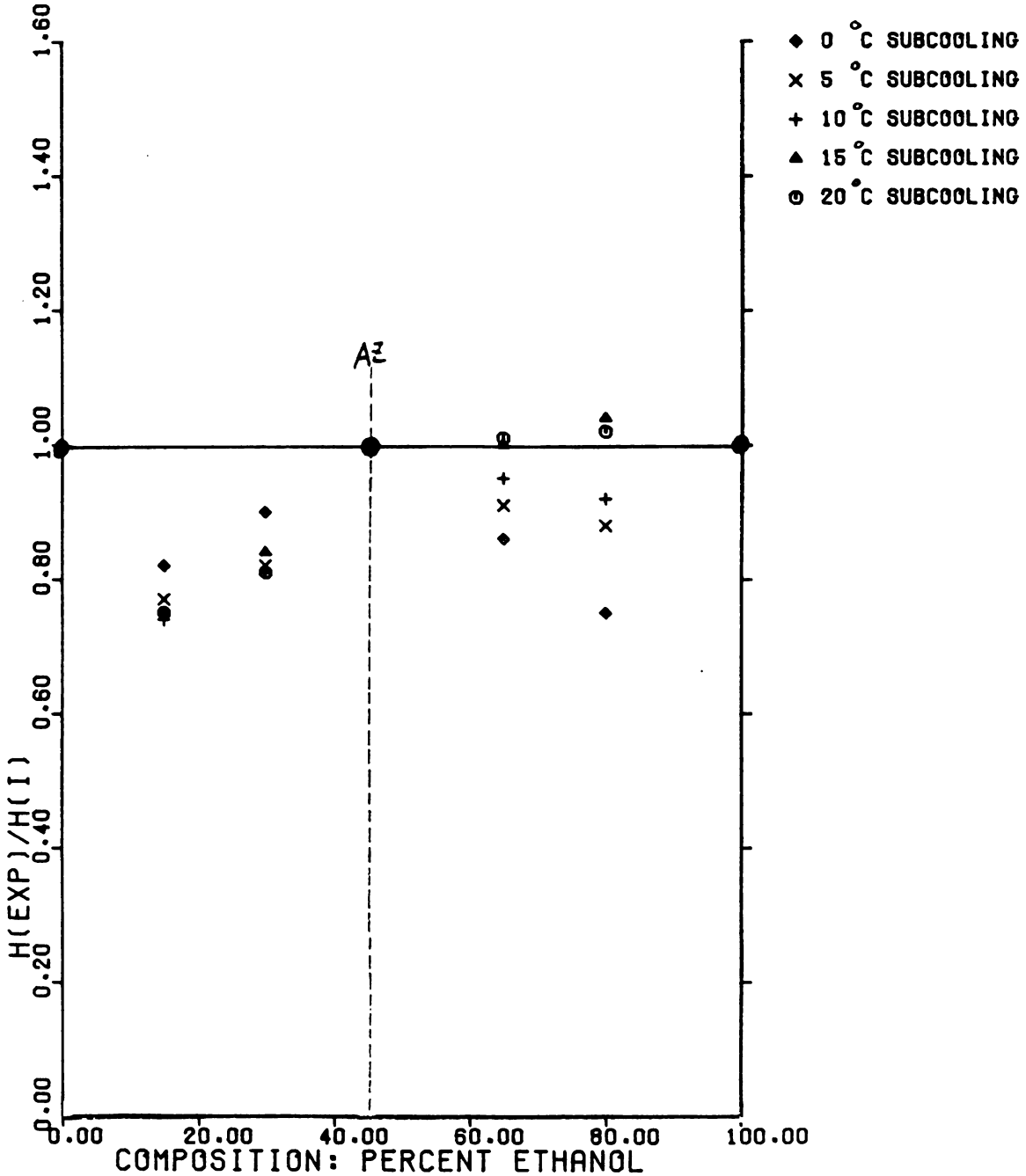

Figure 4.17

SITE DENSITY VS PERCENT ETHANOL
ETHANOL AND WATER MIXTURE
HEAT FLUX IS 97.39 KW/M^2

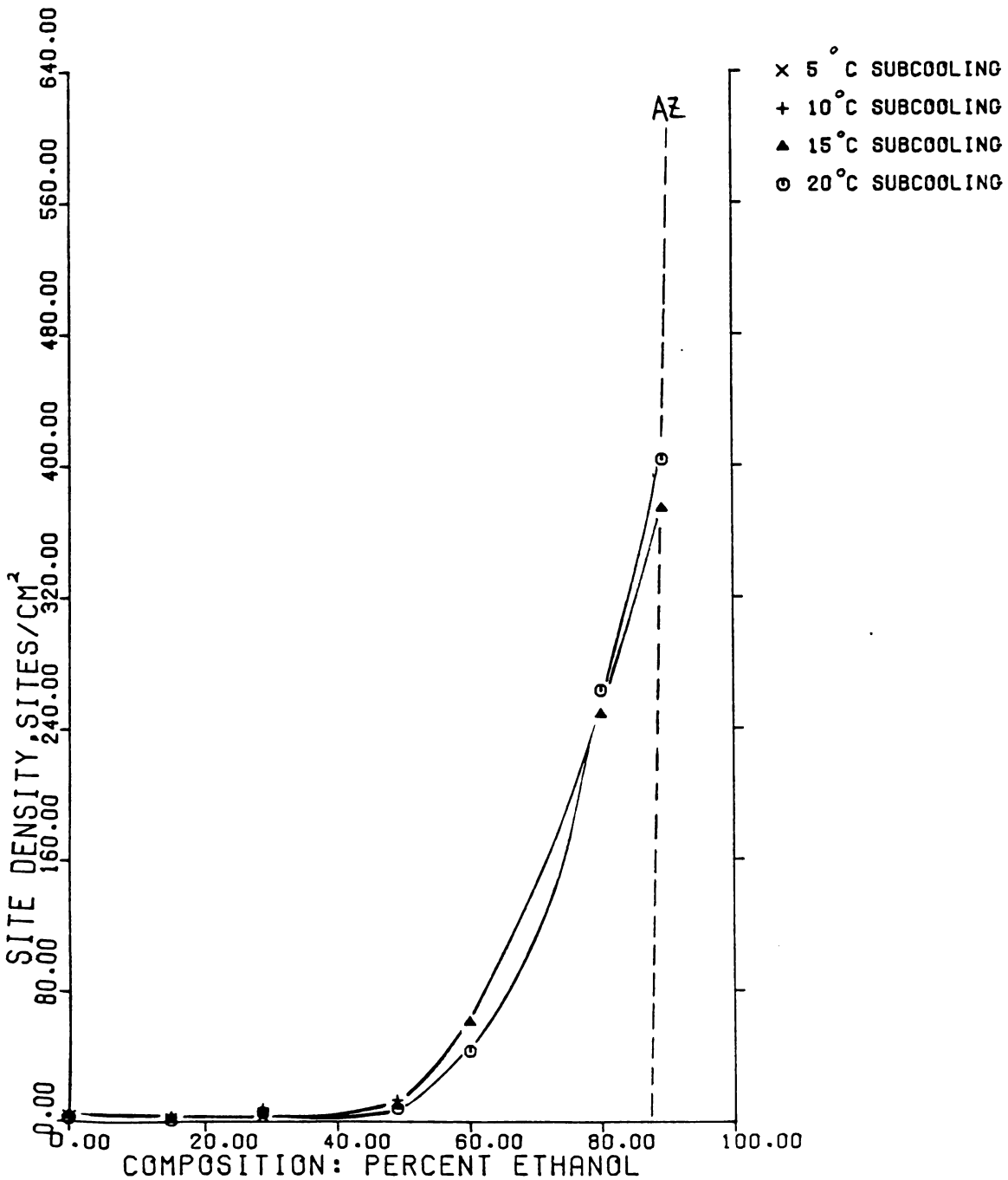

Figure 4.18

SITE DENSITY VS PERCENT ETHANOL
ETHANOL AND WATER MIXTURE
HEAT FLUX IS 74.62 KW/M^2

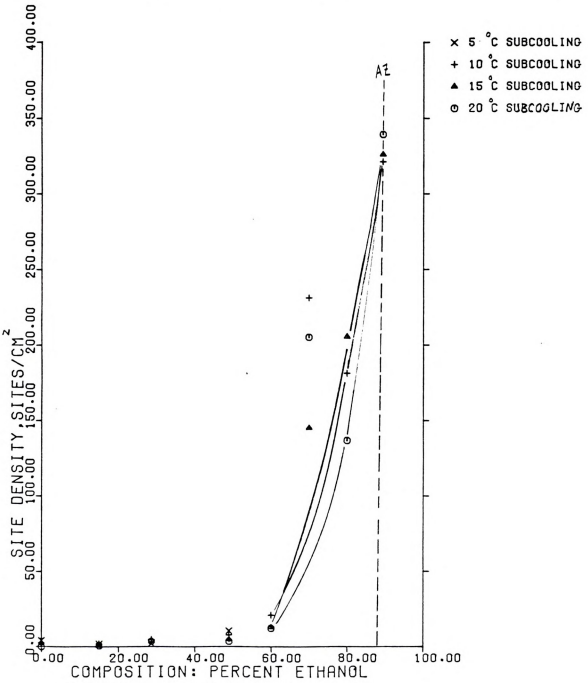

Figure 4.19

SITE DENSITY VS PERCENT ETHANOL
ETHANOL AND WATER MIXTURE
HEAT FLUX IS 38.54 KW/M²

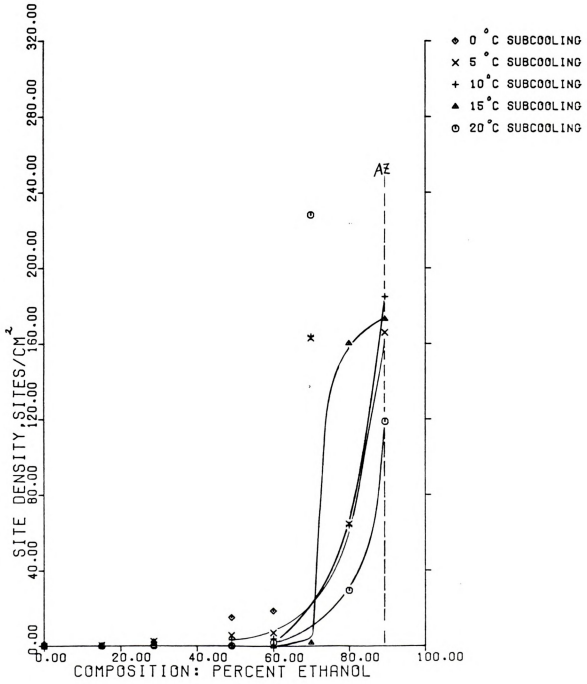

Figure 4.20

SITE DENSITY VS PERCENT ETHANOL
ETHANOL AND WATER MIXTURE
HEAT FLUX IS 24.41 KW/M^2

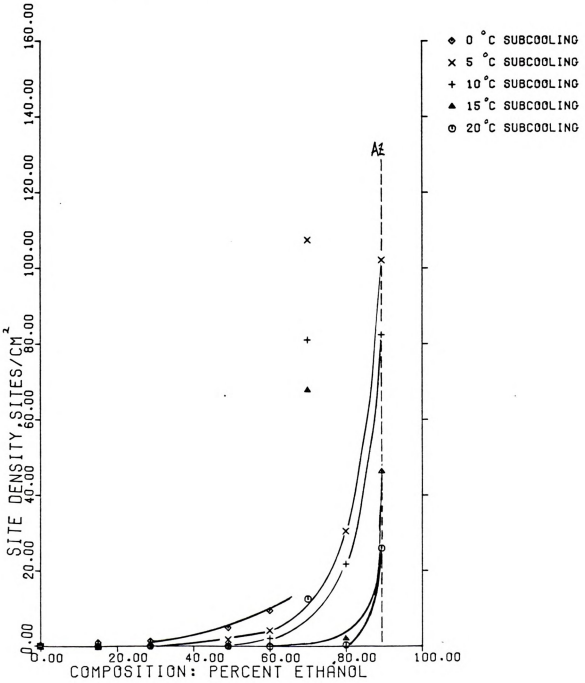

results for the boiling site density as a function of composition at different heat fluxes. Based on the results of Thome, Shakir, and Mercier (12) on the incipient superheats for ethanol-water system (Figure 2.9), a minimum value for the boiling site density is expected in the vicinity of 50% mole fraction of ethanol. The results of the deactivation superheats showed a smaller variation as a function of composition. For the experiments performed in the present study, the deactivation superheat would be more reliable in predicting the boiling site density since all possible sites were activated by using a very high heat flux at the beginning of each trial.

For each of the heat fluxes studied, the boiling site density is relatively small in the composition region from 0% to about 60% mole fraction of ethanol. Beyond this point the boiling site density increases very rapidly, until an increase of two orders of magnitude is reached at the azeotrope. A vapor spreading phenomenon is observed to be responsible for this huge increase in the boiling site density. For mixtures with a relatively large percentage of ethanol, the following observation was noted. When the heat flux through the heating surface is increased gradually to about 200 kW/m^2, the wall temperature can be about 30 to 45 °C above the saturation temperature before boiling takes place. A single site would be activated first and it is surmized that its vapor in turn "seeds" neighboring sites, causing them to be activated also. A "chain reaction

phenomenon" thus occurs, causing the entire heating surface to be activated and hence, a high boiling site density to result.

This aqueous system shows a large negative deviation of the boiling site density from that predicted by an ideal linear mixing law. It is noted, however, that the bubble departure diameter of water is about 3 to 4 times that of the azeotropic mixture. It should be pointed out also that some site density results were not obtainable because the sites were too crowded to be counted. This usually occurs at high heat flux and low subcooling.

4.4.2 Ethanol-benzene mixtures

Figures 4.21, 4.22, 4.23, and 4.24a are results for the site density as a function of composition for ethanol-benzene mixtures. The variation here is much smaller than that found in the ethanol-water system. The results demonstrate a maximum to the left of the azeotrope but a minimum to the right. It is noted that the vapor spreading phenomenon occurred over the entire composition range from pure benzene to pure ethanol while activating the boiling surface.

The following offers a plausible explanation for the observed site density variation. After a bubble departed from the heating surface, a vapor nucleus is left behind in the micro-structure. At the same time, liquid from the bulk rushes in to take up the space that the departed

Figure 4.21
SITE DENSITY VS PERCENT ETHANOL
ETHANOL AND BENZENE MIXTURE
HEAT FLUX IS 97.39 KW/M²

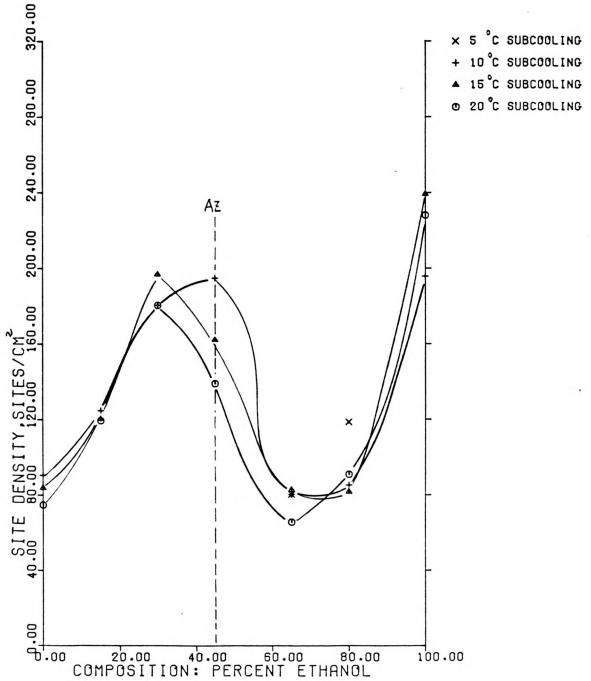

Figure 4.22

SITE DENSITY VS PERCENT ETHANOL
ETHANOL AND BENZENE MIXTURE
HEAT FLUX IS 74.62 KW/M^2

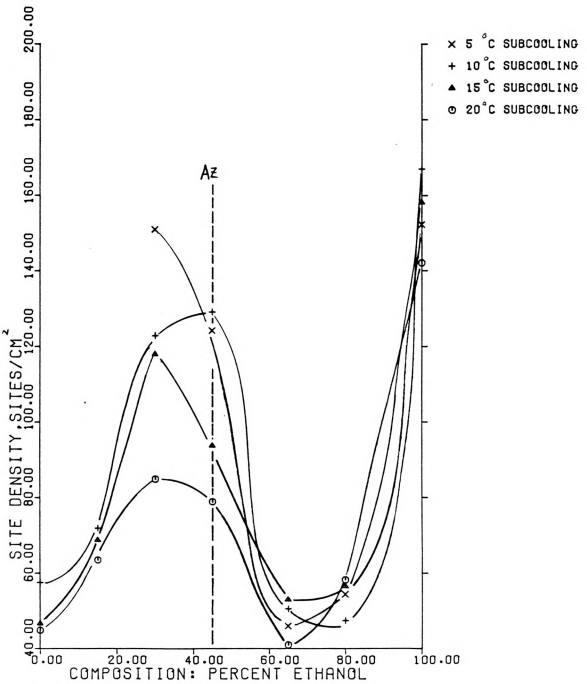

Figure 4.23

SITE DENSITY VS PERCENT ETHANOL
ETHANOL AND BENZENE MIXTURE
HEAT FLUX IS 55.48 KW/M^2

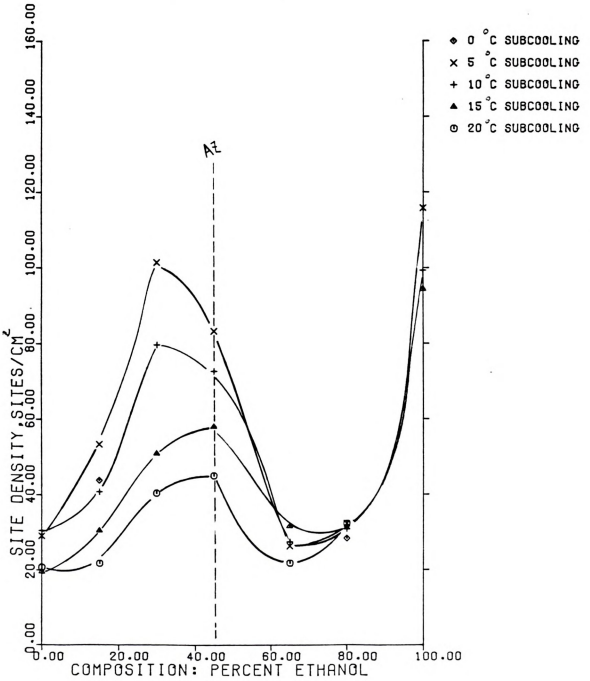

Figure 4.24a

SITE DENSITY VS PERCENT ETHANOL
ETHANOL AND BENZENE MIXTURE
HEAT FLUX IS 24.41 KW/M^2

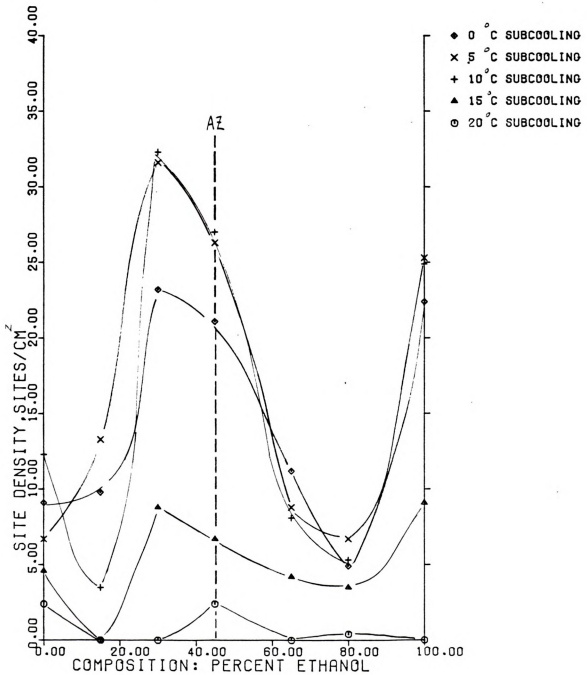

bubble left behind. The composition of the vapor nucleus is likely to have a lower concentration of the more volatile component than the vapor composition corresponding to the bulk liquid due to the preferential evaporation of the more volatile component. Therefore, the vapor nucleus will not be in chemical equilibrium with the bulk liquid.

For $0 \leqslant \tilde{x}_b \leqslant \tilde{x}_{az}$ (see Figure 4.24b for a phase equilibrium diagram for the ethanol-benzene system)

Suppose that the bulk liquid is of composition $\tilde{x}_{b_a}$ with its corresponding vapor composition equal to $\tilde{y}_a$. The vapor nucleus has a vapor composition that is of a value somewhere between $\tilde{x}_{b_a}$ and $\tilde{y}_a$. Therefore the composition of the vapor nucleus has a lower mole fraction of ethanol than the vapor composition, $\tilde{y}_a$, corresponding to the bulk liquid composition, $\tilde{x}_{b_a}$. It is postulated that in order for the vapor nucleus to attain a vapor composition of $\tilde{y}_a$, ethanol is preferentially evaporated at the vapor and liquid interface. Thus the radius of this vapor nucleus is increased and the incipient superheat required is lowered. This would lead to a higher boiling site density. It is also postulated that the maximum in the boiling site density is strongly influenced by the maximum value of $|\tilde{y} - \tilde{x}|$.

For $\tilde{x}_{az} \leqslant \tilde{x}_b \leqslant 1$

For this composition range, the vapor composition of the vapor nucleus has a higher composition of ethanol than the

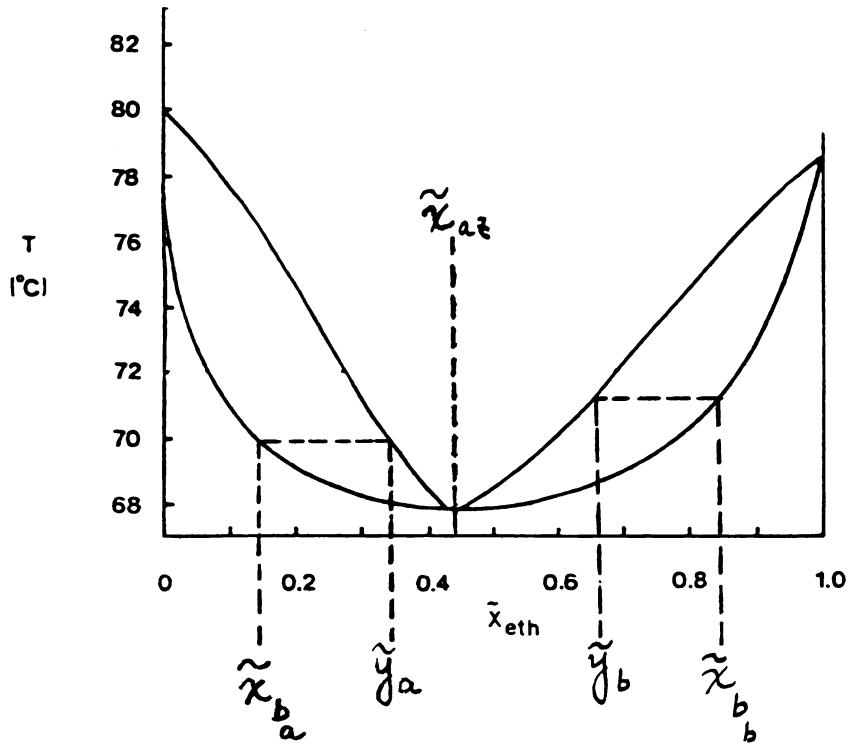

Figure 4.24b Phase equilibrium diagram for ethanol-benzene system.

vapor composition corresponding to the bulk liquid. Therefore, it is postulated that the ethanol component in the vapor nucleus is preferentially condensed so that the vapor nucleus will be in chemical equilibrium with the bulk liquid. Thus the radius of the nucleus is decreased and a higher incipient superheat is required for the nucleus to begin to grow . The resulting effect is a lower boiling site density. Again, the minimum value of the boiling site density is in the vicinity of the maximum value of $|\tilde{y} - \tilde{x}|$. Finally, this non-aqueous mixture system is shown also to have a very nonlinear variation in the boiling site density with composition.

4.5 Boiling site density vs. subcooling

It is seen from Figures 4.25, 4.26, 4.27, 4.28, 4.29, and 4.30 that the site density as a function of subcooling can behave in three different ways (1) monotonically decreasing with subcooling, (2) displaying a maximum, or (3) displaying a minimum value. As discussed in Chapter 2, the wall temperature is a relatively weak function of subcooling and the data from the present study further supports this idea, i.e. T_w drops at a slower rate than that of the decrease in the temperature of the bulk liquid. But at the same time, the heat transfer coefficient is smaller for a higher degree of subcooling used. Since the thickness of the thermal boundary layer is related to the heat transfer coefficient in the form

$$\delta = Ch^d \qquad (2.21)$$

Figure 4.25
SITE DENSITY VS SUBCOOLING
ETHANOL AND WATER MIXTURE
COMPOSITION- 89.40 PERCENT ETHANOL

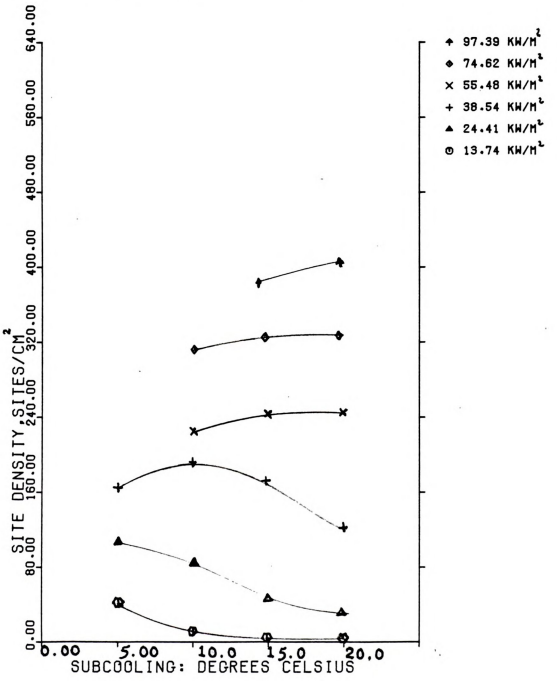

Figure 4.26

SITE DENSITY VS SUBCOOLING
ETHANOL AND WATER MIXTURE
COMPOSITION- 60.00 PERCENT ETHANOL

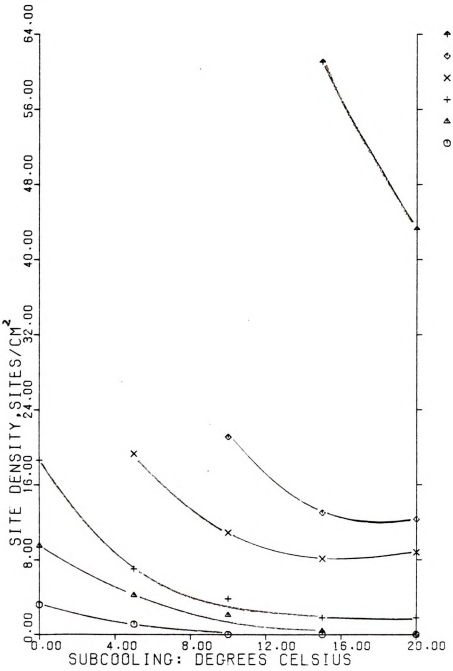

Figure 4.27
SITE DENSITY VS SUBCOOLING
ETHANOL AND WATER MIXTURE
COMPOSITION- 28.67 PERCENT ETHANOL

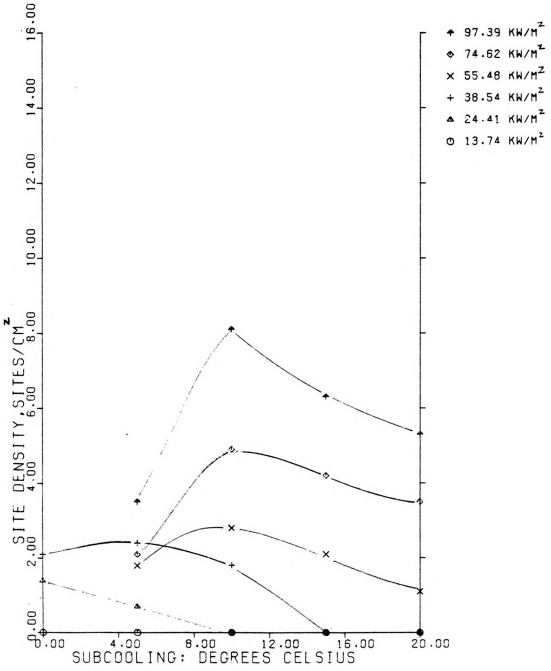

Figure 4.28
SITE DENSITY VS SUBCOOLING
ETHANOL AND BENZENE MIXTURE
COMPOSITION- 100.00 PERCENT ETHANOL

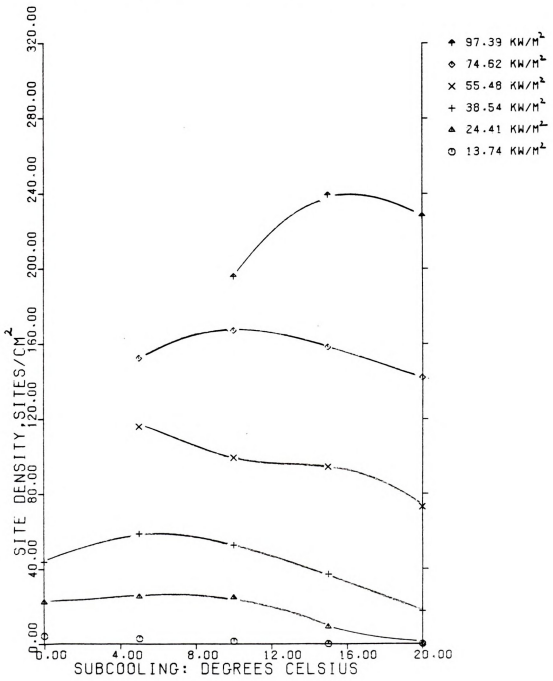

Figure 4.29

SITE DENSITY VS SUBCOOLING
ETHANOL AND BENZENE MIXTURE
COMPOSITION- 80.00 PERCENT ETHANOL

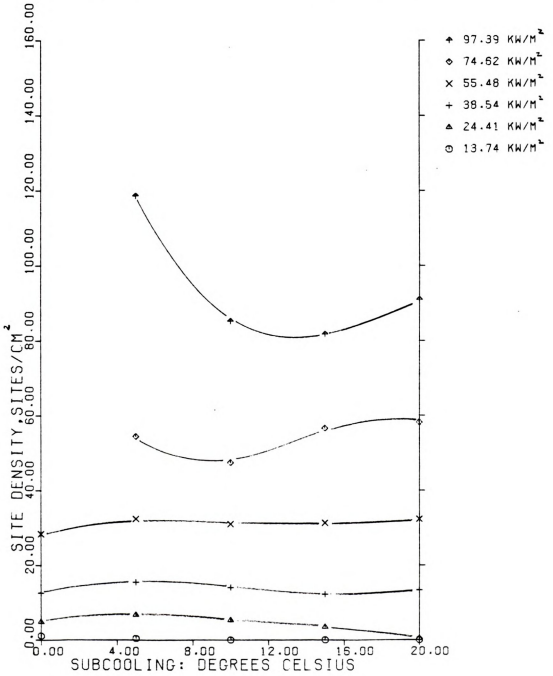

Figure 4.30
SITE DENSITY VS SUBCOOLING
ETHANOL AND BENZENE MIXTURE
COMPOSITION- 15.00 PERCENT ETHANOL

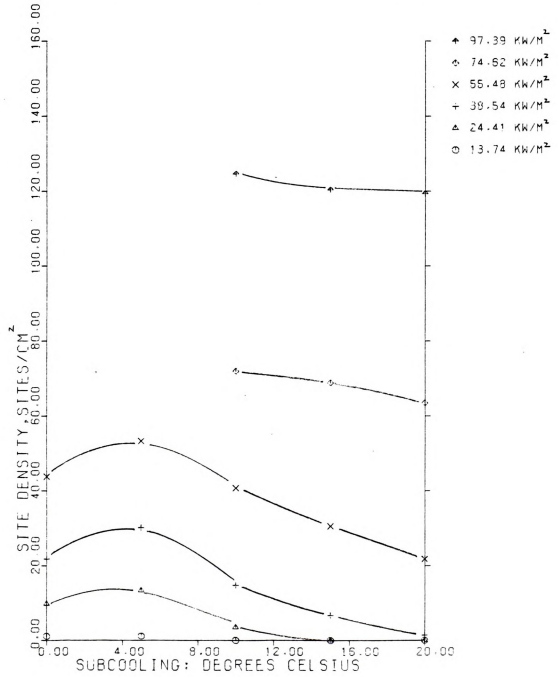

where d is a negative number, the thickness of the thermal boundary layer is expected to increase when a higher degree of subcooling is used. Also, the bubble departure diameter decreases with subcooling as observed here qualitatively and quantitatively in Figure 2.12. Thus, as subcooling increases, there is a possibility of packing boiling sites closer together. Thus three general trends can be caused by an increases in the subcooling: (1) a decrease in the wall temperature, (2) an increase in the thickness of the thermal boundary layer adjacent to the heating surface, and (3) D_d is smaller as subcooling is increased. It can be assumed that a decrease in wall temperature would cause a lower boiling site density to occur. On the other hand, an increase in the thickness of the thermal boundary layer may increase the boiling site density, an idea suggested by Hsu's analysis in Chapter 2. Thus, these three phenomena should be considered in the analysis of the boiling density as a function of subcooling.

4.6 Boiling site density vs. heat flux

As expected, the boiling site density increases as the heat flux is increased as shown in Figures 4.31, 4.32, and 4.33. Note that the slope of the curves gets steeper as the heat flux is increased. An energy balance can be written in the form

$$\frac{\text{Energy}}{(\text{Area})(\text{time})} = (\text{Boiling site density})\ (\text{average energy removed per bubble})\ (\text{Average frequency of bubble cycle}) \qquad (4.1)$$

Figure 4.31

SITE DENSITY VS HEAT FLUX
ETHANOL AND WATER MIXTURE
COMPOSITION- 80.00 PERCENT ETHANOL

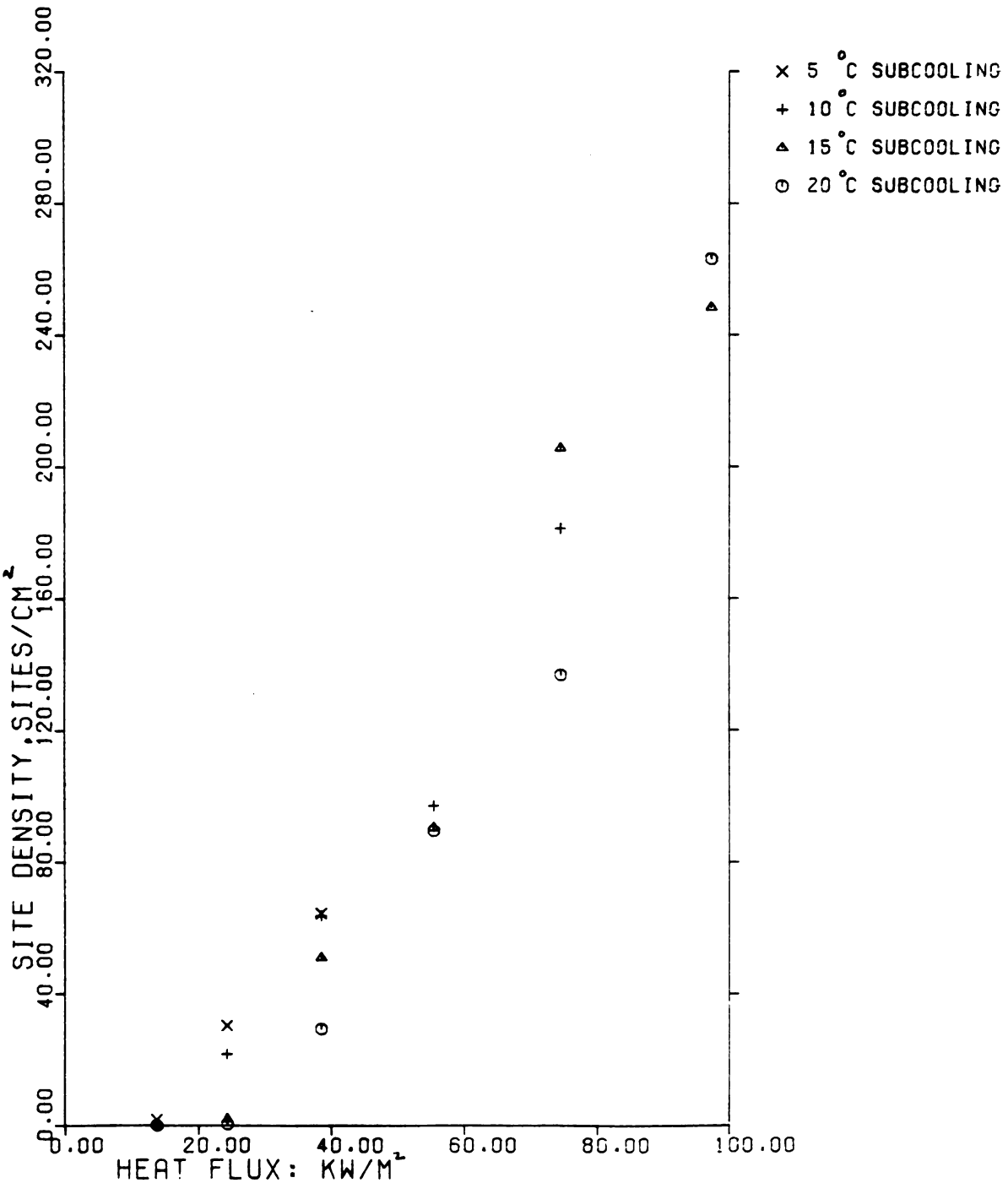

Figure 4.32

SITE DENSITY VS HEAT FLUX
ETHANOL AND BENZENE MIXTURE
COMPOSITION- 100.00 PERCENT ETHANOL

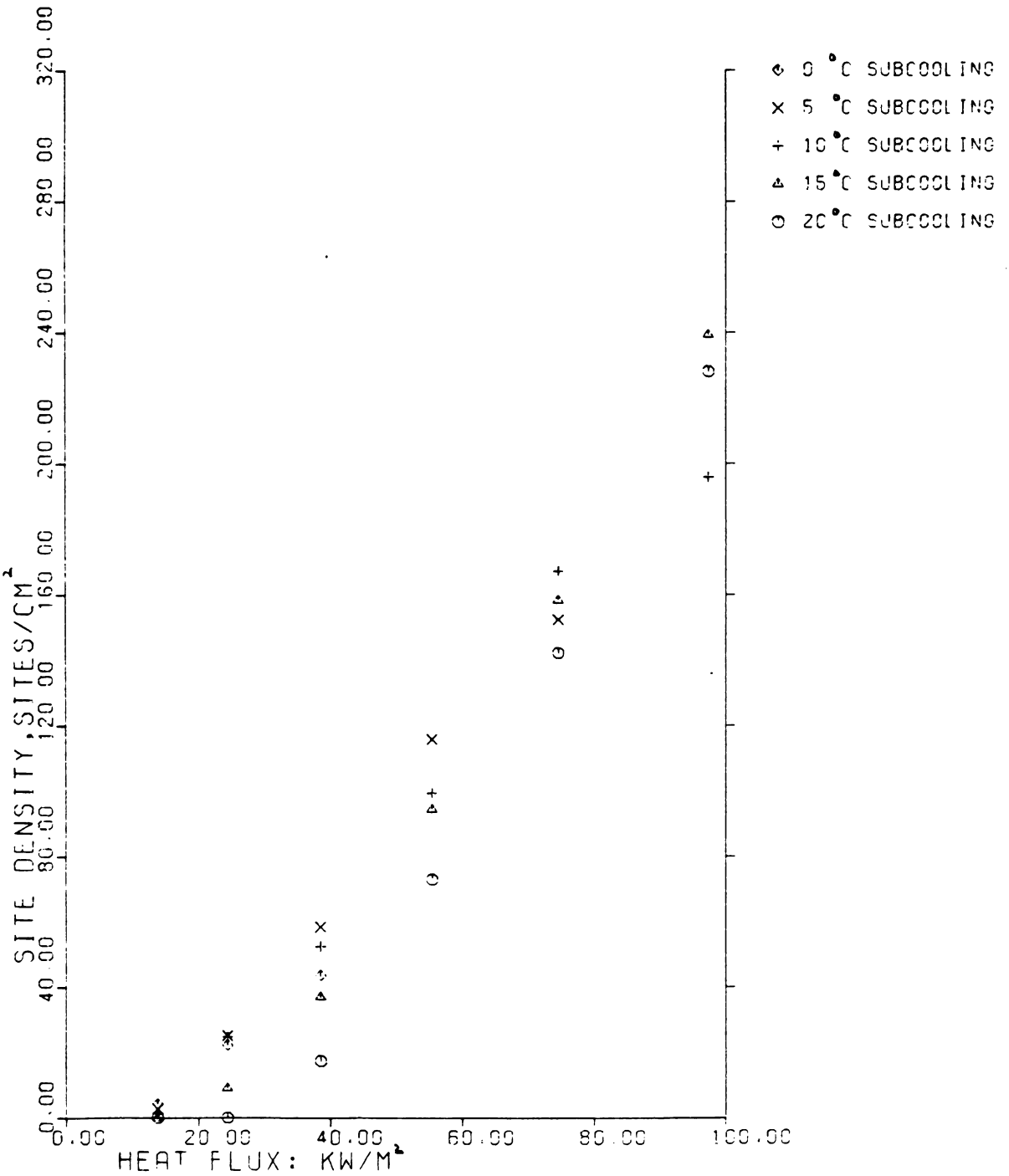

Figure 4.33

SITE DENSITY VS HEAT FLUX
ETHANOL AND BENZENE MIXTURE
COMPOSITION- 45.00 PERCENT ETHANOL

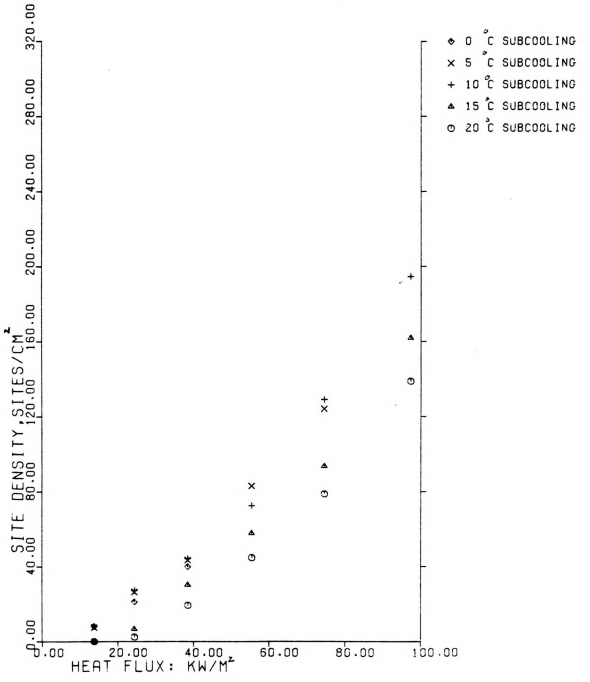

or

$$\frac{\text{Heat flux}}{\text{Boiling site density}} = (\text{Average energy removed per bubble}) \times (1/\tau) \qquad (4.2)$$

Since the experimental data point to the fact that the ratio of (heat flux/boiling site density) is decreasing as heat flux is increased, this shows that the product of (av. energy removed per bubble) X $(1/\tau)$ is therefore also decreasing as the heat flux is increased. Since it is well known that τ decreases as heat flux is increased, this suggests that the average energy removed per bubble decreases at higher heat flux.

4.7 Boiling site density vs. wall temperature

The boiling site density is plotted as a function of wall temperature in Figures 4.34, 4.35, and 4.36. The following observations are noted :

(1) The deactivation superheats can be extrapolated from each curve. Note that the data seem to suggest a higher deactivation superheat for lower subcooling, pointing to the importance of the thickness of the thermal boundary layer suggested earlier.

(2) Within the range of conditions tested, i.e. a heat flux up to about 100kW/m^2, the rate of increase in the boiling site density increase rapidly as the wall termperature is raised.

Figure 4.34
SITE DENSITY VS. WALL TEMPERATURE
ETHANOL AND WATER MIXTURE
COMPOSITION- 80.00 PERCENT ETHANOL

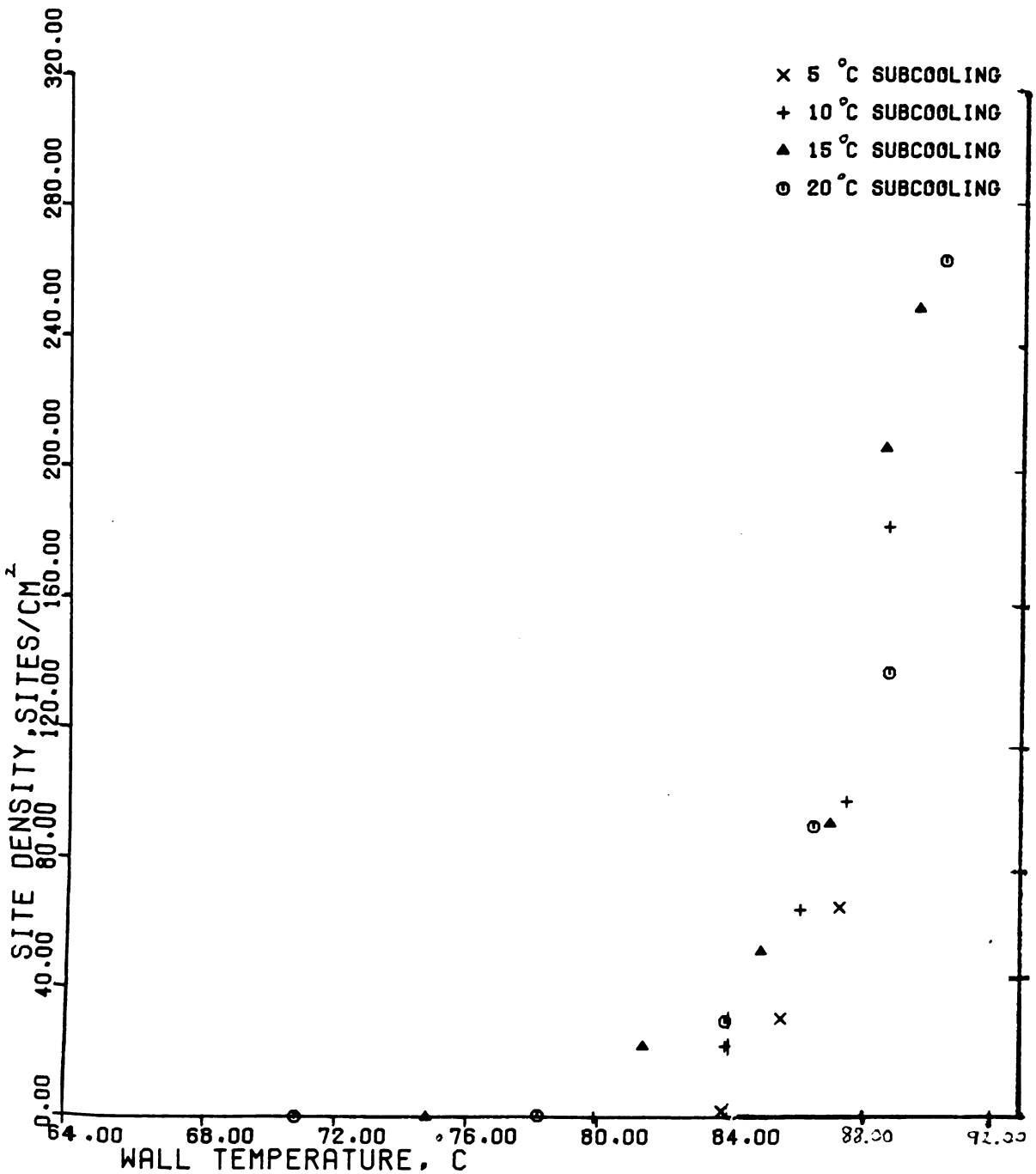

Figure 4.35

SITE DENSITY VS. WALL TEMPERATURE
ETHANOL AND BENZENE MIXTURE
COMPOSITION- 80.00 PERCENT ETHANOL

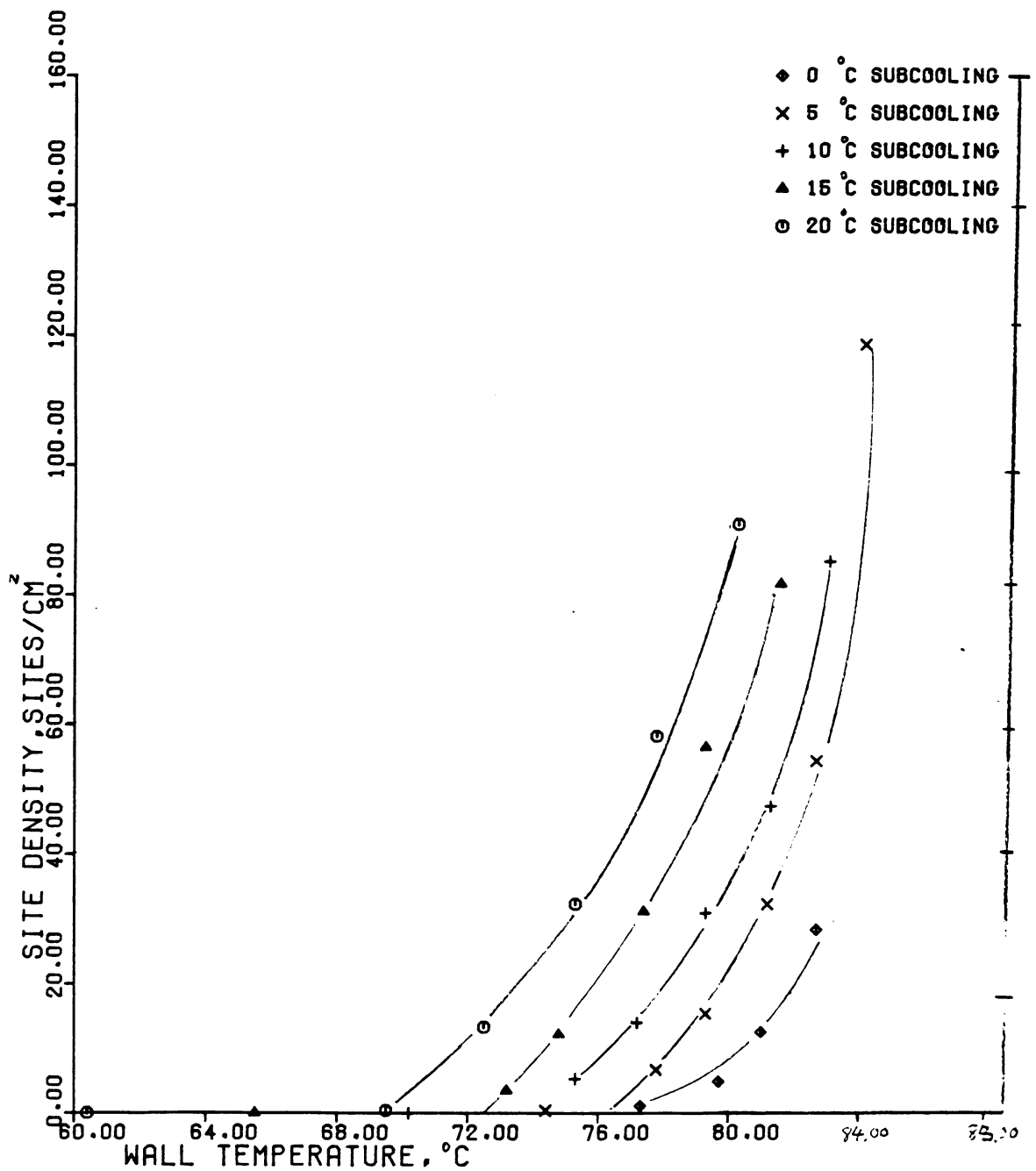

Figure 4.36

SITE DENSITY VS. WALL TEMPERATURE
ETHANOL AND BENZENE MIXTURE
COMPOSITION- 30.00 PERCENT ETHANOL

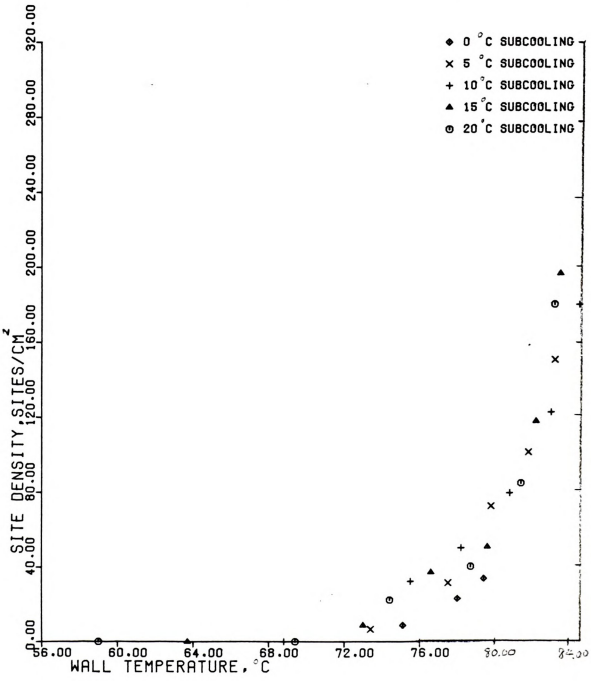

(3) Note that given the same wall temperature, the general trend is for the boiling site density to be larger for higher subcooling. Again, this can be due to a thicker thermal boundary layer at higher subcooling.

4.8 (Experimental boiling site density)/(Ideal linear boiling site density) vs. mixture composition

Figures 4.38, 4.39, and 4.40 show the variation of $(B.S.D._{exp}/B.S.D._I)$ versus the mixture composition ; where $(B.S.D._{exp}/B.S.D._I)$ is the ratio of the experimental boiling site density to that predicted by an ideal linear mixing law. Note the inadequacy of trying to predict the boiling site density from the linear mixing law. This is especially true for the ethanol-water mixtures at the mole fractions of 15%, 28.67%, 49.04%, and 60.0% ethanol where the experimental boiling site densities for these mixtures are less than 10% of the predicted ideal values. For the ethanol-benzene mixture system, the value of $B.S.D_{exp}/B.S.D._I$ is greater that one to the left of the azeotrope and is less than one to the right. For this system, it would also be very inadequate to try to predict the boiling site density based on a linear mixing law.

Figure 4.38

B.S.D.(EXP)/B.S.D.(I) VS. COMPOSITI
ETHANOL AND WATER MIXTURE
HEAT FLUX IS 74.62 KW/M^2

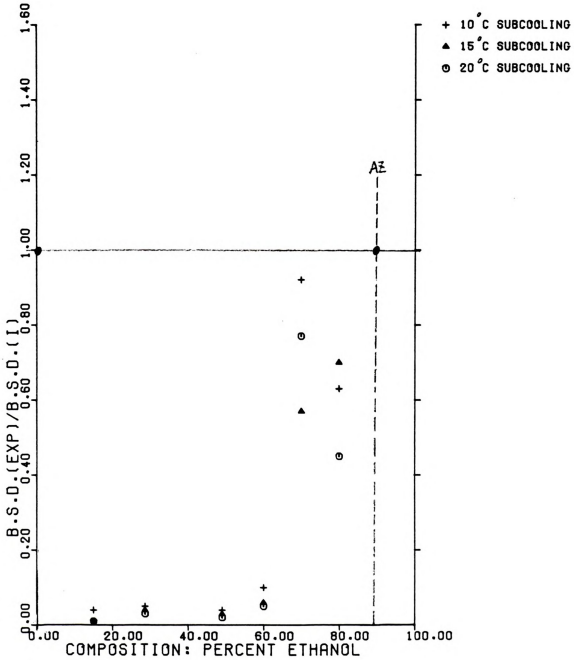

Figure 4.39
B.S.D.(EXP)/B.S.D.(I) VS. COMPOSITI
ETHANOL AND BENZENE MIXTURE
HEAT FLUX IS 97.39 KW/M²

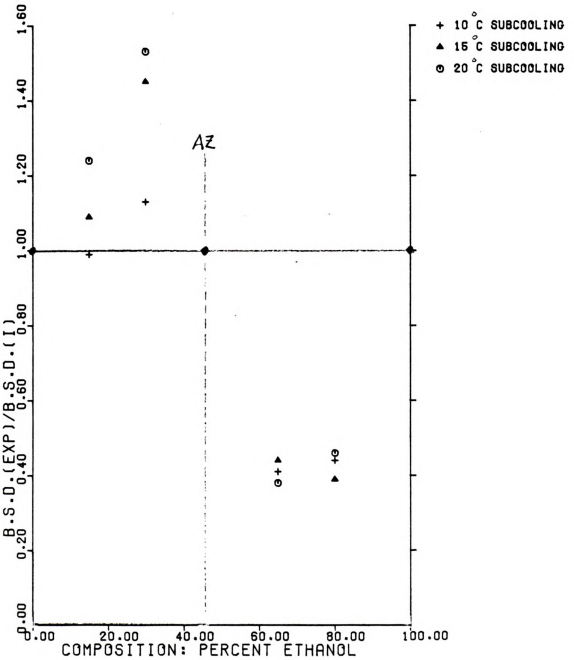

Figure 4.40

B.S.D.(EXP)/B.S.D.(I) VS. COMPOSITI
ETHANOL AND BENZENE MIXTURE
HEAT FLUX IS 74.62 KW/M^2

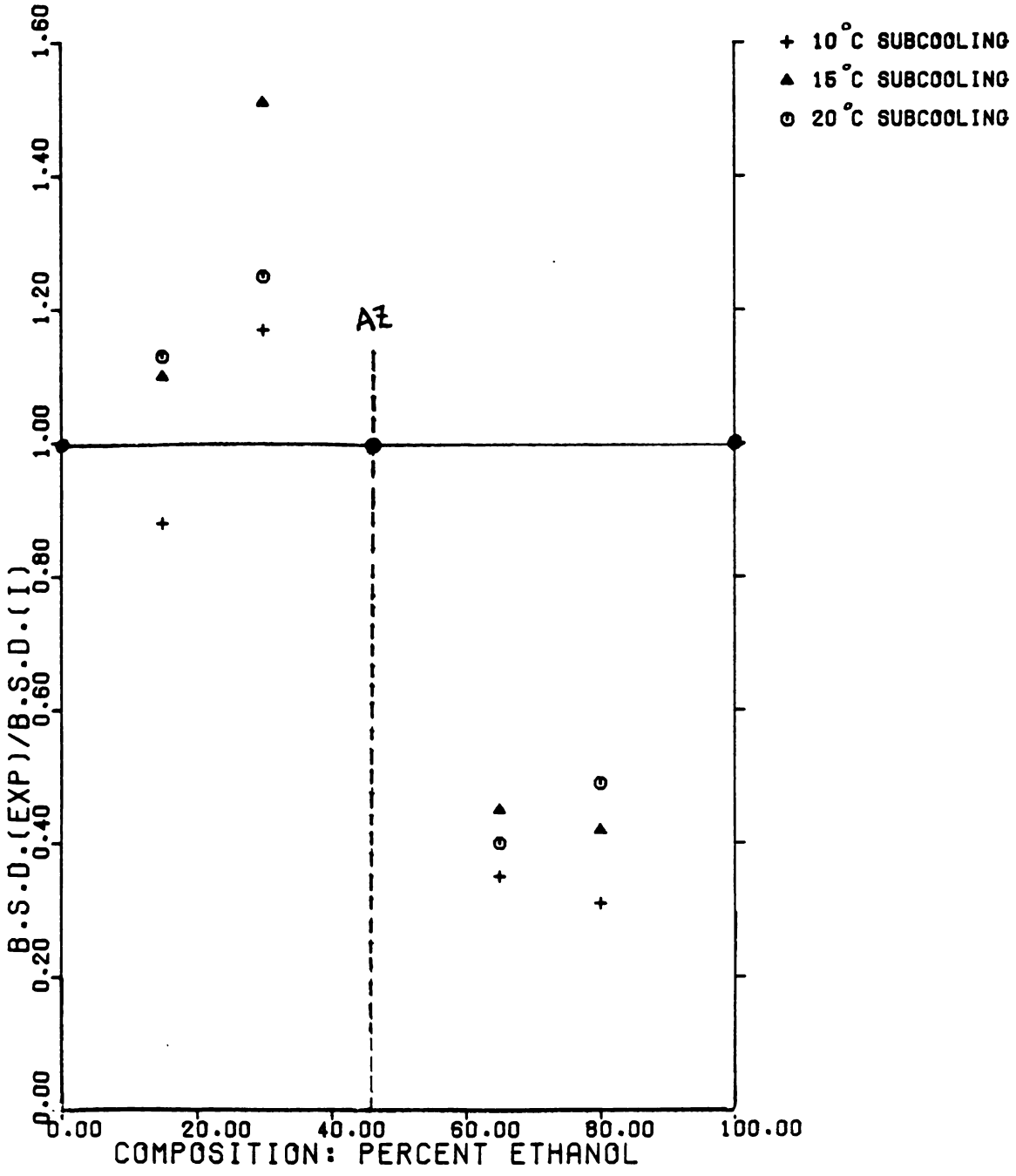

Chapter 5
Conclusions

The following conclusions are made on the effects of subcooling and composition on the boiling heat transfer coefficient and boiling site density for the binary systems tested:

(1) The boiling heat transfer coefficient decreases as the degree of subcooling in the bulk liquid increases.

(2) The ideal linear mixing law is found to be very inadequate in the prediction of the boiling site density of both the aqueous and non-aqueous binary mixture systems studied.

   (a) For the ethanol-water mixture system, the boiling site density can increase by two orders of magnitude from pure water to mixtures close to the azeotrope. A vapor spreading mechanism is proposed as an explanation. The decrease in the actual boiling site density compared to the ideal value is suggested to be due to mass diffusion effects.

   (b) The ethanol-benzene mixture results demonstrate a maximum in the boiling site density to the left of the azeotrope but a minimum to the right. This phenomenon is explained by postulating that during the waiting period of a bubble growth cycle, condensation or evaporation can take place at the surface

of the vapor nucleus so that the vapor nucleus can reach chemical equilibrium with the bulk liquid. Thus the size of the vapor nucleus can be changed and therefore changing the incipient superheat required.

(3) The boiling site density with heat flux and mixture composition being held constant can (1) decrease monotonically , (2) display a maximum value, or (3) display a minimum value when plotted as a function of subcooling. This suggests that the thickness of the thermal boundary layer is a significant parameter in determining the boiling site density.

(4) When the boiling site density is plotted as a function of the wall temperature, it was found that for a given wall temperature the boiling site density is generally greater at a higher degree of subcooling.

Appendix A

Preparation of a mixture of known composition- a sample illustration

To prepare an ethanol-benzene mixture of 15% mole fraction ethanol (at 23 °C).

1. A) Mass of 1 mole of ethanol = 46.06952 gram

   B) Density of ethanol at 23 °C = 0.7903 gram/ml

   C) Molar volume of ethanol at 23 °C =

   molar mass of ethanol/density of ethanol at 23 °C =

   $$\frac{46.06953 \text{ gram}}{0.7903 \text{ gram/ml}} = 58.29 \text{ ml}$$

2. A) Mass of 1 mole of benzene = 78.11472 gram

   B) Density of benzene at 23 °C = 0.875 gram/ml

   C) Molar volume of benzene at 23 °C = molar mass of benzene/density of benzene at 23 °C =

   $$\frac{78.11472 \text{ gram}}{0.8753 \text{ gram/ml}} = 89.24 \text{ ml}$$

3. A) Volume of 15 moles of ethanol =

   $$\frac{58.29 \text{ ml}}{\text{mole of ethanol}} \times 15 \text{ moles of ethanol} = 874.35 \text{ ml}$$

   B) Volume of 85 moles of benzene =

   $$\frac{89.24 \text{ ml}}{\text{moles of benzene}} \times 85 \text{ moles of benzene} = 7585.40 \text{ ml}$$

   C) To prepare a mixture of a total volume of approximately 4400 ml (capacity of boiling vessel) :

   Volume of ethanol = (874.35 ml X 4400 ml)/(874.35 ml + 7585.40 ml)

   = 454.76 ml

Volume of benzene = (7585.40 X 4400 ml)/(874.35 ml + 7585.40 ml)

= 3945.26 ml

Appendix B

Calculation for heat loss

The purpose of this section is to outline the method used in obtaining the experimental heat transfer coefficients. To start, we have an energy balance equation: (also see Figure 3.1)

Power generated by electrical heater = Total heat flux from inner section of heating surface + Total heat flux from outer section of heating surface (A-1)

It is observed experimentally that the mode of heat transfer at the outer section is always by natural convection. Specifically, the outer section of the heating surface is modeled here as that of a case of heat transfer by natural convection through a circumferential fin of rectangular profile .

Let us further assume that for a particular mixture, the heat transfer coefficient for natural convection does not change significantly for different conditions of heat flux and subcooling. This assumption is supported by the experimental data in the present study (Figures 4.9, 4.10, 4.11, 4.12). The heat transfer coefficient approaches an

asymptotic value as the degree of subcooling is increased and this value is relatively the same for different heat fluxes (represented by different curves)used. This suggests that the natural convection heat transfer coefficient is basically a function of the fluid properties only. Applying equation A-1 to situations where natural convection is taking place on the entire heating surface , inner and outer sections:

Power generated by electrical heater $= P = \eta_f h_{n.c.} A_f (T_w - T_b) + h_{n.c.} A_c (T_w - T_b)$ (A-1a)

where η_f = fin efficiency

$h_{n.c.}$ = natural convection heat transfer coefficient

T_w = wall temperature at center of heating surface

T_b = bulk temperature of liquid

A_f = surface area of circumferential fin

A_c = surface area of inner section

Inorder to obtain a value of η_f, it is necessary to have a value for $h_{n.c.}$ in equation A-1. Starting with an equation to get an approximated value for $h_{n.c.}$:

$$h_{n.c.} = \frac{P}{(A_f + A_c)(T_w - T_b)} \qquad \text{(A-2)}$$

Another form of equation A-1 can be rewritten as;

$$h_{n.c.} = \frac{P}{(\eta_f A_f + A_c)(T_w - T_b)} \qquad \text{(A-3)}$$

To summarize the steps that follows:

(1) Equation A-2 is used to get a starting value for $h_{n.c.}$.

(2) Using the value of $h_{n.c.}$ from equation A-2, a value of η_f is obtained from Figure 2.11 of reference (27) and is reproduced here as Figure A-1.

(3) The value of η_f is substituted into equation A-3 and a new value of $h_{n.c.}$ is obtained.

(4) Iteration is used on equation A-3 until the value of $h_{n.c.}$ stabilizes.

The method outlined above is applied to a heating condition of lowest heat flux and highest degree of subcooling. Thus it is a situation where the whole surface is in the natural convection region. To obtain the boiling heat transfer coefficient when boiling is occurring in the inner section and natural convection in the outer region, we have, applying equation A-1:

Power generated by electrical heater = Total boiling heat flux from inner section of heating surface + Total heat flux by natural convection from outer section of heating surface (A-4)

or

$$P = h_b A_c (T_w - T_b) + \eta_f h_{n.c.} A_f (T_w - T_b) \qquad (A-5)$$

where h_b is the boiling heat transfer coefficient. Note that in order to solve for h_b from equation A-5, we use values of η_f and $h_{n.c.}$ obtained by equation A-3.

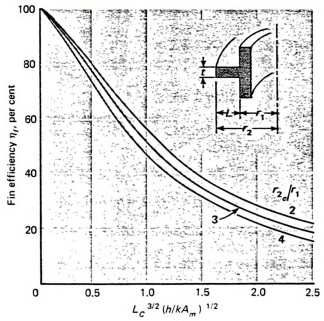

$L_c = L + \frac{t}{2}$

$r_{2c} = r_1 + L_c$

$A_m = t(r_{2c} - r_1)$

Figure A-1 Efficiencies of circumferential fins of rectangular profile

Appendix C

Experimental data

List of symbols used

HFLUX	Power generated by electrical heater
BTEMP	Bulk temperature
T_2, T_4	Temperature readings used to extrapolate the wall temperature
T_w	Wall temperature
QFIN	Heat flux loss at fin
QNET	Heat flux at inner section of heating surface
HEXP	Experimental heat transfer coefficient
HNC	Natural heat transfer coefficient
EFCO	Fin efficiency coefficient

HNC = 883. EFCO = .490

HFLUX	BTEMP	T2	T4	TW	QFIN	QNET	HEXP
49.350	100.000	113.800	115.250	112.350	8.122	41.228	6588.121
37.810	100.000	112.700	113.800	111.600	7.760	30.050	5025.673
28.110	100.000	111.800	112.450	111.150	7.464	20.646	3589.784
19.350	100.000	110.700	111.150	110.250	6.675	12.675	2464.399
12.370	100.000	109.200	109.600	108.800	5.590	6.780	1574.134
6.960	100.000	105.700	105.950	105.450	3.453	3.507	1318.408
49.350	95.500	113.500	115.100	111.900	10.720	38.630	4677.094
37.810	95.500	112.600	113.700	111.500	10.523	27.287	3365.738
28.110	95.500	111.600	112.400	110.800	10.259	17.851	2258.206
19.350	95.500	109.900	110.550	109.250	9.240	10.110	1420.063
12.370	95.500	106.000	106.500	105.500	6.774	5.596	1072.227
6.960	95.500	102.000	102.350	101.650	4.242	2.718	831.655
49.350	90.000	113.000	114.450	111.550	13.778	35.572	3350.905
37.810	90.000	111.600	112.800	110.400	13.022	24.788	2470.699
28.110	90.000	109.900	110.850	108.950	12.463	15.647	1629.556
19.350	90.000	105.800	106.550	105.050	9.898	9.452	1239.468
12.370	90.000	101.000	101.400	100.600	6.774	5.596	1072.227
6.960	90.000	96.300	96.550	96.050	3.979	2.981	972.452
49.350	85.100	112.200	113.800	110.600	16.836	32.514	2506.495
37.810	85.100	110.600	111.900	109.300	15.850	21.960	1798.295
28.110	85.100	108.700	107.750	105.650	13.581	14.529	1388.556
19.350	85.100	101.400	102.150	100.650	10.227	9.123	1157.881
12.370	85.100	96.300	96.900	95.700	6.905	5.465	1027.082
6.960	85.100	91.400	91.700	91.100	3.946	3.014	991.371
49.350	80.000	111.300	112.950	109.650	19.500	29.850	1986.640
37.810	80.000	108.200	109.650	106.750	17.658	20.152	1481.181
28.110	80.000	102.300	103.350	101.250	14.041	14.069	1300.476
19.350	80.000	96.300	97.050	95.550	10.227	9.123	1157.881
12.370	80.000	91.100	91.600	90.600	6.971	5.399	1005.148
6.960	80.000	86.500	86.900	86.300	4.143	2.817	882.359

Ethanol-water system - 0% mole fraction of ethanol

HNC = 709. EFCO = .500

HFLUX	BTEMP	T2	T4	TW	QFIN	QNET	HEXP
49.350	84.450	103.600	104.950	102.250	9.591	39.759	4408.073
37.810	84.450	101.800	102.850	100.750	8.783	29.027	3514.393
28.110	84.450	99.900	100.600	99.200	7.948	20.162	2697.622
19.350	84.450	97.800	98.300	97.300	6.924	12.426	1908.368
12.370	84.450	95.600	95.950	95.250	5.819	6.551	1196.988
6.960	84.450	92.200	92.700	91.700	3.907	3.053	831.159
49.350	79.450	106.600	108.350	104.850	13.687	35.663	2770.939
37.810	79.450	104.100	105.500	102.700	12.528	25.282	2145.977
28.110	79.450	101.100	102.150	100.050	11.100	17.010	1629.565
19.350	79.450	97.200	98.050	96.350	9.106	10.244	1196.198
12.370	79.450	89.700	90.200	89.200	5.254	7.116	1440.414
6.960	79.450	85.400	85.700	85.100	3.044	3.916	1367.672
49.350	74.450	105.600	107.350	103.850	15.842	33.508	2249.260
37.810	74.450	102.500	103.850	101.150	14.387	23.423	1731.282
28.110	74.450	98.300	99.450	97.150	12.232	15.878	1380.436
19.350	74.450	93.200	94.000	92.400	9.672	9.678	1064.021
12.370	74.450	87.300	87.900	86.700	6.601	5.769	929.432
6.960	74.450	81.900	82.200	81.600	3.853	3.107	857.657
49.350	69.450	105.200	107.050	103.350	18.267	31.083	1809.526
37.810	69.450	101.000	102.500	99.500	16.192	21.618	1419.729
28.110	69.450	94.500	95.950	93.050	12.717	15.393	1287.238
19.350	69.450	88.300	88.800	87.800	9.888	9.462	1017.647
12.370	69.450	82.200	82.750	81.650	6.574	5.796	937.599
6.960	69.450	77.000	77.300	76.700	3.907	3.053	831.159
49.350	64.450	103.000	104.900	101.100	19.748	29.602	1593.959
37.810	64.450	97.800	99.400	96.200	17.108	20.702	1286.774
28.110	64.450	91.000	92.150	89.850	13.687	14.423	1120.658
19.350	64.450	84.100	84.950	83.250	10.130	9.220	967.935
12.370	64.450	77.800	78.350	77.250	6.897	5.473	843.802
6.960	64.450	72.500	72.850	72.150	4.149	2.811	720.438

Ethanol-water system - 15% mole fraction of ethanol

HNC = 632. EFCO = .550

HFLUX	BTEMP	T2	T4	TW	QFIN	QNET	HEXP
49.350	81.700	103.400	104.950	101.850	10.646	38.704	3790.658
37.810	81.700	101.100	102.300	99.900	9.616	28.194	3057.189
28.110	81.700	99.000	99.800	98.200	8.718	19.392	2319.424
19.350	81.700	97.000	97.600	96.400	7.767	11.583	1555.068
12.370	81.700	94.100	94.500	93.700	6.340	6.030	991.647
6.960	81.700	89.600	89.900	89.300	4.015	2.945	764.508
49.350	76.700	104.900	106.350	103.450	14.133	35.217	2598.128
37.810	76.700	102.600	103.700	101.500	13.103	24.707	1966.089
28.110	76.700	99.800	100.700	98.900	11.729	16.381	1456.175
19.350	76.700	94.500	95.350	93.650	8.956	10.394	1210.231
12.370	76.700	90.100	90.550	89.650	6.842	5.526	842.409
6.960	76.700	85.100	85.400	84.800	4.280	2.680	653.045
49.350	71.700	101.400	103.200	99.600	14.741	34.609	2448.058
37.810	71.700	99.100	100.400	97.800	13.790	24.020	1816.226
28.110	71.700	96.300	97.400	95.200	12.416	15.694	1317.939
19.350	71.700	92.400	93.000	91.800	10.620	8.730	857.159
12.370	71.700	85.600	86.150	85.050	7.053	5.317	785.926
6.960	71.700	79.900	80.150	79.650	4.200	2.760	685.041
49.350	66.700	101.800	103.450	100.150	17.673	31.677	1868.874
37.810	66.700	98.700	99.950	97.450	15.247	21.563	1383.900
28.110	66.700	94.400	95.550	93.250	14.028	14.082	1046.754
19.350	66.700	87.600	88.350	86.850	10.646	8.704	852.445
12.370	66.700	80.600	81.100	80.100	7.080	5.290	779.103
6.960	66.700	74.500	74.800	74.200	3.963	2.997	788.705
49.350	61.700	99.800	101.450	98.150	19.258	30.092	1629.238
37.810	61.700	97.300	98.650	95.950	18.096	19.714	1135.926
28.110	61.700	91.500	92.600	90.400	15.164	12.946	890.227
19.350	61.700	85.200	85.950	84.450	12.020	7.330	635.857
12.370	61.700	76.000	76.500	75.500	7.291	5.079	726.297
6.960	61.700	70.200	70.500	69.900	4.332	2.628	632.366

Ethanol-water system - 28.67% mole fraction of ethanol

HNC = 492. EFCO = .590

HFLUX	BTEMP	T2	T4	TW	QFIN	QNET	HEXP
49.350	80.000	99.400	101.200	97.600	7.766	41.584	4662.890
37.810	80.000	97.600	98.950	96.250	7.170	30.640	3721.120
28.110	80.000	95.700	96.600	94.800	6.530	21.580	2877.558
19.350	80.000	93.400	94.100	92.700	5.604	13.746	2136.109
12.370	80.000	91.000	91.450	90.550	4.655	7.715	1443.193
6.960	80.000	87.500	87.650	87.350	3.243	3.717	998.025
49.350	75.000	101.000	102.500	99.500	10.810	38.540	3104.434
37.810	75.000	99.800	100.700	98.900	10.545	27.265	2251.335
28.110	75.000	97.000	97.700	96.300	9.398	18.712	1733.705
19.350	75.000	94.200	94.650	93.750	8.273	11.077	1165.893
12.370	75.000	90.400	90.700	90.100	6.663	5.707	745.943
6.960	75.000	84.400	84.550	84.250	4.081	2.879	614.167
49.350	70.000	101.100	102.450	99.750	13.126	36.224	2402.930
37.810	70.000	98.800	99.750	97.850	12.288	25.522	1808.524
28.110	70.000	96.200	96.800	95.600	11.295	16.815	1296.237
19.350	70.000	91.900	92.350	91.450	9.464	9.886	909.531
12.370	70.000	85.800	86.100	85.500	6.839	5.531	704.222
6.960	70.000	78.800	78.900	78.700	3.839	3.121	708.041
49.350	65.000	100.100	101.400	98.800	14.913	34.437	2010.668
37.810	65.000	97.700	98.600	96.800	14.031	23.779	1475.720
28.110	65.000	94.100	94.750	93.450	12.553	15.557	1079.156
19.350	65.000	89.100	89.450	88.750	10.479	8.871	737.124
12.370	65.000	80.400	80.650	80.150	6.685	5.685	740.607
6.960	65.000	74.000	74.200	73.800	3.883	3.077	690.100
49.350	60.000	99.400	100.650	98.150	16.833	32.517	1682.117
37.810	60.000	96.200	97.100	95.300	15.575	22.235	1243.067
28.110	60.000	92.100	92.700	91.500	13.899	14.211	890.355
19.350	60.000	84.800	85.150	84.450	10.788	8.562	691.091
12.370	60.000	76.800	77.050	76.550	7.302	5.068	604.298
6.960	60.000	70.400	70.600	70.200	4.501	2.459	475.865

Ethanol-water system - 49.04% mole fraction of ethanol

HNC = 405. EFCO = .620

HFLUX	BTEMP	T2	T4	TW	QFIN	QNET	HEXP
49.350	79.500	95.800	97.550	94.050	5.553	43.797	5940.394
37.810	79.500	94.900	96.250	93.550	5.286	32.524	4634.354
28.110	79.500	93.700	94.600	92.800	5.076	23.034	3417.829
19.350	79.500	91.500	92.150	90.850	4.370	14.980	2581.899
12.370	79.500	89.800	90.200	89.400	3.702	8.668	1763.491
6.960	79.500	87.000	87.200	86.800	2.672	4.288	1208.993
49.350	75.000	96.800	98.600	95.000	7.824	41.526	3997.611
37.810	75.000	95.900	97.200	94.600	7.481	30.329	3053.813
28.110	75.000	94.500	95.750	94.050	7.485	20.625	2075.688
19.350	75.000	93.500	94.000	93.000	6.985	12.365	1333.504
12.370	75.000	90.300	90.600	90.000	5.840	6.530	842.339
6.960	75.000	85.200	85.400	85.000	3.931	3.029	580.320
49.350	69.700	97.000	98.700	95.300	9.656	39.694	3996.265
37.810	69.700	95.600	96.900	94.300	9.542	28.268	2231.492
28.110	69.700	94.300	95.150	93.450	9.065	19.045	1582.563
19.350	69.700	92.400	93.000	91.800	8.511	10.839	959.202
12.370	69.700	87.500	87.750	87.250	6.775	5.595	622.105
6.960	69.700	79.700	79.950	79.450	3.798	3.162	627.229
49.350	64.400	96.400	98.100	94.700	11.412	37.938	2504.035
37.810	64.400	94.700	96.000	93.400	10.916	26.894	1855.793
28.110	64.400	93.200	94.050	92.350	10.591	17.519	1245.872
19.350	64.400	90.600	91.250	89.950	9.752	9.598	741.378
12.370	64.400	82.300	82.600	82.000	6.756	5.614	625.990
6.960	64.400	75.300	75.550	75.050	4.065	2.895	536.494
49.350	60.000	95.800	97.550	94.050	13.225	36.125	2057.513
37.810	60.000	93.500	94.700	92.300	12.366	25.444	1549.796
28.110	60.000	91.400	92.250	90.550	11.698	16.412	1056.724
19.350	60.000	87.100	87.600	86.600	10.152	9.198	682.380
12.370	60.000	78.600	79.100	78.100	6.908	5.462	595.510
6.960	60.000	71.400	71.550	71.250	4.332	2.628	456.952

Ethanol-water system - 60% mole fraction of ethanol

HNC = 462. EFCO = .600

HFLUX	BTEMP	T2	T4	TW	QFIN	QNET	HEXP
49.350	79.100	90.400	92.200	88.600	4.003	45.347	9420.291
37.810	79.100	89.300	90.650	87.950	3.771	34.039	7505.688
28.110	79.100	88.400	89.300	87.500	3.581	24.529	5694.958
19.350	79.100	87.200	87.800	86.600	3.244	16.106	4127.857
12.370	79.100	85.700	86.050	85.350	2.718	9.652	2953.314
6.960	79.100	84.500	84.650	84.350	2.338	4.622	1643.353
49.350	73.900	90.900	92.650	89.150	6.468	42.882	5513.248
37.810	73.900	90.000	91.300	88.700	6.236	31.574	4210.237
28.110	73.900	89.000	89.950	88.050	5.878	22.232	3145.186
19.350	73.900	87.800	88.300	87.300	5.688	13.662	1997.161
12.370	73.900	85.900	86.250	85.550	4.824	7.546	1300.547
6.960	73.900	83.500	83.700	83.300	3.961	2.999	629.707
49.350	69.000	91.400	93.200	89.600	8.595	40.755	3942.606
37.810	69.000	90.200	91.500	88.900	8.343	29.467	2937.065
28.110	69.000	88.800	89.800	87.800	7.921	20.189	2119.280
19.350	69.000	87.400	88.000	86.800	7.500	11.850	1313.827
12.370	69.000	84.700	85.150	84.250	6.468	5.902	758.949
6.960	69.000	80.300	80.500	80.100	4.719	2.241	394.867
49.350	64.000	91.000	92.800	89.200	10.534	38.816	3064.167
37.810	64.000	89.800	91.200	88.400	10.239	27.571	2239.179
28.110	64.000	88.400	89.250	87.550	9.923	18.187	1524.108
19.350	64.000	86.100	86.800	85.400	9.017	10.333	952.927
12.370	64.000	82.100	82.550	81.650	7.437	4.933	551.605
6.960	64.000	76.500	76.750	76.250	5.204	1.756	280.669
49.350	59.100	91.000	92.800	89.200	12.640	36.710	2414.885
37.810	59.100	89.700	91.000	88.400	12.303	25.507	1723.890
28.110	59.100	87.400	88.700	86.100	11.334	16.776	1230.748
19.350	59.100	83.700	84.600	82.800	9.986	9.364	779.753
12.370	59.100	78.200	78.950	77.450	7.732	4.638	498.842
6.960	59.100	69.800	70.200	69.400	4.466	2.494	464.285

Ethanol-water system - 70% mole fraction of ethanol

HNC = 462. EFCO = .600

HFLUX	BTEMP	T2	T4	TW	QFIN	QNET	HEXP
49.350	78.900	90.000	91.700	88.300	3.961	45.389	9529.353
37.810	78.900	88.800	90.100	87.500	3.624	34.186	7844.993
28.110	78.900	87.800	88.650	86.950	3.476	24.634	5892.730
19.350	78.900	86.700	87.300	86.100	3.034	16.316	4472.259
12.370	78.900	85.300	85.600	85.000	2.612	9.758	3105.928
6.960	78.900	84.200	84.300	84.100	2.233	4.727	1760.093
49.350	73.500	90.200	91.900	88.500	6.194	43.156	5793.799
37.810	73.500	89.200	90.350	88.050	6.131	31.679	4296.865
28.110	73.500	88.100	88.950	87.250	5.541	22.569	3387.115
19.350	73.500	86.900	87.400	86.400	5.183	14.167	2273.130
12.370	73.500	85.200	85.500	84.900	4.593	7.777	1408.129
6.960	73.500	83.200	83.350	83.050	3.855	3.105	669.632
49.350	69.000	90.300	91.900	88.700	8.048	41.302	4267.547
37.810	69.000	89.200	90.350	88.050	7.816	29.994	3191.013
28.110	69.000	88.000	88.900	87.100	7.626	20.484	2233.399
19.350	69.000	86.900	87.500	86.300	7.331	12.019	1363.146
12.370	69.000	84.300	84.650	83.950	6.299	6.071	801.400
6.960	69.000	80.400	80.650	80.150	4.614	2.346	422.867
49.350	63.900	90.400	92.050	88.750	10.470	38.880	3087.682
37.810	63.900	89.300	90.500	88.100	10.239	27.571	2239.179
28.110	63.900	87.800	88.700	86.900	9.733	18.377	1569.996
19.350	63.900	85.500	86.050	84.950	8.869	10.481	982.598
12.370	63.900	81.400	81.800	81.000	7.247	5.123	587.791
6.960	63.900	74.600	74.800	74.400	4.635	2.325	417.165
49.350	59.200	90.400	92.050	88.750	12.619	36.731	2420.305
37.810	59.200	89.000	90.150	87.850	12.240	25.570	1737.885
28.110	59.200	87.400	88.200	86.600	11.545	16.565	1193.116
19.350	59.200	83.600	84.150	83.050	10.175	9.175	749.729
12.370	59.200	78.500	78.950	78.050	7.942	4.428	463.554
6.960	59.200	71.000	71.250	70.750	4.993	1.967	327.597

Ethanol-water system - 70% mole fraction of ethanol

HNC = 403. EFCO = .620

HFLUX	BTEMP	T2	T4	TW	QFIN	QNET	HEXP
49.350	78.410	92.200	93.850	90.550	4.611	44.739	7272.914
37.810	78.410	91.300	92.400	90.200	4.478	33.332	5579.416
28.110	78.410	90.000	90.850	89.150	4.079	24.031	4415.768
19.350	78.410	88.700	89.200	88.200	3.718	15.632	3151.125
12.370	78.410	87.200	87.500	86.900	3.224	9.146	2125.896
6.960	78.410	85.600	85.750	85.450	2.674	4.286	1201.564
49.350	73.400	92.400	93.900	90.900	6.646	42.704	4815.760
37.810	73.400	91.200	92.250	90.150	6.361	31.449	3705.298
28.110	73.400	89.900	90.650	88.950	5.906	22.204	2818.020
19.350	73.400	88.200	88.750	87.650	5.412	13.938	1937.295
12.370	73.400	86.100	86.400	85.800	4.709	7.661	1219.215
6.960	73.400	83.000	83.200	82.800	3.570	3.390	711.720
49.350	68.400	92.000	93.650	90.350	8.336	41.014	3687.493
37.810	68.400	90.500	91.650	89.350	7.957	29.853	2812.210
28.110	68.400	88.800	89.700	87.900	7.406	20.704	2095.366
19.350	68.400	86.700	87.250	86.150	6.741	12.609	1401.883
12.370	68.400	84.000	84.300	83.700	5.811	6.559	846.058
6.960	68.400	80.100	80.350	79.850	4.349	2.611	450.102
49.350	63.400	91.700	93.250	90.150	10.159	39.191	2891.321
37.810	63.400	90.100	91.200	89.000	9.723	28.087	2165.257
28.110	63.400	88.000	88.800	87.200	9.039	19.071	1581.376
19.350	63.400	85.400	85.950	84.850	8.146	11.204	1030.780
12.370	63.400	82.000	82.550	81.450	6.855	5.515	602.966
6.960	63.400	74.700	74.900	74.500	4.216	2.744	487.928
49.350	58.400	90.800	92.350	89.250	11.716	37.634	2407.450
37.810	58.400	88.900	90.000	87.800	11.166	26.644	1788.518
28.110	58.400	86.300	87.150	85.450	10.273	17.837	1301.325
19.350	58.400	83.900	84.350	83.250	9.438	9.912	787.199
12.370	58.400	77.100	77.600	76.600	6.912	5.458	591.819
6.960	58.400	70.800	71.000	70.600	4.633	2.327	376.356

Ethanol-water system - 80% mole fraction of ethanol

HNC = 426. EFCO = .620

HFLUX	BTEMP	T2	T4	TW	QFIN	QNET	HEXP
49.350	78.600	89.100	91.100	87.100	3.412	45.938	10665.623
37.810	78.600	88.100	89.500	86.700	3.292	34.518	8307.474
28.110	78.600	87.100	88.050	86.150	3.111	24.999	6365.789
19.350	78.600	85.800	86.500	85.100	2.730	16.620	4823.482
12.370	78.600	84.400	84.750	84.050	2.308	10.062	3453.313
6.960	78.600	83.300	83.500	83.100	1.927	5.033	2069.289
49.350	73.300	89.300	91.150	87.450	5.600	43.750	6189.235
37.810	73.300	88.000	89.400	86.600	5.339	32.471	4818.093
28.110	73.300	87.000	87.900	86.100	5.219	22.891	3475.028
19.350	73.300	85.400	86.200	84.600	4.577	14.773	2557.471
12.370	73.300	84.100	84.350	83.850	4.316	8.054	1478.616
6.960	73.300	82.400	82.450	82.350	3.714	3.246	692.639
49.350	68.500	89.400	91.400	87.400	7.387	41.963	4500.770
37.810	68.500	87.900	89.300	86.500	7.266	30.544	3330.257
28.110	68.500	86.300	87.400	85.200	6.704	21.406	2529.575
19.350	68.500	84.500	85.100	83.900	6.183	13.167	1687.404
12.370	68.500	82.100	82.550	81.650	5.279	7.091	1064.155
6.960	68.500	79.700	80.000	79.400	4.376	2.584	467.857
49.350	63.700	88.300	90.050	86.550	9.214	40.136	3451.384
37.810	63.700	86.500	88.100	85.100	8.832	28.978	2599.443
28.110	63.700	84.900	85.850	83.950	8.370	19.740	1868.389
19.350	63.700	82.900	83.500	82.300	7.467	11.883	1260.791
12.370	63.700	80.200	80.550	79.850	6.604	5.766	691.738
6.960	63.700	75.100	75.350	74.850	4.516	2.444	428.653
49.350	58.900	87.900	89.700	86.100	11.241	38.109	2686.008
37.810	58.900	85.900	87.250	84.550	10.579	27.231	2039.518
28.110	58.900	73.900	79.750	67.850	3.754	24.356	5140.878
19.350	58.900	81.200	81.750	80.650	8.973	10.377	916.315
12.370	58.900	77.700	78.100	77.300	7.387	4.983	534.464
6.960	58.900	69.900	70.150	69.650	4.516	2.444	428.653

Ethanol-water system - 89.4% mole fraction of ethanol

HNC = 416. EFCO = .630

HFLUX	BTEMP	T2	T4	TW	QFIN	QNET	HEXP
49.350	80.000	95.500	98.450	92.550	4.999	44.351	6974.170
37.810	80.000	94.700	96.850	92.550	4.999	32.811	5159.494
28.110	80.000	93.400	95.050	91.750	4.760	23.350	3856.100
19.350	80.000	92.100	93.300	90.900	4.342	15.008	2717.249
12.370	80.000	90.200	90.850	89.550	3.804	8.566	1770.084
6.960	80.000	86.800	87.150	86.450	2.530	4.430	1376.914
49.350	75.200	94.500	97.300	91.700	6.453	42.897	5225.699
37.810	75.200	93.100	95.300	90.900	6.254	31.556	3966.574
28.110	75.200	91.500	93.100	89.900	5.856	22.254	2987.649
19.350	75.200	89.600	90.700	88.500	5.378	13.972	2042.517
12.370	75.200	87.900	88.650	87.150	4.760	7.610	1256.695
6.960	75.200	83.900	84.250	83.550	3.326	3.634	858.811
49.350	70.000	93.900	96.650	91.150	8.266	41.084	3907.435
37.810	70.000	92.260	94.350	90.050	7.868	29.942	2991.962
28.110	70.000	90.400	91.950	88.850	7.509	20.601	2156.809
19.350	70.000	87.900	89.050	86.750	6.673	12.677	1493.668
12.370	70.000	85.500	86.100	84.900	5.936	6.434	852.236
6.960	70.000	80.700	81.000	80.400	4.143	2.817	534.560
49.350	65.400	93.400	95.950	90.850	10.059	39.291	3070.951
37.810	65.400	91.500	93.450	89.550	9.620	28.190	2303.607
28.110	65.400	89.600	91.000	88.200	9.043	19.067	1657.670
19.350	65.400	86.600	87.600	85.600	8.047	11.303	1104.290
12.370	65.400	83.900	84.400	83.400	7.171	5.199	570.066
6.960	65.400	76.800	77.150	76.450	4.442	2.518	445.722
49.350	60.200	92.400	94.950	89.850	11.652	37.698	2543.482
37.810	60.200	90.200	92.250	88.150	11.055	26.755	1902.772
28.110	60.200	87.600	88.950	86.250	10.258	17.852	1368.206
19.350	60.200	84.000	84.900	83.100	9.083	10.267	888.712
12.370	60.200	80.600	81.000	80.200	7.967	4.403	434.443
6.960	60.200	72.100	72.450	71.750	4.601	2.359	403.059

Ethanol-benzene system - 0% mole fraction of ethanol

HNC = 446. EFCO = .600

HFLUX	BTEMP	T2	T4	TW	QFIN	QNET	HEXP
49.350	69.000	86.500	88.800	84.400	6.264	43.086	5521.445
37.810	69.000	85.300	86.950	83.650	6.000	31.810	4256.125
28.110	69.000	84.300	85.650	82.950	5.634	22.476	3202.696
19.350	69.000	82.900	83.850	81.950	5.145	14.205	2216.028
12.370	69.000	81.000	81.650	80.350	4.535	7.835	1386.709
6.960	69.000	78.000	78.300	77.700	3.579	3.381	756.134
49.350	64.200	87.200	89.200	85.200	8.542	40.808	3835.000
37.810	64.200	85.700	87.250	84.150	8.115	29.695	2937.527
28.110	64.200	84.200	85.450	82.950	7.708	20.402	2124.720
19.350	64.200	82.100	82.900	81.300	6.915	12.435	1443.582
12.370	64.200	79.800	80.500	79.100	6.101	6.269	824.755
6.960	64.200	74.500	74.800	74.400	4.027	2.933	584.705
49.350	59.100	87.800	89.800	85.800	10.820	38.530	2858.637
37.810	59.100	86.300	87.900	84.700	10.372	27.438	2123.472
28.110	59.100	84.500	85.800	83.400	9.884	18.226	1480.200
19.350	59.100	82.100	82.950	81.250	9.132	10.218	898.265
12.370	59.100	78.500	79.100	77.900	7.850	4.520	462.155
6.960	59.100	70.000	70.250	69.750	4.454	2.506	451.664
49.350	54.000	87.400	89.500	85.300	12.853	36.497	2279.307
37.810	54.000	85.900	87.550	84.250	12.264	25.546	1672.168
28.110	54.000	83.700	85.000	82.400	11.470	16.640	1164.477
19.350	54.000	80.300	81.050	79.550	10.393	8.957	691.883
12.370	54.000	74.400	74.950	73.850	8.033	4.337	433.335
6.960	54.000	64.500	64.850	64.150	4.129	2.831	550.532
49.350	49.200	87.100	89.150	85.050	14.501	34.849	1929.175
37.810	49.200	84.900	86.600	83.200	13.830	23.980	1391.923
28.110	49.200	82.500	83.700	81.300	13.057	15.053	925.471
19.350	49.200	77.200	77.900	76.500	11.064	8.286	601.217
12.370	49.200	69.900	70.350	69.450	8.237	4.133	402.815
6.960	49.200	60.300	60.650	59.950	4.413	2.547	463.225

Ethanol-benzene system - 15% mole fraction of ethanol

HNC = 454. EFCO = .600

HFLUX	BTEMP	T2	T4	TW	QFIN	QNET	HEXP
49.350	68.100	84.200	86.600	81.800	5.672	43.678	6291.798
37.810	68.100	82.800	84.750	80.850	5.403	32.407	4900.733
28.110	68.100	81.900	83.350	80.450	5.238	22.872	3568.258
19.350	68.100	80.000	81.100	78.900	4.555	14.795	2654.442
12.370	68.100	78.400	79.150	77.650	4.078	8.292	1661.272
6.960	68.100	75.300	75.700	74.900	2.816	4.144	1202.812
49.350	63.400	85.400	87.600	83.200	8.157	41.193	4126.644
37.810	63.400	84.200	85.900	82.500	7.908	29.902	3089.580
28.110	63.400	82.500	83.950	81.250	7.474	20.636	2256.286
19.350	63.400	80.300	81.250	79.350	6.604	12.746	1577.060
12.370	63.400	77.900	78.650	77.150	5.693	6.677	958.309
6.960	63.400	73.600	73.900	73.300	4.140	2.820	556.432
49.350	58.500	85.700	87.850	83.550	10.496	38.854	3024.779
37.810	58.500	84.000	85.700	82.300	9.979	27.831	2279.060
28.110	58.500	81.500	82.800	80.200	8.985	19.125	1739.332
19.350	58.500	78.700	79.550	77.850	8.053	11.297	1146.230
12.370	58.500	75.900	76.550	75.250	7.018	5.352	623.124
6.960	58.500	69.000	69.250	68.750	4.451	2.509	460.603
49.350	53.100	84.700	86.800	82.600	11.966	37.384	2552.849
37.810	53.100	83.100	84.700	81.500	11.511	26.299	1866.978
28.110	53.100	80.400	81.750	79.050	10.620	17.490	1345.648
19.350	53.100	77.100	77.900	76.300	9.606	9.744	828.877
12.370	53.100	73.300	73.750	72.850	8.136	4.234	425.227
6.960	53.100	63.900	64.200	63.600	4.513	2.447	443.019
49.350	48.400	84.400	86.450	82.350	14.181	35.169	2026.445
37.810	48.400	82.400	84.050	80.750	13.353	24.457	1496.614
28.110	48.400	79.400	80.550	78.250	12.277	15.833	1053.874
19.350	48.400	74.800	75.550	74.050	10.786	8.564	648.797
12.370	48.400	69.700	70.150	69.250	8.633	3.737	353.725
6.960	48.400	59.100	59.350	58.850	4.451	2.509	460.603

Ethanol-benzene system - 30% mole fraction of ethanol

HNC = 438. EFCO = .600

HFLUX	BTEMP	T2	T4	TW	QFIN	QNET	HEXP
49.350	67.700	82.200	84.700	79.700	4.793	44.557	7327.692
37.810	67.700	81.200	83.150	79.250	4.654	33.156	5616.655
28.110	67.700	79.800	81.150	78.450	4.254	23.856	4420.602
19.350	67.700	78.200	79.250	77.150	3.735	15.615	3295.869
12.370	67.700	76.800	77.600	76.000	3.276	9.094	2188.771
6.960	67.700	73.900	74.250	73.550	2.297	4.663	1600.467
49.350	62.900	82.200	84.750	79.650	6.611	42.739	5096.400
37.810	62.900	81.100	82.800	79.400	6.591	31.219	3733.979
28.110	62.900	79.600	80.750	78.450	6.251	21.859	2756.407
19.350	62.900	77.700	78.450	76.950	5.732	13.618	1872.804
12.370	62.900	75.700	76.350	75.050	4.933	7.437	1188.370
6.960	62.900	72.400	72.600	72.200	3.875	3.085	627.711
49.350	57.800	82.000	84.300	79.700	8.668	40.682	3699.795
37.810	57.800	80.600	82.300	78.900	8.429	29.381	2748.073
28.110	57.800	78.500	79.850	77.350	7.809	20.301	2049.274
19.350	57.800	76.000	76.900	75.100	6.911	12.439	1419.028
12.370	57.800	73.500	74.150	72.850	6.012	6.358	833.746
6.960	57.800	68.300	68.550	68.050	4.134	2.826	538.781
49.350	53.100	82.000	84.200	79.800	10.626	38.724	2873.035
37.810	53.100	80.000	81.700	78.300	10.026	27.784	2184.504
28.110	53.100	77.500	78.650	76.350	9.287	18.823	1597.699
19.350	53.100	74.100	74.550	73.650	8.209	11.141	1069.933
12.370	53.100	71.600	72.150	71.050	7.130	5.240	579.304
6.960	53.100	63.800	64.150	63.450	4.374	2.586	466.063
49.350	47.800	80.900	83.000	78.800	12.223	37.127	2394.426
37.810	47.800	78.400	80.000	76.800	11.424	26.386	1820.696
28.110	47.800	75.400	76.550	74.250	10.446	17.664	1333.092
19.350	47.800	71.900	72.750	71.050	9.207	10.143	868.386
12.370	47.800	68.200	68.600	67.800	7.989	4.381	432.283
6.960	47.800	59.100	59.350	58.850	4.454	2.506	443.562

Ethanol-benzene system - 45% mole fraction of ethanol

HNC = 438. EFCO = .600

HFLUX	BTEMP	T2	T4	TW	QFIN	QNET	HEXP
49.350	68.200	84.200	86.250	82.150	5.572	43.778	6193.195
37.810	68.200	82.600	84.150	81.050	5.093	32.717	5064.068
28.110	68.200	81.200	82.450	79.950	4.614	23.496	4014.711
19.350	68.200	79.500	80.600	78.400	3.995	15.355	3030.396
12.370	68.200	77.600	77.300	77.900	3.875	8.495	1728.395
6.960	68.200	75.100	75.550	74.650	2.497	4.463	1409.363
49.350	63.400	83.400	85.400	81.400	7.150	42.200	4652.580
37.810	63.400	82.200	83.650	80.750	6.931	30.879	3512.425
28.110	63.400	80.400	81.650	79.150	6.212	21.898	2779.203
19.350	63.400	78.800	79.600	78.000	5.792	13.558	1845.275
12.370	63.400	76.600	77.300	75.900	4.993	7.377	1164.649
6.960	63.400	73.500	73.750	73.250	3.935	3.025	606.147
49.350	58.500	82.400	84.400	80.400	8.868	40.482	3598.711
37.810	58.500	80.800	82.300	79.300	8.429	29.381	2748.073
28.110	58.500	78.900	80.050	77.550	7.610	20.500	2123.752
19.350	58.500	76.400	77.400	75.400	6.791	12.559	1457.981
12.370	58.500	74.000	74.803	73.200	5.912	6.458	861.146
6.960	58.500	69.000	69.300	68.700	4.234	2.726	507.481
49.350	53.400	81.800	83.800	79.800	10.586	38.764	2886.852
37.810	53.400	79.400	81.000	77.800	9.667	28.143	2295.063
28.110	53.400	77.000	78.250	75.750	8.928	19.182	1693.780
19.350	53.400	74.000	75.000	73.000	7.829	11.521	1160.001
12.370	53.400	72.100	72.650	71.550	7.290	5.080	549.328
6.960	53.400	64.400	64.700	64.100	4.314	2.646	483.485
49.350	48.100	80.200	82.050	78.350	12.004	37.346	2452.679
37.810	48.100	77.700	79.250	76.150	11.245	26.565	1862.403
28.110	48.100	75.300	76.500	74.100	10.306	17.804	1361.871
19.350	48.100	72.000	72.950	71.050	9.168	10.182	875.605
12.370	48.100	68.300	68.750	67.850	7.889	4.481	447.734
6.960	48.100	59.400	59.650	59.150	4.454	2.506	443.562

Ethanol-benzene system - 65% mole fraction of ethanol

HNC = 450. EFCO = .600

HFLUX	BTEMP	T2	T4	TW	QFIN	QNET	HEXP
49.350	69.400	86.400	88.400	84.400	6.156	43.194	5682.891
37.810	69.400	84.800	86.450	83.150	5.643	32.167	4616.842
28.110	69.400	83.400	84.600	82.200	5.212	22.898	3558.193
19.350	69.400	81.500	82.400	80.600	4.555	14.795	2630.366
12.370	69.400	80.100	80.750	79.450	4.083	8.287	1643.563
6.960	69.400	77.500	77.900	77.100	3.160	3.800	973.915
49.350	64.400	85.400	87.400	83.400	7.880	41.470	4262.587
37.810	64.400	83.600	85.150	82.050	7.244	30.566	3417.726
28.110	64.400	81.900	83.050	80.750	6.710	21.400	2583.047
19.350	64.400	79.900	80.850	78.950	6.053	13.297	1779.040
12.370	64.400	78.200	78.900	77.500	5.458	6.912	1025.579
6.960	64.400	74.600	74.950	74.250	4.001	2.959	598.851
49.350	59.500	84.200	86.150	82.250	9.296	40.054	3489.953
37.810	59.500	82.200	83.700	80.700	8.618	29.192	2743.315
28.110	59.500	80.000	81.250	78.750	7.900	20.210	2071.898
19.350	59.500	77.800	78.800	76.800	7.141	12.209	1384.744
12.370	59.500	75.800	76.600	75.000	6.320	6.050	775.283
6.960	59.500	70.400	70.700	70.100	4.309	2.651	498.224
49.350	54.700	82.700	84.550	80.850	10.855	38.495	2872.201
37.810	54.700	80.200	81.800	78.600	9.850	27.960	2299.160
28.110	54.700	78.100	79.250	76.950	9.131	18.979	1683.338
19.350	54.700	75.400	76.400	74.400	8.085	11.265	1128.513
12.370	54.700	73.500	74.000	73.000	7.551	4.819	516.825
6.960	54.700	65.700	66.000	65.400	4.391	2.569	473.773
49.350	49.600	81.400	83.300	79.500	12.435	36.915	2404.340
37.810	49.600	78.800	80.450	77.150	11.224	26.586	1918.340
28.110	49.600	76.000	77.250	74.750	10.322	17.788	1395.844
19.350	49.600	73.000	73.900	72.100	9.234	10.116	887.286
12.370	49.600	69.800	70.250	69.350	8.105	4.265	426.136
6.960	49.600	60.600	60.900	60.300	4.432	2.528	461.887

Ethanol-benzene system - 80% mole fraction of ethanol

HNC = 454. EFCO = .600

HFLUX	BTEMP	T2	T4	TW	QFIN	QNET	HEXP
49.350	78.300	91.300	93.900	88.700	4.306	45.044	8547.513
37.810	78.300	90.100	92.050	88.150	4.078	33.732	6758.311
28.110	78.300	89.200	90.550	87.850	3.954	24.156	4991.786
19.350	78.300	87.900	88.950	86.850	3.540	15.810	3649.218
12.370	78.300	86.800	87.600	86.000	3.147	9.223	2395.007
6.960	78.300	84.900	85.250	84.550	2.546	4.414	1416.301
49.350	73.000	90.800	93.350	88.250	6.231	43.119	5654.120
37.810	73.000	89.600	91.300	87.900	6.169	31.641	4190.798
28.110	73.000	88.400	89.550	87.250	5.776	22.334	3159.585
19.350	73.000	87.200	87.950	86.450	5.362	13.988	2131.697
12.370	73.000	85.600	86.250	84.950	4.824	7.546	1278.344
6.960	73.000	83.200	83.400	83.000	3.933	3.027	628.725
49.350	68.400	90.500	92.800	88.200	8.115	41.235	4151.867
37.810	68.400	89.200	90.900	87.500	7.743	30.067	3173.146
28.110	68.400	87.400	88.650	86.150	7.349	20.761	2308.233
19.350	68.400	85.200	86.100	84.300	6.666	12.684	1554.754
12.370	68.400	83.400	84.050	82.750	6.024	6.346	860.690
6.960	68.400	79.100	79.350	78.850	4.451	2.509	460.603
49.350	63.600	89.800	92.000	87.600	10.061	39.289	3190.787
37.810	63.600	87.900	89.600	86.200	9.357	28.453	2484.559
28.110	63.600	86.000	87.150	84.850	8.799	19.311	1793.469
19.350	63.600	83.300	84.250	82.350	7.763	11.587	1219.528
12.370	63.600	81.600	82.150	81.050	7.349	5.021	558.211
6.960	63.600	74.900	75.250	74.550	4.658	2.302	403.815
49.350	58.000	88.800	90.900	86.700	11.800	37.550	2600.147
37.810	58.000	86.900	88.500	85.300	11.386	26.424	1896.259
28.110	58.000	84.500	85.650	83.350	10.372	17.738	1397.451
19.350	58.000	81.900	82.750	81.050	9.502	9.848	846.808
12.370	58.000	78.200	78.600	77.800	8.198	4.172	415.815
6.960	58.000	69.000	69.250	68.750	4.451	2.509	460.603

Ethanol-benzene system - 100% mole fraction of ethanol

LIST OF REFERENCES

1. S.J.D. Van Stralen and R. Cole, "Boiling Phenomena", p. 38, Hemisphere Publishing Corp., Washington, 1978.

2. S.J.D. Van Stralen, "Heat Transfer to Boiling Binary Liquid Mixtures", Br. Chem. Eng. 4(1959) 8-17, 78-82, 6(1961) 834-840, 7(1962) 90-97.

3. J.R. Thome, "Nucleate Pool Boiling of Binary Liquid - an Analytical Equation", AICHE Symposium Series, No. 208, 77(1981) 238-250.

4. M.S. Plesset and S.A. Zwick, "The Growth of Vapor Bubble in Superheated Liquids", J. Appl. Physics 25(1954) 493-500.

5. V.I. Tolubinskiy and Y.N. Ostrovskiy, "Mechanism of Heat Transfer in Boiling Binary Mixture", Heat Transfer-Soviet Research 1(16) 1969, p.6-11.

6. J.R. Thome, "Bubble Growth and Nucleate Pool Boiling in Liquid Nitrogen, Argon, and Their Mixtures", D.Phil. Thesis, Oxford University (1978).

7. E.G. Keshock and R. Siegel, "Forces Acting on Bubbles in Nucleate Boiling Under Normal and Reduces Gravity Conditions", NASA TN-D-2299 (1964).

8. J.R. Thome and G. Davey, "Effect of Mass Diffusion Controlled Growth and Wall Superheat On Bubble Departure in a Cryogenic Binary Mixture System", Proc. of 8th International Cryogenic Engineering Conference (Guildford, IPC Science and Technology Press, 1980, Genoa, Italy, p.243-250.

9. J.R. Thome, "Latent and Sensible Heat Transfer Rates in the Boiling of Binary Liquids", J. Heat Transfer, 104, 474-478(1982).

10. R.A.W. Shock, "The Evaporation of Binary Mixtures in Forced Convection", AERE Report R7593(1973).

11. A. Singh, B.B. Mikic, and W.M. Rohsenow, "Active Sites in Boiling", J. Heat Transfer 98(1976) 401-406.

12. J.R. Thome, S. Shakir, and C. Mercier, "Effect of Composition on Boiling Incipient Superheats in Binary Liquid Mixtures", Proc. of 7th Int. Heat Transfer Conference, Munich (1982).

13. Y.Y. Hsu and R.W. Graham, "An Analytical and Experimental Study of the Thermal Boundary Layer and Ebullition Cycle in Nucleate Boiling", NASA TN D-594, May, 1961.

14. Y.Y. Hsu "On the Size Range of Active Nucleation Cavities on a Heating Surface", J. of Heat Transfer, 84(1962) 207-216.

15. Chi-Yeh Han, and P. Griffth, "The Mechanism of Heat Transfer in Nucleate Pool Boiling- Part I : Bubble Initiation, Growth, and Departure", Int. J. of Heat and Mass Transfer, 8(1965) 887-892.

16. J.R. Howell and R. Siegel, "Incipience, Growth, and Detachment of Bubble in Saturated Water from Artificial Nucleation Sites of Known Geometry and Sizes", Proc. from 3rd Int. Heat Transfer Conf., Chicago, IV (1966) 12-23.

17. B.D. Marcus and D. Dropkin, "Measured Temperature Profile Within the Superheated Boundary Layer Above a Horizontal Surface in Saturated Nucleate Pool Boiling of Water", J. of Heat Transfer, (1965) 333-341.

18. T.E. Lippert and R.S. Dougall, "A Study of the Temperature Profiles Measured in the Thermal Sublayer of Water, Freon-113, and Methyl Alcohol During Pool Boiling", J. of Heat Transfer, (1968) 347-352.

19. J.R. Wiebe and R.L. Judd, "Superheated Layer Thickness Measurements in Saturated and Subcooled Nucleate Boiling", J. of Heat Transfer, (1971) 455-461.

20. K. Engelberg-Forster and R. Greif, "Heat Transfer to a Boiling Liquid- Mechanism and Correlation", J. of Heat Transfer,(1959) 43-53.

21. V.I. Tolubinskiy and D.M. Konstanchuk, "The Rate of Vapor Bubble Growth in Boiling of Water", Heat Transfer-Soviet Research, vol. 4, No. 6, (1972) 7-12.

22. M.E. Ellion, "A Study of the Mechanism of Boiling Heat Transfer", Memo No. 22-88, Jet Propulsion Lab., California Institute of Technology, (1954) 72-82.

23. R.M. Fand and K.K. Keswani, "The Influence of Subcooling on Pool Boiling Heat Transfer from a Horizontal Cylinder to Water", J. Heat Transfer, 87(1963) 231-242.

24. M.Sultan, and R.L. Judd, "Spatial Distribution of Active site and Bubble Flux Density", J. of Heat Transfer, vol. 100 (1978) 56-62.

25. L.S. Sterman, J.V. Vilemas, A.I. Abramov, "On Heat Transfer and Critical Heat Flux in Organic Coolants and Their Mixtures Boiling", Proc. of 3rd International Heat Transfer Conference, p. 258- , Chicago, 1979.

26. R.I Eddington and D.B.R. Kenning, "The Effect of Contact Angle on Bubble Nucleation", Int. J. of Heat and Mass Transfer, 22(1979) 1231-1236.

27. J.P. Holman, "Heat Transfer", p. 40, McGraw-Hill, Inc, New York, 1976.